



## PROTON-EXCHANGE BIOMIMETIC MEMBRANES BASED ON COLUMNAR SIDE-CHAIN LIQUID-CRYSTALLINE POLYETHERS

**Suryakant Bhosale**

**Dipòsit Legal: T.188-2014**

**ADVERTIMENT.** L'accés als continguts d'aquesta tesi doctoral i la seva utilització ha de respectar els drets de la persona autora. Pot ser utilitzada per a consulta o estudi personal, així com en activitats o materials d'investigació i docència en els termes establerts a l'art. 32 del Text Refós de la Llei de Propietat Intel·lectual (RDL 1/1996). Per altres utilitzacions es requereix l'autorització prèvia i expressa de la persona autora. En qualsevol cas, en la utilització dels seus continguts caldrà indicar de forma clara el nom i cognoms de la persona autora i el títol de la tesi doctoral. No s'autoritza la seva reproducció o altres formes d'explotació efectuades amb finalitats de lucre ni la seva comunicació pública des d'un lloc aliè al servei TDX. Tampoc s'autoritza la presentació del seu contingut en una finestra o marc aliè a TDX (framing). Aquesta reserva de drets afecta tant als continguts de la tesi com als seus resums i índexs.

**ADVERTENCIA.** El acceso a los contenidos de esta tesis doctoral y su utilización debe respetar los derechos de la persona autora. Puede ser utilizada para consulta o estudio personal, así como en actividades o materiales de investigación y docencia en los términos establecidos en el art. 32 del Texto Refundido de la Ley de Propiedad Intelectual (RDL 1/1996). Para otros usos se requiere la autorización previa y expresa de la persona autora. En cualquier caso, en la utilización de sus contenidos se deberá indicar de forma clara el nombre y apellidos de la persona autora y el título de la tesis doctoral. No se autoriza su reproducción u otras formas de explotación efectuadas con fines lucrativos ni su comunicación pública desde un sitio ajeno al servicio TDR. Tampoco se autoriza la presentación de su contenido en una ventana o marco ajeno a TDR (framing). Esta reserva de derechos afecta tanto al contenido de la tesis como a sus resúmenes e índices.

**WARNING.** Access to the contents of this doctoral thesis and its use must respect the rights of the author. It can be used for reference or private study, as well as research and learning activities or materials in the terms established by the 32nd article of the Spanish Consolidated Copyright Act (RDL 1/1996). Express and previous authorization of the author is required for any other uses. In any case, when using its content, full name of the author and title of the thesis must be clearly indicated. Reproduction or other forms of for profit use or public communication from outside TDX service is not allowed. Presentation of its content in a window or frame external to TDX (framing) is not authorized either. These rights affect both the content of the thesis and its abstracts and indexes.

# **Proton-Exchange Biomimetic Membranes Based On Columnar Side-Chain Liquid-Crystalline Polyethers**

**Suryakant Vilasrao Bhosale**

**Doctoral Thesis**

**UNIVERSITAT ROVIRA I VIRGILI**



UNIVERSITAT ROVIRA I VIRGILI

PROTON-EXCHANGE BIOMIMETIC MEMBRANES BASED ON COLUMNAR SIDE-CHAIN LIQUID-CRYSTALLINE POLYETHERS

Suryakant Bhosale

Dipòsit Legal: T.188-2014

UNIVERSITAT ROVIRA I VIRGILI

PROTON-EXCHANGE BIOMIMETIC MEMBRANES BASED ON COLUMNAR SIDE-CHAIN LIQUID-CRYSTALLINE POLYETHERS

Suryakant Bhosale

Dipòsit Legal: T.188-2014

UNIVERSITAT ROVIRA I VIRGILI

PROTON-EXCHANGE BIOMIMETIC MEMBRANES BASED ON COLUMNAR SIDE-CHAIN LIQUID-CRYSTALLINE POLYETHERS

Suryakant Bhosale

Dipòsit Legal: T.188-2014

Department of Analytical And Organic Chemistry

**Proton-Exchange Biomimetic Membranes Based On  
Columnar Side-Chain Liquid-Crystalline Polyethers**

by

**Suryakant Vilasrao Bhosale**  
**Doctoral Thesis**

Thesis Supervisor: Dr. José Antonio Reina Lozano

Thesis Co-Supervisor: Dr. Marta Giamberini



**UNIVERSITAT ROVIRA I VIRGILI**

Tarragona

2013

UNIVERSITAT ROVIRA I VIRGILI

PROTON-EXCHANGE BIOMIMETIC MEMBRANES BASED ON COLUMNAR SIDE-CHAIN LIQUID-CRYSTALLINE POLYETHERS

Suryakant Bhosale

Dipòsit Legal: T.188-2014



## UNIVERSITAT ROVIRA I VIRGILI

DEPARTAMENT DE QUÍMICA ANALÍTICA  
I QUÍMICA ORGÀNICA

C/ Marcel·lí Domingo s/n  
Campus Sescelades  
43007 Tarragona (Spain)  
Tel. 34 977 55 97 69  
Fax 34 977 55 84 46  
e-mail: secqao@urv.net

Dr. José Antonio Reina Lozano, Associate Professor at the University of Rovira i Virgili, Department of Analytical Chemistry and Organic Chemistry and Dr. Marta Giamberini, Associate Professor at the University of Rovira I Virgili, Department of Chemical Engineering,

CERTIFY that the present study, entitled “**Proton-Exchange Biomimetic Membranes Based On Columnar Side-Chain Liquid-Crystalline Polyethers**”, presented by Suryakant Vilasrao Bhosale for the award of the degree of Doctor, has been carried out under our supervision at the Department of Analytical and Organic Chemistry, and that it fulfils all the requirements to be eligible for the European Doctorate Award.

Tarragona, December 2013

Thesis Supervisor

Thesis Co-Supervisor

Dr. José Antonio Reina Lozano

Dr. Marta Giamberini



UNIVERSITAT ROVIRA I VIRGILI

PROTON-EXCHANGE BIOMIMETIC MEMBRANES BASED ON COLUMNAR SIDE-CHAIN LIQUID-CRYSTALLINE POLYETHERS

Suryakant Bhosale

Dipòsit Legal: T.188-2014

## **Acknowledgements**

After lots of hard work and patience when doctoral thesis comes to the end, still there remains a difficult part of writing acknowledgements. During this stage, we work with a great number of people directly or indirectly whose contribution in assorted ways to the research and the making of the thesis deserve special mention. It is a pleasure to convey my gratitude to them all in my humble acknowledgment.

In the first place I would like to record my gratitude to my thesis supervisors, respected Dr José Antonio Reina and Dr. Marta Giamberini for their supervision, advice, and guidance from the very early stage of this research as well as giving me extraordinary experiences through out the work. Above all and the most needed, they provided me unflinching encouragement and support in various ways. Yours truly scientist intuition has made you as a constant oasis of ideas and passions in science, which exceptionally inspire and enrich my growth as a student, a researcher and a scientist want to be. I am indebted to them more than they know.

Many thanks go in particular to Dr. Angels Serra. I am much indebted to her for her recommendation of mine to my thesis supervisors to accept me as a PhD student.

Also I would like to thank my other colleagues from lab 330 for their supporting and kind nature. To the role model for hard workers in the lab, Asta, I would like to thank you for being the person who taught me tricks in organic chemistry. I am proud to record that I had several opportunities to work with an exceptionally experienced scientist like her. Adrian: it's reminding me lots of things those happened in past 4 years. Thank you very much for the time that we spend together by sharing many things and thoughts.

*Marjorie: my great gratitude to you for providing hyperbranched polyglycidol without this I would have never finished my chapter 3. Also thank you and Enrique for being always there to solve my laptop problems. Cristina Acebo: it has been always nice to talk to you. Your presence was keeping the lab 330 alive. Best wishes for your PhD. Cristina Mas: you have been always a wonderful person to me. It's my fate having opportunity to spend some time with you and even my Spanish is not so good but was always nice to talk to you, muchas gracias. Kris: I remember we were living together when you came to tarragona for your research stay and now you are continuing to PhD. Best wishes for your PhD and thank you very much for your help in membrane stuff. Also some ex-labmates Azam, David, Mireia and Silvana, I would like to thank you all for your presence during this PhD period, especially Azam: without your help it was not possible to finish my chapter 2. Also, I would like to thank Dr. Bartosz Tylkowski for your help in membrane preparation.*

*Apart from the lab 330, during this PhD, I got lots of friends like Rodolfo, Maryluz, Camilo, Cristina Lluch, Zynep and Alev from lab 327. It is always nice to have friends like you people. I would like to thank you all from bottom of my heart and wishing you the best in future.*

*This PhD also gave some fantastic flatmates like Lin and Silvana. Thank you very much you both for being there.*

*Here I would like to acknowledge people from Katholieke Universiteit of Leuven (KU Leuven) where I spent 3 months of my research stay. I would like to thank you Prof. Ivo Vankelecom for accepting me to work in his research group and providing all necessary information and material to carry out my research. Also I would like to thank you Parimal Naik and Hubei Yu for helping me during this research stay.*

Where would I be without my family? My parents deserve special mention for their inseparable support and prayers. My Father, Mr. Vilasrao Bhosale, in the first place is the person who put the fundamentals of my learning character, showing me the joy of intellectual pursuit ever since I was a child, letting me to live my life at my own terms and being supportive during failures of my early career stage, thank you very much *Bapu*. My Mother, Minakshi, is the one who sincerely raised me with her caring and gently love, thank you very much *Aai*. My brother, Chandrakant, my best buddy, and his wife Rajashri, thank you very much both of you for your support and encouragement.

Words fail me to express my appreciation to my wife Komal whose dedication, love and persistent confidence in me, has taken the load off my shoulder. Therefore, I would also thank Katkar family, Mr. Kishor Katkar, Mrs Sanjivani Katkar and Kiran for letting me to take her hand in marriage, and accepting me as a member of the family, warmly.

And finally handsome, gorgeous, incredible, dazzling, stunning, amazing, fabulous, outstanding...that is my wonderful son Aaryan Bhosale. Thank you very much my lad for being my inspiration.

In conclusion, I would like to thank everybody who was important to the successful realization of thesis.

Finally, I thank God for His love and care in fulfilling this goal.

UNIVERSITAT ROVIRA I VIRGILI

PROTON-EXCHANGE BIOMIMETIC MEMBRANES BASED ON COLUMNAR SIDE-CHAIN LIQUID-CRYSTALLINE POLYETHERS

Suryakant Bhosale

Dipòsit Legal: T.188-2014

## List of abbreviations

AFC	Alkaline Fuel Cells
AFM	Atomic Force Microscopy
Col	Columnar
Col <sub>h</sub>	Columnar Hexagonal
Col <sub>r</sub>	Rectangular Columnar
CP	Copolymer
DCC	N,N'-Dicyclohexylcarbodiimide
DMAP	4-Dimethylaminopyridine
DMFC	Direct Methanol Fuel Cells
DSC	Differential Scanning Calorimetry
EIS	Electrochemical Impedance Spectroscopy
ESEM	Environmental Scanning Electron Microscopy
HBP	Hyperbranched Polymer
HP	Homopolymer
LC	Liquid Crystal
LPG	Linear Polyglycidol
MCFC)	Molten Carbonate Fuel cells
MCLCP	Main Chain Liquid Crystalline Polymer
MEA	Membrane Electrode Assembly
M <sub>n</sub>	Number Average Molecular Weight
M <sub>w</sub>	Weight Average Molecular Weight
NMR	Nuclear Magnetic Resonance
P(ECH-co-EO)	Polyepichlorohydrin-co-Ethylene Oxide
PAFC	Phosphoric Acid Fuel Cells
PECH	Polyepichlorohydrin
PEM	polymer electrolyte membrane
PEMFC	Polymer Electrolyte Membrane Fuel Cells
PEMFC	Proton Exchange Membrane Fuel Cells
PFSA	Perfluorosulfonated acid
POM	Polarised Optical Microscopy
PSSA	Poly(propylene)-Grafted-Polystyrene Sulfonic Acid
PVA	Polyvinyl Alcohol
ROMBP	Ring-Opening Multibranching Polymerization
SCLCP	Side Chain Liquid Crystalline Polymer
SEC	Size Exclusion Chromatography
SOFC	Solid Oxide Fuel Cells
SPEEK	Sulphonated Poly(ether ether ketone)
TBAB	Tetrabutylammonium bromide
TMS	Tetramethyl Silane
TMV	Tobacco Mosaic Virus
XRD	X-ray Diffraction

UNIVERSITAT ROVIRA I VIRGILI

PROTON-EXCHANGE BIOMIMETIC MEMBRANES BASED ON COLUMNAR SIDE-CHAIN LIQUID-CRYSTALLINE POLYETHERS

Suryakant Bhosale

Dipòsit Legal: T.188-2014

## Table of contents

<b>Chapter 1: Introduction</b>	<b>1</b>
1.1 Introduction	3
1.2 Direct Methanol Fuel Cell	7
1.3 Polymer electrolytes for DMFC	10
1.4 Proton exchange membranes based on side chain liquid crystalline polymers (SCLCPs)	16
1.5 Liquid Crystalline Side Chain Polymers	21
1.6 References	26
1.7 General objectives of the thesis	32
<b>Chapter 2: Side-Chain Liquid Crystalline Polymers Based On Chemical Modification Of Commercial Polyethers</b>	<b>33</b>
2.1 Introduction	35
2.2 Experimental	38
2.2.1 Materials	38
2.2.2 Synthesis of Dendritic mesogenic groups	38
2.2.3 PECH Modification	38
2.2.4 P(ECH-co-EO) modification	39
2.3 Characterization and measurements	40
2.4 Results and discussion	43
2.4.1 Synthesis of Potassium-3,4,5-tris[4-(n-dodecan-1-yloxy)benzyloxy]benzoate	43
2.4.2 Modification of PECH	45
2.4.3 Modification of P(ECH-co-EO)	48
2.5 Conclusions	61
2.6 References	62
<b>Chapter 3: Side-Chain Liquid Crystalline Polymers Based On Chemical Modification Of Polyglycidol</b>	<b>65</b>
3.1 Introduction	67
3.2 Experimental	69
3.2.1 Materials	69
3.2.2 Synthesis of 3,4,5-tris[4-(n-dodecan-1-yloxy)benzyloxy]benzoic Acid (2)	69
3.2.3 Synthesis of linear polyglycidol (LPG)	72
3.2.4 Synthesis of hyperbranched polyglycirol	77
3.2.5 Modification of linear polyglycidol	77
3.2.6 Modification of hyperbranched polyglycidol	78
3.3 Characterization and Measurements	80
3.4 Results and discussion	82
3.4.1 Synthesis of 3,4,5-Tris[4-(n-dodecan-1-yloxy)benzyloxy]benzoic acid	82
3.4.2 Synthesis of linear polyglycidol	82
3.4.3 Chemical modification of linear polyglycidol	83
3.4.4 Chemical modification of hyperbranched polyglycidol	96



3.5 Conclusions	101
3.6 References	102
<b>Chapter 4: Preparation And Assessment Of Proton-Conducting Membranes Based On Homeotropically Aligned Side-Chain Liquid Crystalline Polyethers</b>	<b>105</b>
4.1 Introduction	107
4.2 Experimental	113
4.2.1 Materials	113
4.2.2 Preparation of hydrophilic glass substrate	113
4.2.3 Preparation of membranes based on SCLCPS by immersion precipitation	113
4.2.4 Preparation of membranes based on SCLCPS by vapor precipitation	114
4.2.5 Membrane orientation by baking process	115
4.2.6 Preparation of membranes based on SCLCPs by shearing process	116
4.3 Characterisation techniques	117
4.4 Results and discussion	120
4.5 Conclusion	143
4.6 References	144
<b>Chapter 5: General Conclusions</b>	<b>147</b>
<b>Appendices</b>	<b>151</b>
Appendix A: List of figures, schemes and tables	153
Appendix B: Publications, meeting contributions and abroad research stay	160
Appendix C: New Liquid Crystalline Columnar Poly(epichlorohydrin-co-ethylene oxide) derivatives leading to biomimetic ion channels	161

---

*Chapter 1*  
*Introduction*

UNIVERSITAT ROVIRA I VIRGILI

PROTON-EXCHANGE BIOMIMETIC MEMBRANES BASED ON COLUMNAR SIDE-CHAIN LIQUID-CRYSTALLINE POLYETHERS

Suryakant Bhosale

Dipòsit Legal: T.188-2014

## 1.1 Introduction

Throughout the world, now there is a need to look for other alternatives of power generation against natural resources. Fuel cells are the best alternative to these natural resources which has been invented by William Grove in 1839. Although fuel cells are not a recent development, “Fuel cells” have always fascinated scientist from all over the world. Savings in fossil fuels, due to high efficiency of energy conversion, low pollution level, low noise and low maintenance costs render fuel cells preferable over other energy conversion devices. A fuel cell produces electricity directly from the electrochemical reaction of hydrogen, from a hydrogen-containing fuel, and oxygen from the air. All fuel cells consist of a pair of electrodes, i.e. cathode and anode, and an electrolyte, plus an external circuit for electrical current and internal mechanism for allowing ion migration to complete the circuit. Electrolytes transport protons from one compartment to other converting the chemical energy stored in hydrogen fuel directly and efficiently to electrical energy with water as the only byproduct. A simple and general scheme of fuel cell has been given in **(Figure 1.1)**.

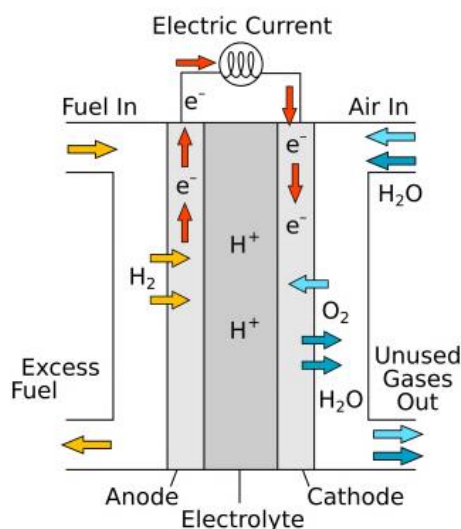


**Figure 1.1. General scheme of fuel cell**

In general fuel cells are classified by the sort of electrolyte they utilize. This classification determines the kind of chemical reactions that take place in the cell, the kind of catalysts required, the temperature range in which the cell operates, the fuel required, and other factors. These characteristics, in turn, affect the applications for which these cells are most suitable. There are several types of fuel cells currently under development, each with its own advantages, limitations, and potential applications<sup>1</sup> :

- Alkaline Fuel Cells (AFC)
- Phosphoric Acid Fuel Cells (PAFC)
- Molten Carbonate Fuel cells (MCFC)
- Solid Oxide Fuel Cells (SOFC)
- Proton Exchange Membrane Fuel Cells (PEMFC) [Polymer Electrolyte Membrane Fuel Cells (PEMFC) and Direct Methanol Fuel Cells (DMFC)]

### **AFC**

Alkaline fuel cells (AFC) were developed by F.T. Bacon in 1930. They use alkaline potassium hydroxide as the electrolyte and generate power efficiencies of up to 70 percent. AFC were long used by NASA on space missions on the Apollo spacecraft to provide electricity and drinking water, for example. Their operating temperature is 150 °C to 200 °C. However, they were too costly for commercial applications and several companies are now examining ways to reduce costs and improve operating flexibility.

### **PAFC**

Phosphoric acid fuel cells (PAFC) were manufactured in the 1970s in the background of the energy crises. This type of fuel cell is the one that has been commercially developed the most and is used in a wider range of applications in hospitals, nursing homes, hotels, office buildings, schools, utility power plants and airport terminals. These cells generate electricity with an efficiency of over 40% and their operating temperatures are around 150 °C.

## **MCFC**

Molten carbonate fuel cells (MCFC) use a liquid solution of lithium, sodium and/or potassium carbonates soaked in a matrix for an electrolyte. They promise high fuel-to-electricity efficiencies normally of about 60%, or 85% with cogeneration, and operate at about 650 °C.

## **SOFC**

Another highly promising fuel cell, the solid oxide fuel cell (SOFC), is used for stationary power plants. A solid oxide system usually uses a hard ceramic material instead of a liquid electrolyte. This allows operating temperatures to reach 1000 °C. Power generating efficiencies can reach 60% and 85% with cogeneration and with a cell output of up to 100 kW.

## **PEMFC**

Proton exchange membrane fuel cells (PEMFC) operate at relatively low temperatures (about 80 °C), have high power density, can vary their output quickly to meet shifts in power demand, and are suitable for automobile applications. In the 1960s, driven by the need for very compact units for producing electricity and water, NASA developed PEMFC in their Gemini space program. They were chosen for the Apollo program and launched in the space shuttles, but were found to be inferior to the AFC in terms of performance and durability. In the 1980s PEMFCs achieved significant progress when membranes with greater stability and performance were discovered. PEMFCs use polymer membranes, which are able to conduct protons, as the electrolyte. The electrolyte is sandwiched between two electrodes, which contain Pt-based catalysts that help the oxidation and reduction reactions to take place. According to the U.S. Department of Energy, they are "the primary candidates for light-duty vehicles, for buildings, and potentially for much smaller applications such as replacements for rechargeable batteries in video cameras." PEMFCs mainly include hydrogen fuel cells and direct methanol fuel cells (DMFC). Most relevant characteristics of all fuel cells are summarized in the following **Table 1.1**.

**Table 1.1. Classification of fuel cells and their main features**

<b>Fuel cell Characteristics</b>	<b>PEMFC /DMFC</b>	<b>AFC</b>	<b>PAFC</b>	<b>MCFC</b>	<b>SOFC</b>
<b>Electrolyte</b>	Cationic Exchange Membrane	Potassium hydroxide	Phosphoric acid	Molten carbonate	Ceramics
<b>Operation Temperature</b>	80 °C	65 °C - 220 °C	205 °C	650 °C	800 °C - 1000 °C
<b>Charge carrier</b>	H <sup>+</sup>	OH <sup>-</sup>	H <sup>+</sup>	CO <sub>3</sub> <sup>-2</sup>	O <sup>-2</sup>
<b>Cell materials</b>	Carbon	Carbon	Graphite	Iron steel	Ceramics
<b>Catalyst</b>	Platinum	Platinum	Platinum	Nickel	Nickel
<b>Heat management</b>	Gas processing refrigerant	Gas processing Refrigerant	Gas processing refrigerant	Internal reforming gas processing	Internal reforming gas processing

## 1.2 Direct Methanol Fuel Cell

In the year 1990, Dr. Surya Prakash and Dr. George Olah invented DMFC which is capable of producing electrical energy by use of methanol as a fuel. Basically, the direct methanol fuel cell is a proton exchange membrane fuel cell that is fed with an aqueous solution of methanol. The two catalytic electrodes where the methanol oxidation (anode) and the oxygen reduction (cathode) occur are separated by a membrane which conducts protons from anode to cathode, while other compound's diffusion is blocked. The combination of electrodes and membranes is called membrane electrode assembly (MEA). Here, the state of the art in membranes is Nafion®. It was created by addition of sulfonic acid groups into the bulk polymer matrix of Teflon. These sites have strong ionic properties and act as proton exchange sites. Aqueous methanol is fed at the anode side. It diffuses through the diffusion layer to the catalytic layer where it is electrochemically oxidized into mainly carbon dioxide, six protons and six electrons. These six protons react at the cathode with oxygen to form water<sup>2</sup>. The overall reaction looks like a combustion reaction and is thus sometimes referred to as cold combustion. Actually the cell is a mean to control this reaction and use it to produce current directly. Oxygen may be pure but can also come from air. Electrons are collected by graphite bipolar plates which are the two poles of the cell. The working principle of the direct methanol fuel cell is shown in **(Figure 1.2)**.

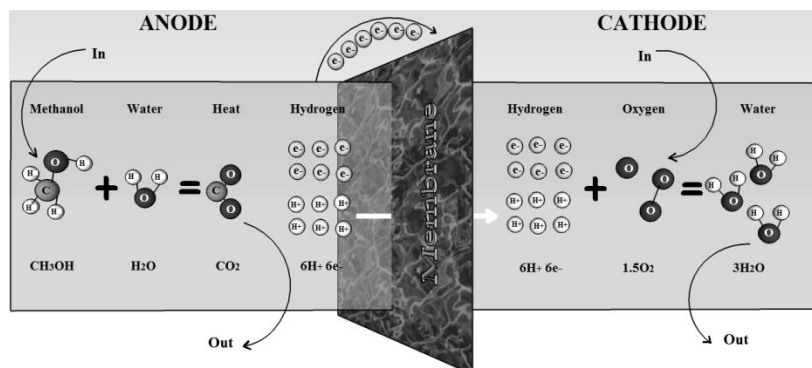


Figure 1.2. The working principle of the direct methanol fuel cell

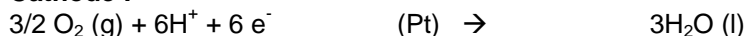


## Reactions

### Anode :



### Cathode :



### Overall :



The high energy density of methanol makes it as a suitable fuel for fuel cells<sup>3</sup>. DMFC are fed with a dilute aqueous solution of methanol in water. Also in mobile applications, liquid fuels are usually preferable to gaseous ones, and often to solid ones as well. So, not surprisingly, researchers have long been on the lookout for a fluid that would also be a suitable fuel. Methanol was an obvious candidate, because it:

- is inexpensive and can be readily made via a well known manufacturing process from plentiful raw materials,
- is easy to handle, store and transport,
- remains liquid under normal storage conditions (unlike, say, butane, which tends to evaporate much more easily),
- is compatible with the existing fuel distribution infrastructure,
- is relatively hydrogen-dense, *i.e.* four of the six atoms in methanol ( $\text{CH}_3\text{OH}$ ) are hydrogen, and
- is environmentally acceptable.

Fuel Cells are considered as environmentally friendly as they do not produce toxic byproducts. However, they are not emission-free. They still produce carbon dioxide which is a green house gas. This is also true for hydrogen which produces  $\text{CO}_2$  indirectly during reforming step in the water-gas shift reaction. Methanol and other alcohols also produce some other byproducts like aldehydes, ketones and carboxylic acids but in very low concentrations. If the methanol produced from biomass, the  $\text{CO}_2$  formed during cell operation would nevertheless be balanced by  $\text{CO}_2$  consumed in photosynthesis. Consequently,

this form of energy would contribute no more to green house effect and will be renewable.

### 1.3 Polymer electrolytes for DMFC

One of the functions of the electrolyte is to separate the hydrogen ( $H_2$ ) and oxygen ( $O_2$ ) streams. The membrane must be also electrically isolating in order to drive the electrons to flow through an external circuit, and also must provide a pathway for the protons from the anode to the cathode, so that the electrochemical reactions can occur. The performance of fuel cells depends not only on the yield of the reactions, but also on complex mass and energy transfer processes. Therefore, the proton transport through the electrolyte is crucial to the whole fuel cell performance. The most common electrolytes used in DMFC are perfluorinated polymers containing proton conducting groups attached via side chains. In particular, DuPont's Nafion® is the benchmark material in DMFC<sup>4</sup>, and its chemical structure can be seen in **Figure 1.3**.

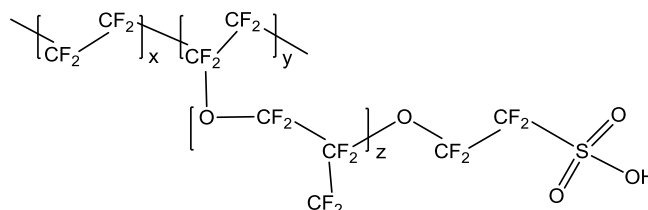


**Figure 1.3. Chemical structure of Nafion®**

The substitution of the hydrogen atoms by fluorine in the main chain leads to a very stable and chemical resistant material while the presence of ionic groups gives high proton conductivity. Even though there are numerous hypotheses about the detailed morphology of Nafion<sup>5</sup>, it is widely accepted that microphase separation occurs. The ionic groups tend to form ion-rich aggregates (ionic clusters). The ionic clusters are nanometer sized (approximately, diameter 5 nm) and are connected by small narrow ionic channels (approximately, 1 nm). The proton conductivity depends on the ionic sites in the polymer. When the membrane is swollen in water, the ion clusters become interconnected and then the proton conductivity increases. The transport of molecules and ions is enhanced through this interconnected ionic network. Several investigations have

shown that the diffusion of protons and water molecules is strongly affected by the ionic nanostructure.

It is widely assumed that there are two main mechanisms for proton transport through these electrolytes, namely, well known “proton hopping” invented by De Grotthuss (1806), also known as Grotthuss mechanism and the “vehicular or electroosmotic drag”<sup>6</sup> mechanisms. The hopping mechanism occurs when protons ( $H^+$ ) hop from one hydrolysed site ( $SO_3^-H_3O^+$ ) to another by the formation and destruction of hydrogen bonds (**Figure 1.4**). On the other hand, protons transported by the vehicular mechanism are bound with water ( $H^+$  ( $H_2O$ )<sub>x</sub>) and drag one or more water molecules across the membrane, as seen in **Figure 1.5**. Therefore, these membranes must be designed to retain a certain degree of hydration since water is involved in proton transport. Several experiments have shown that proton conductivity increases with increasing water content, ionic group concentration and temperature. In membranes with higher ionic group concentration there is an increase in the hydrophilic and ionic nature of the polymer which promotes higher conductivities and water levels<sup>7</sup>. However, when the water content reaches a certain value, the mechanical stability of the membrane suffers a drastic reduction. Moreover, high water content causes swelling of the membrane and promotes methanol crossover: methanol is transported through the membrane by means of diffusion and active transport with proton and water. This high methanol crossover reduces cell efficiency in various aspects: first, the methanol that crosses over is oxidized in the cathode, thus consuming extra energy; second, overall fuel efficiency is reduced because fuel that could have been separated into protons and carbon dioxide is wasted; finally, the catalyst on the cathode side is easily poisoned by carbon monoxide that sticks to the catalyst and inactivates it. Increasing temperature also promotes proton conductivity. However, over 80°C there is a risk of membrane dehydration which leads to a reduction in the proton conductivity and poor water management<sup>8</sup>. Therefore, it is important to achieve a balance of water in the electrolyte.

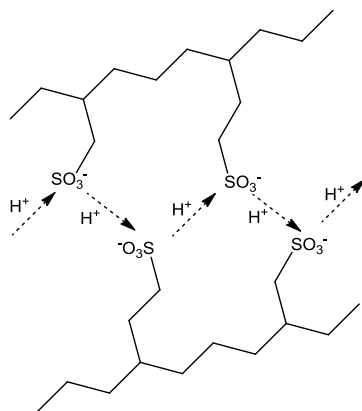


Figure 1.4. Schematic representation of the hopping (Grotthus) mechanism

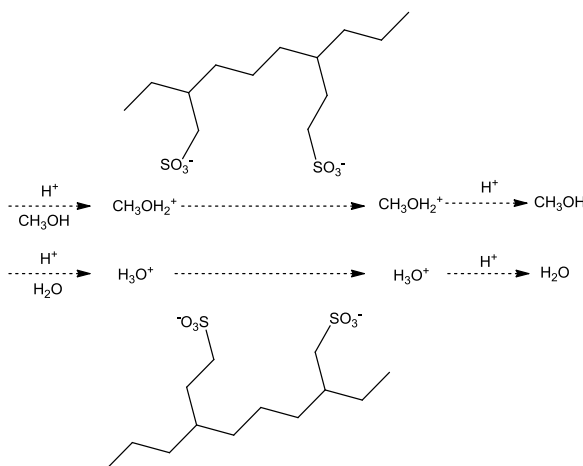
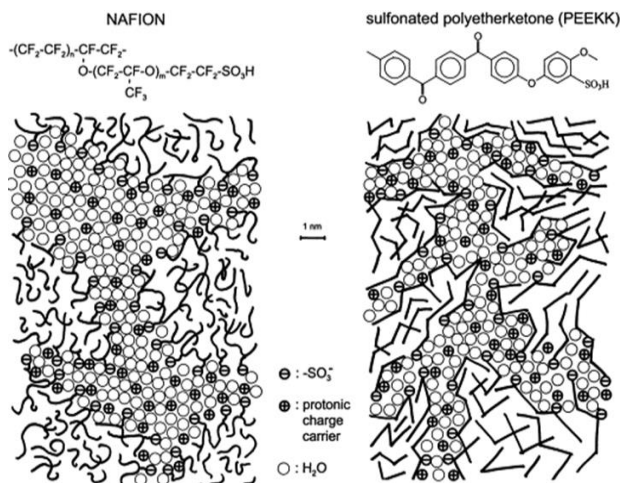


Figure 1.5. Schematic representation of the vehicular mechanism

Two different pathways exist to solve the problem of methanol cross-over, the first being the development of ion-conductive membranes based on alternative polymers or polymer composites, the second being the modification of the existing Nafion® membrane, in order to prevent cross-over.

Even though Nafion shows excellent performance in hydrogen fuel cells, its application to *DMFC* is more restricted due to its high methanol crossover<sup>9</sup>. The nature of the hydrophobic backbone and the hydrophilic groups play an

important role in the resulting microphase structure. If the chemical nature of the hydrophobic and hydrophilic segments is very different, the resulting material will have a highly phase separated structure. This will lead to a material with large hydrophilic domains which are separated from each other. This structure will probably limit the proton conductivity. On the other hand, if the hydrophilic and hydrophobic segments are more similar, the phase separation will be less pronounced. In this case, the resulting microstructure will consist of narrower ionic channels but also with more interfacial regions. Examples of these possible structures can be seen in **Figure 1.6**. It has been shown that the existence of narrower and highly interconnected ionic channels promotes the proton conductivity, and at the same time reduces the methanol permeability. Moreover, the use of narrower channels also reduces the water mobility, promoting Grotthuss mechanism instead of vehicular transport<sup>10</sup>. As a consequence, in recent years the search for new polymeric materials for application in DMFC has increased enormously to obtain polymer electrolyte membrane (PEM) with high proton conductivity and low methanol permeability.



**Figure 1.6. Phase separation in membranes : broader (left) and narrower (right) ionic channels for proton transport<sup>11</sup>**

The first strategy to improve the properties of commercial membranes is to modify Nafion or to prepare similar perfluorosulfonated acid (PFSA) polymer membranes.

The development of improved PFSA membranes has been carried out by addition of inorganic solid proton conductors (such as silica-phosphotungstic acid)<sup>12</sup>. Alternatively, sulfonated polymer membranes (hydrocarbon polymers) have been prepared as an attempt to obtain less expensive materials for low temperature PEM. In this case, the stability of the materials is a critical factor due to the introduction of tertiary carbon bonds in some of the polymer structures. For this reason, a wide range of different structures and compositions have been developed in an attempt to enhance mechanical and thermal stability, including crosslinked polymers<sup>13</sup> or the addition of inorganic fillers and plasticizers. Different strategies have been followed to obtain new hydrocarbon PEM exhibiting high proton conductivity and low methanol permeability. A set of ionic copolymers with sulfonate moieties in their structure have been prepared in the past, including random copolymers<sup>14-18</sup>, graft copolymers<sup>19,20</sup>, block copolymers<sup>21,22</sup>

Another strategy to obtain new materials for DMFC electrolytes is the preparation of blends of different polymers. Polymer blends can combine the good characteristics of two components. This may be an effective low cost method for the preparation of new materials<sup>23</sup>. An alternative strategy to enhance the mechanical and chemical stability and also to reduce methanol diffusion is to carry out chemical crosslinking between the blend components, thus creating 3D networks<sup>24</sup>. Crosslinked materials are easily prepared and the water contents and transport of proton and methanol can be adjusted by the crosslinking density. Some interesting results have been obtained for polyvinyl alcohol (PVA) crosslinked materials, in which different crosslinkers have been used, such as glutaraldehyde<sup>25</sup>. Some crosslinkers have sulfonic groups to enhance the proton conductivity of the membrane<sup>26,27</sup>. In this case, the studies have shown that there are two main factors affecting the transport of the solutes in the membranes. At low degrees of crosslinking, there is a considerable increase in the proton conductivity due to the presence of ionic conducting groups. However, at higher crosslinking densities the reduction of the free volume becomes limiting and the

water swellability is drastically reduced, leading to a decrease in the proton conductivity. For such systems, it is paramount to establish an equilibrium point between the number of sulfonic groups and the hydrophilicity. Another strategy to reduce crossover is to use composite membranes. Inorganic fillers act as blockers to methanol without causing a drastic drop in the proton conductivity. The incorporation of the inorganic phase also enhances thermal and mechanical stability<sup>28</sup>. Several membranes have been prepared containing, for example, silica, zirconium phosphate, phosphotungstic acid, molybdophosphoric acid, Aerosil (silicon dioxide), ORMOSILS (organically modified silicates), silane-based fillers, titanium oxide, hydroxyapatite, laponite, montmorillonite, zeolites and palladium<sup>9</sup>. A wide range of polymers have been used in this composites, such as Nafion<sup>29</sup>, PVA/phosphotungstic acid (PWA)<sup>30</sup>, and macroporous silica matrix<sup>31</sup>. Hybrid membranes also have some shortcomings, usually due to a poor water management and brittleness at high inorganic contents. Several groups have prepared coated membranes, for example, Nafion has been coated with *sulfonated poly(ether ether ketone)* (SPEEK)<sup>32</sup> and poly(propylene)-grafted-polystyrene sulfonic acid (PSSA)<sup>33</sup>.

In general terms, it is necessary to obtain well dispersed and interconnected ionic channels to ensure high proton conductivity. This implies that not only the chemical composition but also the resulting morphology of the membranes plays an important role in the cell performance<sup>34</sup>. Therefore it is vital to control the phase separation morphology in order to discriminate between the transport processes of protons, water and methanol through the membrane with the aim to optimize the use of PEM in DMFC.



## 1.4 Proton exchange membranes based on side chain liquid crystalline polymers (SCLCPs)

In biological systems, transport mainly occurs by means of three different mechanism: carriers, channels and doors. Among them, proteic channels are the most commonly used systems to transport ions through the membranes in the cells (**Figure 1.7**). However, although proteic channels are very effective in ion transport through a cell membrane, they are inadequate for technological applications, both because these proteins are too difficult to purify and because their structure is too complex to be chemically modified to get tailor-made systems. For this reason, the design, synthesis and study of supramolecular assemblies capable of transporting ions across membranes by the channel mechanism have been the subject of increasing interest. Various approaches dealing with polyether-based structures were tested, due to the weak coordinative capability of oxygen, which makes it particularly suitable for the transport of cations like sodium and potassium.

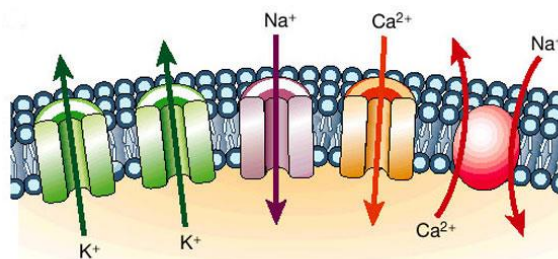


**Figure 1.7.** Ion transportation through the cell membrane

In the literature, the first reported synthetic strategy consisted of stacking of transmembrane, carriers: thus, for example, ion channels were formed by cylindrical packing of crown ether molecules<sup>35</sup> (**Figure 1.8**); however, this kind of molecular devices led to an unfavourable energy barrier associated with a discontinuous transport process.

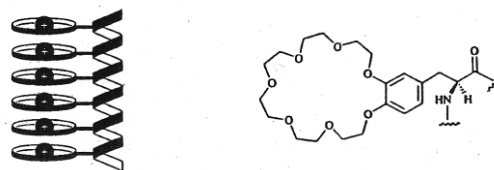


**Figure 1.8.** Ion channels formed by cylindrical packing of crown ether molecules<sup>36</sup>

A polyether helix structure should prevent this barrier as it implies a continuous transport process: therefore, it should be considered an effective way of obtaining ion channels. This possibility was explored in the second strategy to get channels, that is the use of systems having a tunnel geometry. In 1994, Koert and coworkers reported<sup>37</sup> the stereoselective synthesis of an oligo(tetrahydrofuran) (**Figure 1.9**) which tended to adopt a helical conformation, thus leading to a biomimetic ion channel: however, this example had a limited interest as the synthesis involved multiple and complex steps.

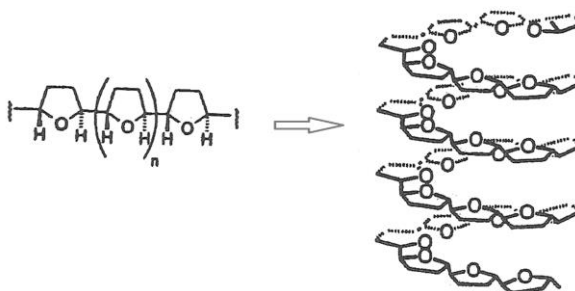


**Figure 1.9.** C<sub>2</sub>-symmetric tetrahydrofuran pentamer prepared in enantiomerically pure form by a convergent synthesis. Compounds of this type are of interest for the construction of synthetic ion channels from polyether helices<sup>37</sup>

On the other hand, the use of polyethers obtained by conventional ring-opening polymerization is not possible in principle, since polyethers generally tend to adopt a random-coil conformation. A way of forcing a polymer chain to adopt a helical conformation could be found by the aid of supramolecular

chemistry, that is the chemistry of the entities generated via inter- and intra-molecular non-covalent interactions. This approach considers the molecular recognition as a mean for controlling the evolution and the architecture of polymolecular species as they spontaneously build up from their components through self-organization and has very clear example in the nature, investigated by Klug in 1983, i.e. the self-assembling of the Tobacco Mosaic Virus (TMV)<sup>38</sup>. The TMV consists of 2130 units of a single type of protein molecule, which has a tapered shape, and a chain of ribonucleic acid. The TMV self-assembles upon mixing of its individual components, leading to a cylindrical structure in which the proteins organize in a regular helical array and force the RNA to adopt a helical conformation in the inner part of the structure (**Figure 1.10**).

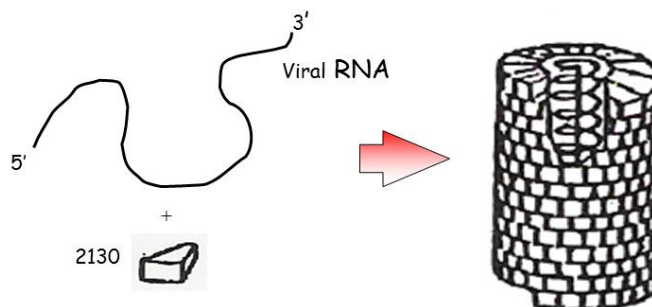


**Figure 1.10. Supramolecular self-assembly of TMV into a helical conformation**

The protein units act as exo-receptor, that is like molecules with a big surface of interaction, similar shape or dimension or complementary geometries; those characteristics can lead to the process of exo-recognition, which occurs through specific non-bonding interactions (such as hydrogen bonds, Van Der Waals forces, etc.) between surfaces. The main driving force for the self-assembly of TMV lies in the exo-recognition of the proteins, due to their tapered shape. Therefore it can be deduced that if tapered moieties are linked to a polyether chain, the exo-recognition and the consequent self-assembling of these groups would probably lead to a tubular supramolecular structure where the polymer chain, which lies in the inner part of the generated column, would be

forced to adopt a helical conformation. In this way a biomimetic ion channel could be built up.

The first examples of polymers containing tapered minidendritic side groups that self-assembled intramolecularly in cylindrical macromolecules, which subsequently self-organized in hexagonal columnar lattices, were discovered and reported by the group of Percec in 1991<sup>39</sup>. Since then, that group has been extensively investigating on the self-organization into liquid crystalline phases of supramolecular monodendrons, styrene- and methacrylate-based networks and poly(oxazolines), for the design of ion-active nanostructured supramolecular systems<sup>40,41</sup>. They synthesized and studied tapered minidendritic units containing crown-ethers or oligo(ethylene oxide) units at their core, leading to the development of ion-active systems;<sup>42</sup> they demonstrated the structure of these assemblies and reported enhanced conductivity along these ion-channels which were organized in a hexagonal columnar bidimensional lattice.<sup>43</sup> They also showed the dependence of the shape of the supramolecular architecture on the molecular taper angle and an increased ionic conductivity also in other liquid crystalline states.<sup>44</sup>

Very recently, two types of one-dimensional ion-conductive polymer films containing ion nanochannels were prepared (**Figure 1.11**), obtained by photopolymerization of aligned columnar liquid crystals of a fan-shaped imidazolium salt having acrylate groups at the periphery<sup>45</sup>. These films have been obtained by photopolymerization of aligned columnar liquid crystals of a fan-shaped imidazolium salt having acrylate groups at the periphery. In the columnar structure, the ionic part self-assembles into the inner part of the column. The column is oriented macroscopically in two directions by different methods: orientation perpendicular to the modified surfaces of glass and indium tin oxide with 3-(aminopropyl)triethoxysilane and orientation parallel to a glass surface by mechanical shearing. Ionic conductivities have been measured for the films with columnar orientation vertical and parallel to the surface. Anisotropic ionic conductivities are observed for the oriented films fixed by photopolymerization.

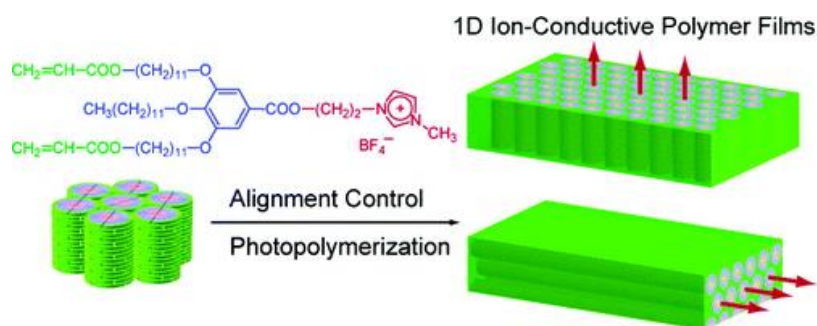


**Figure 1.11. One-dimensional ion-conductive polymer films containing ion nanochannels**<sup>45</sup>

The ionic conductivities parallel to the columnar axis are higher than those perpendicular to the columnar axis because the lipophilic part functions as an ion-insulating part. The film with the columns oriented vertically to the surface shows an anisotropy of ionic conductivities higher than that of the film with the columns aligned parallel to the surface.

Likewise, different research groups proposed synthetic biomimetic transport approaches, for instance, 'ion-transporting molecular cable' and 'proton-conductive materials formed by the self-organization' introduced by Bennin et al and Ueda et al respectively<sup>46,47</sup>.

## 1.5 Liquid Crystalline Side Chain Polymers

Liquid crystals (LCs) are soft materials that can spontaneously self-organize into ordered phase structures while retaining the fluid properties at the same time and the LCs which are obtained by melting a crystalline solid or by cooling from isotropic melt are called thermotropic. Liquid crystalline behavior is also found in certain colloidal solutions, such as aqueous solutions of tobacco mosaic virus and certain polymers. This class of liquid crystals is called lyotropic. For this class, concentration (and secondarily temperature) is the important controllable parameter, rather than temperature (and secondarily pressure) as in the thermotropic phase.

The essential requirement for a molecule to be a thermotropic LC is a structure consisting of a central rigid core (often aromatic), a flexible peripheral moiety (generally aliphatic groups) and strong dipoles and/or easily polarisable substituents (-CN, -COOH, etc). This structural requirement leads to two general classes of LCs:

1. Calamitic LCs, and
2. Discotic LCs

Liquid crystals consist of rod-shaped molecules are called as calamitic liquid crystals, while disc-shaped as discotic liquid crystals as shown in **Figure 1.12**.



**Figure 1.12. a) Calamitic (rod-like) liquid crystals b) Discotic (disc-like) liquid crystals**

Discotic liquid crystals can give rise to the several mesophases, depending on the level of order of the disk-like units. Discotic liquid crystal phases are classified into two main categories: discotic nematic mesophases ( $N_D$ ) and discotic columnar mesophases. The discotic nematic phase is the least ordered mesophase formed by disc-like molecules and is analogous to the nematic phase formed by rod-like molecules. It is characterized by possessing 1-dimensional long-range orientational and no long-range positional order. Discotic columnar mesophases are obtained when the disc-like molecules stack on top of each other. These phases have both long-range orientational and 2-dimensional positional order. General classification of these phases is shown in **Figure 1.13**.

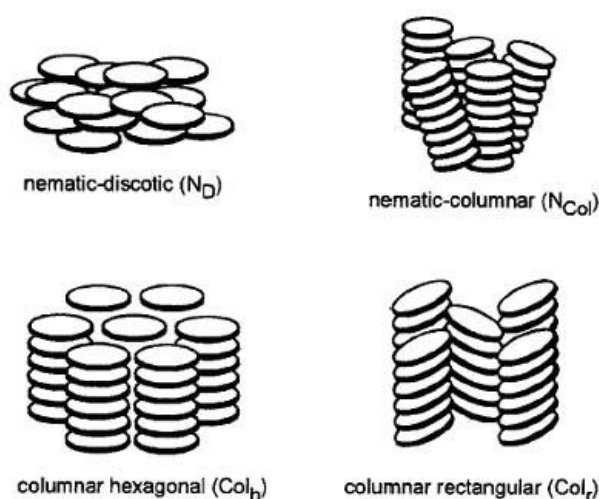


**Figure 1.13. Several mesophases shown by discotic liquid crystals.**

Columnar phases with long-range order are classified by their two-dimensional lattices as: hexagonal, rectangular, oblique and square phases. First of all, thermotropic columnar mesophases have been observed by S. Chandrasekhar in the year 1977<sup>48</sup>. In particular, synthetically, hexagonal columnar mesophases are formed by a variety of molecular structures;<sup>49</sup> for example, disk-shaped molecules such as hexaalkoxytriphenylenes show evidence of this type of arrangement (discotic hexagonal mesophase)<sup>50,51</sup>. The formation of columnar mesophases is not restricted to disk-shaped molecules

only, but also those molecules which due to specific noncovalent interactions form disk like aggregates which then act as mesogenic units<sup>52</sup>.

When LC meets polymers, the resulting liquid crystalline polymers (LCPs) show both anisotropic properties which originate from mesogenic units and good mechanical properties which come from long-chain structures. LCP are polymers containing mesogenic groups in either their backbone or their side chains. This difference leads to the so-called main-chain liquid crystalline polymers (MCLCP) and (SCLCP), respectively. Schematic representations of both sorts of LCP can be seen in **Figures 1.14 and 1.15**.

SCLCPs have been the subjects of intensive research during the last decades. Systematic investigation of the synthesis of SCLCPs began only after discovery of Finkelmann et al, that a flexible spacer should be inserted between the polymeric backbones and mesogenic side groups to decouple the motions of the backbone and side groups in the liquid-crystalline state<sup>53</sup>.



**Figure 1.14. Schematic representation of a main-chain liquid-crystalline polymer (MCLCP)**

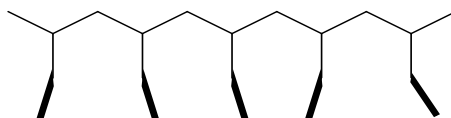


**Figure 1.15. Schematic representation of a side-chain liquid-crystal polymer (SCLCP)**

The SCLCPs studied in this thesis are showing columnar, rectangular columnar and hexagonal columnar mesophases depending on degree of modification. The columnar phase is a class of liquid-crystalline phases in which molecules assemble into cylindrical structures.



Traditionally, SCLCPs have been prepared by two different approaches: i) polymerization or copolymerization of monomers containing the desired mesogen, ii) chemical modification of a suitably functionalized non-mesogenic polymer with mesogenic reagents. In fact, these two approaches are complementary, since both of them show advantages and drawbacks. The polymerization or copolymerization approach allows, in many cases, the control of the monomer sequence, of the microstructure and of the molecular weight of the polymer by suitably choosing the initiator and polymerization conditions. As main drawbacks, it should be mentioned that often a very high purity of the monomers is required for an effective polymerization to take place and, that in many cases functional groups responsible of the mesogenic character are incompatible with the polymerization conditions. On the other hand, the chemical modification approach is attractive due to its apparent simplicity, but in most cases the reactions are not quantitative and, therefore, non-reacted groups and functionalities due to side-reactions are present in the final polymer, which can negatively affect its mesomorphic behaviour.

In the last decade, our group published several papers regarding the synthesis and characterization of some sets of side-chain liquid-crystalline polyethers which self-assemble into supramolecular columnar structures.<sup>54,55</sup> These polymers were prepared by reacting poly(epichlorohydrin) (PECH) with tapered mesogenic carboxylates. Different types of columnar mesophases were obtained depending on the tapered group introduced and the modification degree achieved. More recently, our group reported the preparation of membranes based on a side-chain liquid-crystalline polyether, obtained by chemically modifying PECH with a tapered group, which exhibited a columnar structure. The columns were successfully oriented, i.e. perpendicularly to the membrane surface, by taking advantage of surface interactions between the polymer and hydrophilic substrates, and the oriented membranes exhibited proton transport comparable to Nafion<sup>®</sup>N117 and no water uptake. On the other hand, poor proton transport could be detected on unoriented membranes based on the same liquid-crystalline polyether or on unmodified poly(epichlorohydrin). However, the procedure used to prepare the oriented membranes has limited reproducibility

and must therefore be improved in order to obtain, in all cases, membranes with a suitable degree of orientation.

## 1.6 References

1. Simader, G. R., *Fuel Cells and Their Applications*. John Wiley & Sons, Limited: 2005.
2. Aricò, A. S.; Srinivasan, S.; Antonucci, V., DMFCs: From Fundamental Aspects to Technology Development. *Fuel Cells* **2001**, 1 (2), 133-161.
3. Zhao, T. S.; Xu, C.; Chen, R.; Yang, W. W., Mass transport phenomena in direct methanol fuel cells. *Progress in Energy and Combustion Science* **2009**, 35 (3), 275-292.
4. Grot, W. G., Perfluorinated ion exchange polymers and their use in research and industry. *Macromolecular Symposia* **1994**, 82 (1), 161-172.
5. Mauritz, K. A.; Moore, R. B., State of Understanding of Nafion. *Chemical Reviews* **2004**, 104 (10), 4535-4586.
6. Kreuer, K.-D.; Rabenau, A.; Weppner, W., Vehicle Mechanism, A New Model for the Interpretation of the Conductivity of Fast Proton Conductors. *Angewandte Chemie International Edition in English* **1982**, 21 (3), 208-209.
7. Elabd, Y. A.; Napadensky, E.; Walker, C. W.; Winey, K. I., Transport Properties of Sulfonated Poly(styrene-*b*-isobutylene-*b*-styrene) Triblock Copolymers at High Ion-Exchange Capacities. *Macromolecules* **2005**, 39 (1), 399-407.
8. Yang, C.; Costamagna, P.; Srinivasan, S.; Benziger, J.; Bocarsly, A. B., Approaches and technical challenges to high temperature operation of proton exchange membrane fuel cells. *Journal of Power Sources* **2001**, 103 (1), 1-9.
9. Elmér, A. M.; Jannasch, P., Synthesis and characterization of poly(ethylene oxide-co-ethylene carbonate) macromonomers and their use in the preparation of crosslinked polymer electrolytes. *Journal of Polymer Science Part A: Polymer Chemistry* **2006**, 44 (7), 2195-2205.
10. Kreuer, K.-D., Proton Conductivity: Materials and Applications. *Chemistry of Materials* **1996**, 8 (3), 610-641.
11. Kreuer, K. D., On the development of proton conducting polymer membranes for hydrogen and methanol fuel cells. *Journal of Membrane Science* **2001**, 185 (1), 29-39.
12. Staiti, P.; Aricò, A. S.; Baglio, V.; Lufrano, F.; Passalacqua, E.; Antonucci, V., Hybrid Nafion-silica membranes doped with heteropolyacids for

application in direct methanol fuel cells. *Solid State Ionics* **2001**, *145* (1–4), 101-107.

13. Tanaka, R.; Yamamoto, H.; Shono, A.; Kubo, K.; Sakurai, M., Proton conducting behavior in non-crosslinked and crosslinked polyethylenimine with excess phosphoric acid. *Electrochimica Acta* **2000**, *45* (8–9), 1385-1389.

14. Carretta, N.; Tricoli, V.; Picchioni, F., Ionomeric membranes based on partially sulfonated poly(styrene): synthesis, proton conduction and methanol permeation. *Journal of Membrane Science* **2000**, *166* (2), 189-197.

15. Jung, B.; Kim, B.; Yang, J. M., Transport of methanol and protons through partially sulfonated polymer blend membranes for direct methanol fuel cell. *Journal of Membrane Science* **2004**, *245* (1–2), 61-69.

16. Gil, M.; Ji, X.; Li, X.; Na, H.; Eric Hampsey, J.; Lu, Y., Direct synthesis of sulfonated aromatic poly(ether ether ketone) proton exchange membranes for fuel cell applications. *Journal of Membrane Science* **2004**, *234* (1–2), 75-81.

17. Okamoto, K.-i.; Yin, Y.; Yamada, O.; Islam, M. N.; Honda, T.; Mishima, T.; Suto, Y.; Tanaka, K.; Kita, H., Methanol permeability and proton conductivity of sulfonated co-polyimide membranes. *Journal of Membrane Science* **2005**, *258* (1–2), 115-122.

18. Sumner, M. J.; Harrison, W. L.; Weyers, R. M.; Kim, Y. S.; McGrath, J. E.; Riffle, J. S.; Brink, A.; Brink, M. H., Novel proton conducting sulfonated poly(arylene ether) copolymers containing aromatic nitriles. *Journal of Membrane Science* **2004**, *239* (2), 199-211.

19. Hatanaka, T.; Hasegawa, N.; Kamiya, A.; Kawasumi, M.; Morimoto, Y.; Kawahara, K., Cell performances of direct methanol fuel cells with grafted membranes. *Fuel* **2002**, *81* (17), 2173-2176.

20. Shen, M.; Roy, S.; Kuhlmann, J. W.; Scott, K.; Lovell, K.; Horsfall, J. A., Grafted polymer electrolyte membrane for direct methanol fuel cells. *Journal of Membrane Science* **2005**, *251* (1–2), 121-130.

21. Kim, B.; Kim, J.; Jung, B., Morphology and transport properties of protons and methanol through partially sulfonated block copolymers. *Journal of Membrane Science* **2005**, *250* (1–2), 175-182.

22. Zhang, X.; Liu, S.; Liu, L.; Yin, J., Partially sulfonated poly(arylene ether sulfone)-b-polybutadiene for proton exchange membrane. *Polymer* **2005**, *46* (6), 1719-1723.

23. Manea, C.; Mulder, M., Characterization of polymer blends of polyethersulfone/sulfonated polysulfone and polyethersulfone/sulfonated polyetheretherketone for direct methanol fuel cell applications. *Journal of Membrane Science* **2002**, *206* (1–2), 443-453.
24. Qiao, J.; Hamaya, T.; Okada, T., New highly proton-conducting membrane poly(vinylpyrrolidone)(PVP) modified poly(vinyl alcohol)/2-acrylamido-2-methyl-1-propanesulfonic acid (PVA–PAMPS) for low temperature direct methanol fuel cells (DMFCs). *Polymer* **2005**, *46* (24), 10809-10816.
25. Shen, C.-C.; Joseph, J.; Lin, Y.-C.; Lin, S.-H.; Lin, C.-W.; Hwang, B. J., Modifying microphase separation of PVA based membranes for improving proton/methanol selectivity. *Desalination* **2008**, *233* (1–3), 82-87.
26. Rhim, J.-W.; Yeom, C.-K.; Kim, S.-W., Modification of poly(vinyl alcohol) membranes using sulfur-succinic acid and its application to pervaporation separation of water–alcohol mixtures. *Journal of Applied Polymer Science* **1998**, *68* (11), 1717-1723.
27. Yang, C.-C.; Chiu, S.-J.; Chien, W.-C., Development of alkaline direct methanol fuel cells based on crosslinked PVA polymer membranes. *Journal of Power Sources* **2006**, *162* (1), 21-29.
28. Chang, H. Y.; Lin, C. W., Proton conducting membranes based on PEG/SiO<sub>2</sub> nanocomposites for direct methanol fuel cells. *Journal of Membrane Science* **2003**, *218* (1–2), 295-306.
29. Xu, W.; Lu, T.; Liu, C.; Xing, W., Low methanol permeable composite Nafion/silica/PWA membranes for low temperature direct methanol fuel cells. *Electrochimica Acta* **2005**, *50* (16–17), 3280-3285.
30. Kim, D. S.; Park, H. B.; Rhim, J. W.; Lee, Y. M., Proton conductivity and methanol transport behavior of cross-linked PVA/PAA/silica hybrid membranes. *Solid State Ionics* **2005**, *176* (1–2), 117-126.
31. Munakata, H.; Yamamoto, D.; Kanamura, K., Properties of composite proton-conducting membranes prepared from three-dimensionally ordered macroporous polyimide matrix and polyelectrolyte. *Chemical Communications* **2005**, *0* (31), 3986-3988.
32. Ren, S.; Li, C.; Zhao, X.; Wu, Z.; Wang, S.; Sun, G.; Xin, Q.; Yang, X., Surface modification of sulfonated poly(ether ether ketone) membranes using

- Nafion solution for direct methanol fuel cells. *Journal of Membrane Science* **2005**, *247* (1–2), 59-63.
33. Sauk, J.; Byun, J.; Kang, Y.; Kim, H., Preparation of laminated composite membranes by impregnation of polypropylene with styrene in supercritical CO<sub>2</sub> for direct methanol fuel cells. *Korean J. Chem. Eng.* **2005**, *22* (4), 605-610.
34. Kreuer, K. D., On the development of proton conducting materials for technological applications. *Solid State Ionics* **1997**, *97* (1–4), 1-15.
35. Dulyea, L. M.; Fyles, T. M.; David Robertson, G., Coupled transport membranes incorporating a polymeric crown ether carboxylic acid. *Journal of Membrane Science* **1987**, *34* (1), 87-108.
36. Voyer, N., Preparation of supramolecular devices using peptide synthesis: design and synthesis of a tubular hexa-crown molecule. *Journal of the American Chemical Society* **1991**, *113* (5), 1818-1821.
37. Koert, U.; Stein, M.; Harms, K., A Convergent Synthesis of 2,5-trans-Linked Oligo (tetrahydrofuran): Potential Building Blocks for a Polyether Helix with Ion Channel Activity. *Angewandte Chemie International Edition in English* **1994**, *33* (11), 1180-1182.
38. Klug, A., From Macromolecules to Biological Assemblies (Nobel Lecture). *Angewandte Chemie International Edition in English* **1983**, *22* (8), 565-582.
39. Percec, V.; Heck, J., Liquid crystalline polymers containing mesogenic units based on half-disc and rod-like moieties. *Polymer Bulletin* **1991**, *25* (4), 431-438.
40. Percec, V.; Glodde, M.; Bera, T. K.; Miura, Y.; Shiyanovskaya, I.; Singer, K. D.; Balagurusamy, V. S. K.; Heiney, P. A.; Schnell, I.; Rapp, A.; Spiess, H. W.; Hudson, S. D.; Duan, H., Self-organization of supramolecular helical dendrimers into complex electronic materials. *Nature* **2002**, *417* (6905), 384-387.
41. Percec, V.; Ahn, C. H.; Ungar, G.; Yeardeley, D. J. P.; Moller, M.; Sheiko, S. S., Controlling polymer shape through the self-assembly of dendritic side-groups. *Nature* **1998**, *391* (6663), 161-164.
42. Percec, V.; Schlueter, D.; Ungar, G.; Cheng, S. Z. D.; Zhang, A., Hierarchical Control of Internal Superstructure, Diameter, and Stability of Supramolecular and Macromolecular Columns Generated from Tapered Monodendritic Building Blocks. *Macromolecules* **1998**, *31* (6), 1745-1762.

43. Percec, V.; Johansson, G.; Heck, J.; Ungarb, G.; Battyb, S. V., Molecular recognition directed self-assembly of supramolecular cylindrical channel-like architectures from 6,7,9,10,12,13,15,16-octahydro-1,4,7,10,13-pentaoxabenzocyclopentadecen-2-ylmethyl 3,4,5-tris(p-dodecyloxybenzyloxy)benzoate. *Journal of the Chemical Society, Perkin Transactions 1* **1993**, 0 (13), 1411-1420.
44. Percec, V.; Cho, W.-D.; Ungar, G.; Yeardley, D. J. P., Synthesis and Structural Analysis of Two Constitutional Isomeric Libraries of AB<sub>2</sub>-Based Monodendrons and Supramolecular Dendrimers. *Journal of the American Chemical Society* **2001**, 123 (7), 1302-1315.
45. Yoshio, M.; Kagata, T.; Hoshino, K.; Mukai, T.; Ohno, H.; Kato, T., One-Dimensional Ion-Conductive Polymer Films: Alignment and Fixation of Ionic Channels Formed by Self-Organization of Polymerizable Columnar Liquid Crystals. *Journal of the American Chemical Society* **2006**, 128 (16), 5570-5577.
46. Beginn, U.; Zipp, G.; Möller, M., Functional Membranes Containing Ion-Selective Matrix-Fixed Supramolecular Channels. *Advanced Materials* **2000**, 12 (7), 510-513.
47. Ueda, S.; Kagimoto, J.; Ichikawa, T.; Kato, T.; Ohno, H., Anisotropic Proton-Conductive Materials Formed by the Self-Organization of Phosphonium-Type Zwitterions. *Advanced Materials* **2011**, 23 (27), 3071-3074.
48. Chandrasekhar, S.; Sadashiva, B. K.; Suresh, K. A., Liquid crystals of disc-like molecules. *Pramana - J Phys* **1977**, 9 (5), 471-480.
49. Ungar, G., Thermotropic hexagonal phases in polymers: common features and classification. *Polymer* **1993**, 34 (10), 2050-2059.
50. Bauer, S.; Plesnivý, T.; Ringsdorf, H.; Schuhmacher, P., Molecular engineering of discotic liquid crystals. *Makromolekulare Chemie. Macromolecular Symposia* **1992**, 64 (1), 19-32.
51. Chandrasekhar, S., Discotic liquid crystals. A brief review. *Liquid Crystals* **1993**, 14 (1), 3-14.
52. Brienne, M.-J.; Gabard, J.; Lehn, J.-M.; Stibor, I., Macroscopic expression of molecular recognition. Supramolecular liquid crystalline phases induced by association of complementary heterocyclic components. *Journal of the Chemical Society, Chemical Communications* **1989**, 0 (24), 1868-1870.

53. Finkelmann, H.; Ringsdorf, H.; Siol, W.; Wendorff, J. H., Synthesis of cholesteric liquid crystalline polymers. Polyreactions in ordered systems, 15. *Die Makromolekulare Chemie* **1978**, *179* (3), 829-832.
54. Ronda, J. C.; Reina, J. A.; Cádiz, V.; Giamberini, M.; Nicolais, L., Self-organized liquid-crystalline polyethers obtained by grafting tapered mesogenic groups onto poly(epichlorohydrin): Toward biomimetic ion channels. *Journal of Polymer Science Part A: Polymer Chemistry* **2003**, *41* (19), 2918-2929.
55. Ronda, J. C.; Reina, J. A.; Giamberini, M., Self-organized liquid-crystalline polyethers obtained by grafting tapered mesogenic groups onto poly(epichlorohydrin): Toward biomimetic ion channels 2. *Journal of Polymer Science Part A: Polymer Chemistry* **2004**, *42* (2), 326-340.



## **1.7 General objectives of the thesis**

The objectives of this thesis can be summarized as follows.

1. The preparation of polyethers with tapered side-groups leading to supramolecular columnar mesophases; in such structures, the polymer backbone is expected to form a helical structure which gives rise to a channel in the inner part of each column. The presence of basic oxygen atoms in the inner helical backbone is expected to confer to these materials the ability to transport proton ions by the channel mechanism.
2. The selection of the suitable techniques for membrane preparation in order to obtain the proper orientation of the transmembrane channels, i.e. perpendicular to the membrane surface, for the channel mechanism to be the main responsible for the proton transport.
3. The assessment of the membranes which are successfully homeotropically oriented to check proton transport by means of conductivity.

## *Chapter 2*

---

### *Side-Chain Liquid Crystalline Polymers Based On Chemical Modification Of Commercial Polyethers*

UNIVERSITAT ROVIRA I VIRGILI

PROTON-EXCHANGE BIOMIMETIC MEMBRANES BASED ON COLUMNAR SIDE-CHAIN LIQUID-CRYSTALLINE POLYETHERS

Suryakant Bhosale

Dipòsit Legal: T.188-2014

## 2.1 Introductions

Since the first introduction of side-chain liquid-crystal polymers (SCLCPs) by Finkelmann et al.<sup>1</sup>, SCLCPs continue to be the focus of much research interest. The main reason is that SCLCPs can combine the unique properties of low-molar mass liquid crystals and polymers together, which made it easier to form films during material processing. The side-chain liquid crystalline properties depend on the polymer chemical structure (the nature of the polymer backbone, the flexibility and length of spacer group, and the mesogenic unit), molar mass, polydispersity, and tacticity. The spacer connecting the mesogenic unit to polymer backbone is regarded as an important constituent, in order to decouple the motion of backbone component from the arrangement of the mesogenic side chains. Because of the complexity of the system, it is difficult to determine the effect of individual variables on liquid crystalline behaviour. Until now, there have been several systematic investigations into the correlation between the above-mentioned variables and liquid crystalline behaviour<sup>2,3</sup>. For conventional side-chain liquid crystalline polymers, mesogenic units based on homologs of low molecular weight liquid crystals were attached to polymer backbones as pendant groups through flexible aliphatic spacers using covalent bonding. The most frequently used polymers in this research area have been polyacrylate<sup>4,5</sup>, poly(methyl acrylate)<sup>6</sup> and polystyrene<sup>7</sup>. Percec and coworkers<sup>8</sup> have comprehensively investigated the self-organization of supramolecular monodendrons and styrene-, methacrylate or oxazoline-based polymers for the design of ion-active nanostructured supramolecular systems.

There has been only limited research on the polyepichlorohydrin-based SCLCPs polymers<sup>9,10</sup>. Of the commercially available polymers, homopolymer poly(epichlorohydrin) (PECH) and its copolymer with ethylene oxide, poly(epichlorohydrin-co-ethylene oxide) P(ECH-co-EO) are very interesting because of the presence of a chlorine atom that can be substituted by nucleophiles and also a flexible backbone. The fact that the chlorine atom is not directly attached to the main chain makes nucleophilic substitution easier and stereochemical preferences observed in polymers such as PVC<sup>11</sup> can be avoided. Several authors have described the modification reaction of PECH with

a large number of nucleophiles such as carbazole<sup>12</sup>, azides<sup>13</sup>, and phenolates<sup>9</sup> under phase transfer catalyst conditions. Polymer modification in the broadest sense means organic chemistry with macromolecular substrates. The reactions may take place either at the chain ends, on pendant functional groups or on functional groups along the main chain. Chemical modification of PECH, which has pendant chloromethyl group, has already been considered from the point of view of the synthesis of functional polymers and their applications, using phase-transfer catalysis conditions<sup>12,13</sup>. Likewise, recently, few examples of liquid crystalline polyethers based on modification of PECH have been reported in our research group<sup>14-16</sup>.

In this chapter we have studied the synthesis and the characterization of a series of PECH- as well as P(ECH-co-EO)-based side chain liquid crystalline polymers prepared by nucleophilic substitution with bulky tapered group potassium 3,4,5-tris[4-(*n*-dodecan-1-yloxy)benzyloxy]benzoate and their thermotropic properties depending on different degrees of modifications. An overview of the results contained in this chapter is given below:

1) Improvement of mesogenic group synthesis

SCLCPs based on chemical modification of polyethers are supposed to be obtained by using the bulky tapered group, potassium 3,4,5-tris[4-(*n*-dodecan-1-yloxy)benzyloxy]benzoate which includes 5 steps of synthesis. We modified this synthesis so that the tapered group was obtained in 4 steps instead of 5 steps. It makes work easier than the previous synthesis strategy with improved product yield.

2) Improvement of PECH modification

Compared to previous report<sup>15</sup>, where the highest obtained value of degree of modification of PECH was 58%, which was an apparent modification plateau, we modified PECH by using more concentrated polymer solution, increasing the amount of tapered group and temperature of the reaction, which allowed to reach a new plateau of degree of modification, equal to 80%.

3) Modification of P(ECH-co-EO)

A new family of liquid crystalline columnar polyethers was obtained by modification of P(ECH-co-EO) with the same dendron potassium 3,4,5-tris[4-(*n*-dodecan-1-yloxy)benzyloxy]benzoate. A modification plateau of 69% was achieved. Further investigation confirmed stable columnar mesophases with average number per unit cell ranging from 5 to 6. This piece of work of this chapter is contained in an article which was published in *Polymer Engineering and Science*<sup>17</sup>.

## 2.2 Experimental

### 2.2.1 Materials

All organic and inorganic reagents were supplied by Fluka or Aldrich and used as received. Tetrahydrofuran (THF) was freshly distilled from sodium benzophenone ketyl under argon. Polyethers, PECH of weight-average molecular weight ( $M_w$ )  $8.52 \times 10^5$  and number-average molecular weight ( $M_n$ )  $3.2 \times 10^5$  and, P(ECH-co-EO) with PECH/PEO 1:1  $M_w$   $5.01 \times 10^5$  and  $M_n$   $1.08 \times 10^5$ , were used for the modification.

### 2.2.2 Synthesis of Dendritic mesogenic groups

4-(*n*-Dodecan-1-yloxy)benzyl chloride was prepared by following a reported procedure<sup>18</sup>, while as shown in **Scheme 2.1** (Results and discussion part), potassium carboxylate, Potassium 3,4,5-Tris[4-(*n*-dodecan-1-yloxy)benzyloxy]benzoate (**3**) was prepared from methyl 3,4,5-Tris[4-(*n*-dodecan-1-yloxy)benzyloxy]benzoate (**1**) as described elsewhere.<sup>15</sup> The reported procedure was slightly modified, in order to convert **1** directly to **3**, instead of converting it before to 3,4,5-Tris[4-(*n*-dodecan-1-yloxy)benzyloxy]benzoic acid (**2**), as follows: a solution of 6 N KOH in C<sub>2</sub>H<sub>5</sub>OH (34.3 g KOH in 102 mL ethyl alcohol) was added to **1** (10.2 g, 0.01 mol) in a 500 mL round bottom flask. The reaction mixture was heated to 100 °C on oil bath. After one hour, the reaction mixture was poured into ice cold water (500 mL). A yellow solid material was filtered and vacuum dried at room temperature. It was recrystallized twice from hot absolute ethanol with active charcoal to yield a light yellow solid (Yield 90%). Its structure was confirmed by <sup>1</sup>H and <sup>13</sup>C NMR spectroscopy.

### 2.2.3 PECH Modification

In a 125-mL Schlenk flask under argon, 1 g (0.01 mol) of PECH was dissolved in anhydrous THF (100 mL) by stirring overnight at room temperature. Over the resulting viscous solution, the necessary amounts of **3** and Tetrabutylammonium bromide (TBAB) were added, in this order, with inert

atmospheric techniques. The mixture was heated at 65 °C, and magnetically stirred for 8 days. The reaction mixture was then diluted with hot THF to reach a total volume of 200 mL, and the solution was precipitated into 1 L of warm water. The copolymer obtained was dissolved in hot THF and precipitated again in boiling 96% ethanol twice (400 mL per gram of polymer). After the second precipitation, the rubbery polymer mass was collected and dried at 55 °C under vacuum for 48 h. **Table 2.1** (Results and discussion part) shows the experimental details, reaction conditions, and the yield and degree of modification for the various experiments.

#### 2.2.4 P(ECH-co-EO) modification

0.5 g (0.0036 mol) of P(ECH-co-EO) were dissolved in a 125 mL round bottom flask under argon in freshly prepared dried THF (60 mL) by stirring overnight at room temperature. A viscous solution was obtained. The necessary amounts of potassium carboxylate and TBAB were added under Argon atmosphere, with inert atmospheric techniques. The reaction mixture was heated under magnetic stirring at the desired temperature. It was heated to 65 °C in THF, and in case of N-methyl-2-pyrrolidone (NMP), it was heated to 80 °C. In experiment **CP3**, THF/DMF were used in equal ratio and heated to 80 °C. After 8 days, the reaction mixture was poured into 500 mL approximately ice cold water. The modified copolymer obtained after filtration was re-dissolved in 125 mL of hot THF and precipitated again in 96% ethanol twice (about 400 mL per gram of copolymer). After the second precipitation, the rubbery modified copolymer was collected by filtration and dried at 55 °C under vacuum for 48 hours. **Table 2.2** (Results and discussion part) shows the experimental conditions, the yield and degree of modification for the various experiments.



### 2.3 Characterization and measurements

Elemental analyses were carried out on a Carlo Erba EA1106 device. The chlorine content was determined with Schöninger's method, which involves the combustion of the sample in a platinum closed vessel and the potentiometric measurement of the HCl evolved.

Average molecular weights were determined in THF by Size exclusion chromatography (SEC); analyses were carried out with an Agilent 1200 series system with PLgel 3  $\mu\text{m}$  MIXED-E, PLgel 5  $\mu\text{m}$  MIXED-D and PLgel 20  $\mu\text{m}$  MIXED-A columns in series, and equipped with an Agilent 1100 series refractive-index detector. Calibration curves were based on polystyrene standards having low polydispersities. THF was used as an eluent at a flow rate of 1.0 mL/min, the sample concentrations were 5-10 mg/mL, and injection volumes of 100  $\mu\text{L}$  were used.

$^1\text{H}$  NMR and  $^{13}\text{C}$  NMR spectra were recorded at 400 and 100.4 MHz, respectively, on a Varian Gemini 400 spectrometer with proton noise decoupling for  $^{13}\text{C}$  NMR. The  $^{13}\text{C}$  NMR spectra of the polymers were recorded at 30  $^{\circ}\text{C}$ , with a flip angle of 45 $^{\circ}$ , and the number of transients ranged from 20,000 to 40,000 with 10–20% (w/v) sample solutions in  $\text{CDCl}_3$ . The central peak of  $\text{CDCl}_3$  was taken as the reference, and the chemical shifts were given in parts per million from TMS with the appropriate shift conversions.

HR-MAS on P(ECH-co-EO) spectra were recorded on a Bruker Avance III 500 Spectrometer operating at a proton frequency of 500.13 MHz. The instrument was equipped with a 4-mm triple resonance ( $^1\text{H}$ ,  $^{13}\text{C}$ ,  $^{31}\text{P}$ ) gradient HR-MAS probe. A Bruker Cooling Unit (BCU-Xtreme) was used to keep the sample temperature at 293 K or 323 K. Samples conveniently prepared with  $\text{CDCl}_3$  were spun at 6 kHz in order to keep the rotation sidebands out of the spectral region of interest. One-dimensional (1D)  $^{13}\text{C}$  spectra were acquired using power gate decoupling (zgpg Bruker® pulse program) and inverse gate decoupling (zg0ig Bruker® pulse program) with 4096 scans. The spectral width of 250 ppm was acquired in 64 K points at different temperatures (293 K or 323

K). These sets up parameters for  $^{13}\text{C}$  were used for longitudinal relaxation ( $T_1$ ) calculation experiments. For  $T_1$  calculation, a relaxation time of 8 seconds (d1) was left between scans and an inversion recovery experiment (t1irpg Bruker® pulse) was performed sampling points at 0.0125, 0.05, 0.1, 0.15, 0.2, 0.3, 0.4, 0.5, 0.6, 0.7, 0.9, 1.2, 2.4 and 4.8 s. The following equation was used for curves fitting the magnetization recovery <sup>19</sup> :

$$\ln(M_0 - M(\tau)) = \ln 2 + \ln M_0 - \tau / T_1 \quad (2.1)$$

where  $\tau$  is the decay time of the experiment and  $M(\tau) = -M_0$  at  $\tau = 0$

If relaxation was due to a single component, then experimental data resulted in a straight line; if this was not the case, multi-component analysis by computer-aided non-linear least squares method had to be performed.

Densities were determined by gas pycnometry using Micrometric AccuPyc 1330 machine at 30 °C.

Thermal transitions were detected with a Mettler-Toledo differential scanning calorimeter mod. 822 in dynamic mode at a heating or cooling rate of 10 °C/min. Nitrogen was used as the purge gas. The calorimeter was calibrated with an indium standard (heat flow calibration) and an indium-lead-zinc standard (temperature calibration).

Clearing temperature were roughly estimated using polarized optical microscopy (POM); textures of the samples were observed with an Axiolab Zeiss optical microscope equipped with a Linkam TP92 hot stage.

For X-ray experiments, the polymers were mechanically oriented by shearing below clearing temperature on a glass plate. Measurements were made using a Bruker-AXS D8-Discover diffractometer equipped with parallel incident beam (Göbel mirror), vertical  $\theta$ - $\theta$  goniometer, XYZ motorized stage. The GADDS detector was a HI-STAR (multiwire proportional counter of 30 x 30 cm with a 1024 x 1024 pixel). Samples were placed directly on the sample holder for transmission mode. An X-ray collimator system allowed to analyze areas of 100  $\mu\text{m}$  and 500  $\mu\text{m}$ . The X-ray diffractometer was operated at 40 kV and 40 mA to generate  $\text{CuK}_\alpha$  radiation. The GADDS detector was 30x30 cm with a 1024 x

1024 pixel CCD sensor placed at 30 and 9 cm from the sample. Two analytical conditions were used to measure the sample.

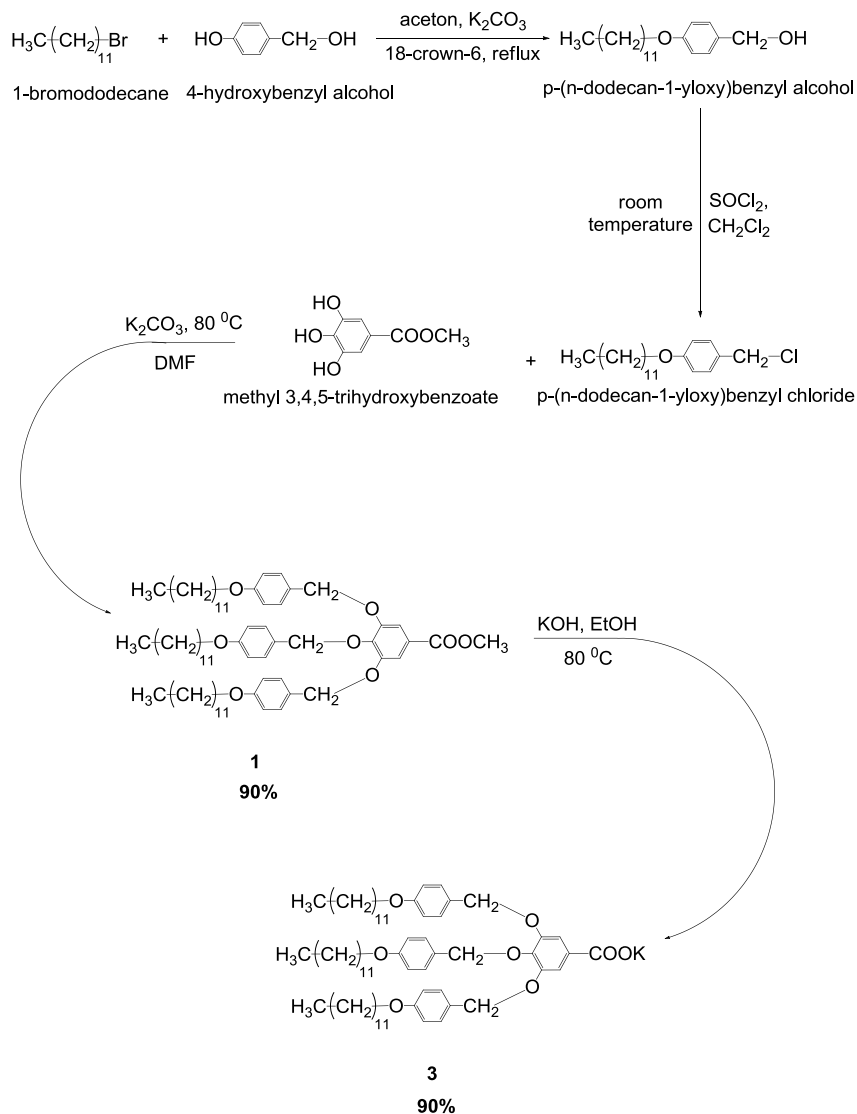
For low  $2\theta$  range: collimator, 100  $\mu\text{m}$ ; distance sample-detector, 30 cm. The collected *frame* (2D XRD pattern) covers a range from 0.9 up to 9.2 $^\circ$   $2\theta$ . The diffracted X-ray beam travelled through a He filled chamber (SAXS attachment) to reduce the air scattering at low angles. The direct X-ray beam was stopped by a beam stop placed directly on the detector face. The exposition time was of 1800s per frame and it was first chi-integrated to generate the conventional  $2\theta$  vs. intensity diffractogram and after it was 2theta-integrated to generate a Chi vs. intensity diffractogram.

Medium  $2\theta$  range: collimator, 500  $\mu\text{m}$ ; distance sample-detector, 9 cm. The collected *frame* (2D XRD pattern) covers a range from 3.0 up to 25.5 $^\circ$   $2\theta$ . The direct X-ray beam is stopped by a beam stop placed behind the sample with an aperture of 4 $^\circ$ . The exposition time was of 300s per frame and it was first chi-integrated to generate the conventional  $2\theta$  vs. intensity diffractogram and after it was 2theta-integrated to generate a Chi vs. intensity diffractogram.

## 2.4 Results and discussion

### 2.4.1 Synthesis of Potassium-3,4,5-tris[4-(*n*-dodecan-1-yloxy)benzyloxy] benzoate

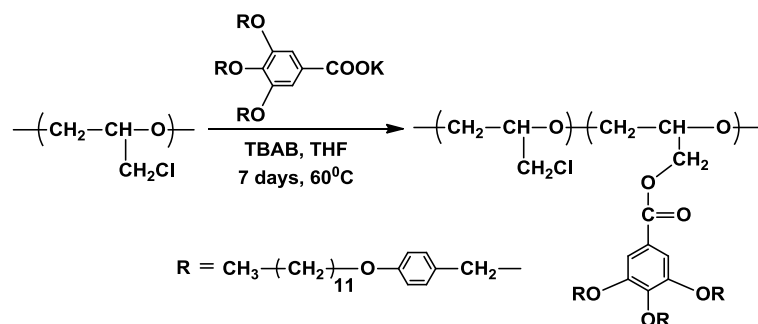
The *p*-(*n*-dodecan-1-yloxy)benzyl alcohol was obtained by refluxing a solution of 4-hydroxybenzyl alcohol, 1-bromododecane, anhydrous potassium carbonate and catalytic amount of 18-crown-6 ether in acetone under argon for 24 hours<sup>15</sup>. Further *p*-(*n*-dodecan-1-yloxy)benzyl alcohol converted into 4-(*n*-Dodecan-1-yloxy)benzyl chloride by reacting with thionyl chloride in dichloromethane at room temperature. In order to obtain **1**, 4-(*n*-Dodecan-1-yloxy)benzyl chloride allowed to react with methyl 3,4,5-hydroxy benzoate. Subsequently, **3** was prepared from **1** as shown in **Scheme 2.1** by converting **1** directly into **3** instead of **2** by reaction with ethanolic KOH which led to minimize one step of synthesis. As compared to previous report<sup>15</sup>, it improved the yield of the product to 90% as well.



**Scheme 2.1. Synthetic path for potassium 3,4,5-tris[4-(n-dodecan-1-yloxy)benzyloxy]benzoate)**

## 2.4.2 Modification of PECH

The SCLCPs were obtained via PECH modification by a bulky tapered group potassium 3,4,5-tris[4-(*n*-dodecan-1-yloxy)benzyloxy]benzoate in order to get the hexagonal columnar mesophases. Anhydrous THF as a solvent, stoichiometric amounts of TBAB, reaction duration of 8 days and 65 °C were selected in all cases. Compared to previous report<sup>15</sup>, in order to obtain higher degree of modification, we increased concentration of PECH solution from 0.083 M to 0.1 M while, amount of tapered group increased by 4 times. Moreover, temperature was increased from 60 to 65 °C as a limiting temperature to avoid unnecessary dehydrochlorination reaction. As per previous report<sup>15</sup>, the bimolecular substitution of the chlorine atom in PECH with the appropriate tapered potassium carboxylate should give the desired polymer with no substantial modification in either the backbone size or the polymer structure (Scheme 2.2).



**Scheme 2.2. Synthetic path for chemical modification of PECH**

**Table 2.1** summarizes the OCH<sub>2</sub>Cl/Nu ratio used and the modification degree and polymer yield obtained in these experiments. Yields were calculated on the basis of the polymer recovery, expected theoretical mass and average degree of modification estimated by <sup>1</sup>H.

**Table 2.1** The modification degree and yield obtained in the modification of PECH

Sample	PECH/ RCOOK <sup>a</sup>	PECH (mol)	Solvent	Time (days)	Modification (%) <sup>b</sup>	Yield (%) <sup>c</sup>
HP1	1:0.8	0.01	THF	8	44	90
HP2	1:1.0	0.01	THF	8	63	89
HP3	1:1.2	0.01	THF	8	80	85

<sup>a</sup> Stoichiometric amounts of TBAB used in each case.

<sup>b</sup> Average value determined by <sup>1</sup>H NMR.

<sup>c</sup> Calculated from average degree of modification

These results have shown better reproducibility of the synthesis with significant increase in degree of modification on increasing amount of potassium carboxylate. As compared to published report<sup>15</sup>, in case of sample **HP3**, we found increased degree of modification of 80%, estimated by <sup>1</sup>H NMR and. Consequently, we have established an improved plateau of degree of modification, which is 80%.

The structure and composition of the modified PECH were characterized by NMR spectroscopy and confirmed by comparing with published report<sup>15</sup>. Neither <sup>1</sup>H NMR nor <sup>13</sup>C NMR spectra showed detectable amounts of any of the signals corresponding to unsaturated vinyl ether units,<sup>20</sup> indicating that the dehydrohalogenation reaction does not take place under given experimental conditions.

The materials were mesomorphically characterized on the basis of DSC, polarized optical microscopy, and X-ray diffractogram experiments. **Table 2.2** lists the glass transition, clearing temperatures and densities which increase with the degree of modification.

**Table 2.2. Clearing temperatures and densities of the modified PECH**

Sample	Modification (%)	$T_g$ (°C) <sup>a</sup>	$T_c$ (°C) <sup>a</sup>	$\rho$ (g/cm <sup>3</sup> ) <sup>b</sup>
HP1	44	-25	85	1.20
HP2	63	-23	116	1.72
HP3	80	-20	142	1.81

<sup>a</sup> Determined by DSC from the second heating scan.

<sup>b</sup> Determined at 30°C. Error: ± 3%

POM and XRD investigations confirmed that HP1-HP3 exhibit hexagonal columnar mesophase (Col<sub>h</sub>), as expected on the basis of previously published report<sup>15</sup>. Table 2.3 shows the results of X-ray diffraction experiments performed at room temperature on the samples oriented by shearing in the rubbery state.

**Table 2.3. X-ray patterns of samples oriented at room temperature**

Sample	Modification (%)	$d_{100}$ <sup>a</sup> (Å)	$d_{001}$ <sup>b</sup> (Å)	$a$ <sup>c</sup> (Å)	Mesophase <sup>d</sup>
HP1	44	41.4	4.5	47	Col <sub>h</sub>
HP2	63	41.0	4.5	47	Col <sub>h</sub>
HP3	80	42.3	4.4	49	Col <sub>h</sub>

<sup>a,b</sup> Experimental planes spacings

<sup>c</sup> Dimension of the hexagonal unit cell

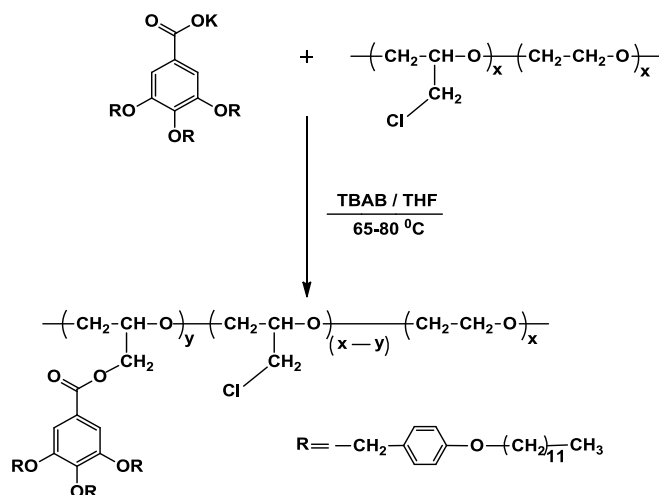
<sup>d</sup> Col<sub>h</sub>: hexagonal columnar

As given in previous report<sup>15</sup>, also in this case, the XRD patterns showed three sharp reflection at low 2θ, and centered broad diffuse halo. This diffractogram is compatible with a columnar mesophase, the lower spacing corresponding to the planar distance between disks and the higher one corresponding to the lateral distance between columns. The former 2θ value corresponded to the  $d_{100}$  plane of a columnar phase and allowed to calculate the dimensions of the unit cell, while the latter corresponded to  $d_{001}$  plane and could be referred to the distance between dendrons<sup>15</sup>.



### 2.4.3 Modification of P(ECH-co-EO)

This section deals with the copolyether, P(ECH-co-EO) modified with the dendron potassium 3,4,5-tris[4-(*n*-dodecan-1-yloxy)benzyloxy]benzoate. Also in this case, the formation of hexagonal columnar mesophases could be induced (Scheme 2.3).



**Scheme 2.3. Synthetic path for chemical modification of P(ECHco-EO)**

Since we obtained good modification degrees and detected no dehydrochlorination side reactions in the chemical modification of PECH, we were encouraged to use the same strategy and reaction conditions for chemically modifying P(ECH-co-EO). The given reactions were performed for 8 days in different solvents like THF, THF/DMF and NMP. As previously stated, the temperature ranged from 65 °C to 80 °C, depending on the solvent. These conditions were selected on the basis of our previous experience, various substrates and nucleophiles, as they gave high and almost quantitative modification degrees<sup>21</sup>. In this way, the P(ECH-co-EO) solutions in different solvents were heated with different ratios of potassium carboxylate in the presence of a stoichiometric amount of TBAB. **Table 2.4** summarizes the

OCH<sub>2</sub>Cl/Nu ratio used, the modification degrees and polymer yields obtained in these experiments.

**Table 2.4. The modification degree and copolymer yield obtained in the modification of P(ECH-co-EO)**

Sample	RCOOK <sup>a</sup> (mmol)	P(ECH- co-EO)/ COOK	Solvent	Time (days)	Modification (%) <sup>b</sup>	Modification (%) <sup>c</sup>	Yield (%) <sup>d</sup>
CP1	5.4	1:1.0	THF	8	67	69	83
CP2	7.3	1:1.2	THF	8	58	59	88
CP3	3.6	1:1.2	THF/DMF	8	64	65	85
CP4	3.6	1:1.2	NMP	8	60	62	87
CP5	5.4	1:1.5	THF	8	56	57	82

<sup>a</sup> Stoichiometric amounts of TBAB referred to chlorine were used in each case.

<sup>b</sup> Average value determined by <sup>1</sup>H NMR.

<sup>c</sup> Determined by chlorine elemental analysis.

<sup>d</sup> Calculated from the average degree of modification.

In this case, the modification degree could not be further improved by increasing the nucleophile/CH<sub>2</sub>Cl ratio beyond the stoichiometric (see comparison of experiments CP1, CP2 and CP5). Neither, we could get higher modification degrees by increasing solvent polarity (compare experiments CP2, CP3 and CP4). In this case, the modification degree reached a plateau value around 69%. This plateau seems to be related to a progressive compaction of the conformational coil which is induced by the gradual displacement of chlorine: this would finally lead to a decrease in the percentage of accessible reactive sites

22

Average molecular weights were determined in THF on a SEC system with polystyrene as a reference sample. All values of molecular weights and polydispersity are reported in **Table 2.5**. One could expect an increasing trend of the molecular weight with modification degree, since considerably heavy dendritic groups were introduced: however, one should keep in mind that molecular weight values are obtained under the assumption that the copolymer behaves like polystyrene in THF. The introduction of dendrons into the P(ECH-co-EO) is expected to greatly modify the hydrodynamic volume of the system. For this reason, it is not easy to predict a trend of the molecular weight with the modification degree, since the introduction of the dendritic groups can lead to

significant changes in the hydrodynamic volume with respect to the starting polymer. Density values of modified polymers (**Table 2.5**) greatly decrease with respect to the starting P(ECH-co-EO), that suggests a considerable change in polymer conformation after modification.

**Table 2.5. Molecular weight and densities of the synthesized copolymers**

Polymer	Modification (%) <sup>b</sup>	$M_n \cdot 10^{-4c}$	$M_w \cdot 10^{-5c}$	$M_w / M_n^c$	$\rho(\text{g/cm}^3)^d$
CP1	69	15.40	7.00	4.55	1.053
CP2	59	9.70	3.85	3.97	1.058
CP3	65	5.59	2.33	4.17	1.074
CP4	62	5.88	2.02	3.44	1.057
CP5	57	5.67	2.03	4.16	1.059
P(ECH-co-EO) <sup>a</sup>	—	10.80	5.01	4.61	1.308

<sup>a</sup> Starting copolymer.

<sup>b</sup> Determined by chlorine elemental analysis.

<sup>c</sup> Determined by SEC.

<sup>d</sup> Determined at 30<sup>o</sup>C. Error:  $\pm$  3%

The structure and composition of the copolymer were characterized by NMR spectroscopy. **Figure 2.1** reports the <sup>1</sup>H NMR spectrum of CP1 copolymer as an example. All <sup>1</sup>H NMR spectra are characterized by broad signals in three regions. The aromatic region shows three partially overlapped signals at 7.20, 6.75, and 6.62 ppm. Considering the relative integration areas and by comparison with the spectrum of methyl 3,4,5-tris(*n*-dodecan-1-yloxy)benzoate, the signal at 7.20 (8H) can be assigned to the protons of the benzoate group plus the benzylic protons ortho to the -CH<sub>2</sub>O-. The signals at 6.75 and 6.62 ppm (4H+2H) correspond to the benzylic protons meta to the -CH<sub>2</sub>O- of the lateral and central alkyloxybenzyloxy substituents. The characteristic signals, corresponding to most protons of the dodecyloxy alkyl chains in the dendron, can be observed in the high-field region at 1.7, 1.4, 1.2, and 0.8 ppm. The most interesting region lies between 5 and 3.4 ppm in which five signals can be observed. The two signals centered at 4.42 and 4.24 ppm correspond to the two methylenic carbon **c'** protons in the modified monomeric unit; the signal centered at 3.90 ppm

corresponds to the methylene attached to the oxygen in the alkyl chains of the mesogenic unit and to the methynic proton **b'**. The partially overlapped broad signal between 3.9 and 3.4 ppm corresponds to the methylenic and methynic protons **a**, **a'**, **b**, and **c** in the modified and unmodified monomeric units, as well as to the methylenic protons **a''** of the ethylene oxide unit. Finally, the signal centered at 4.82 ppm can be assigned to the benzylic methylenes of the dodecyloxybenzyloxy substituent.

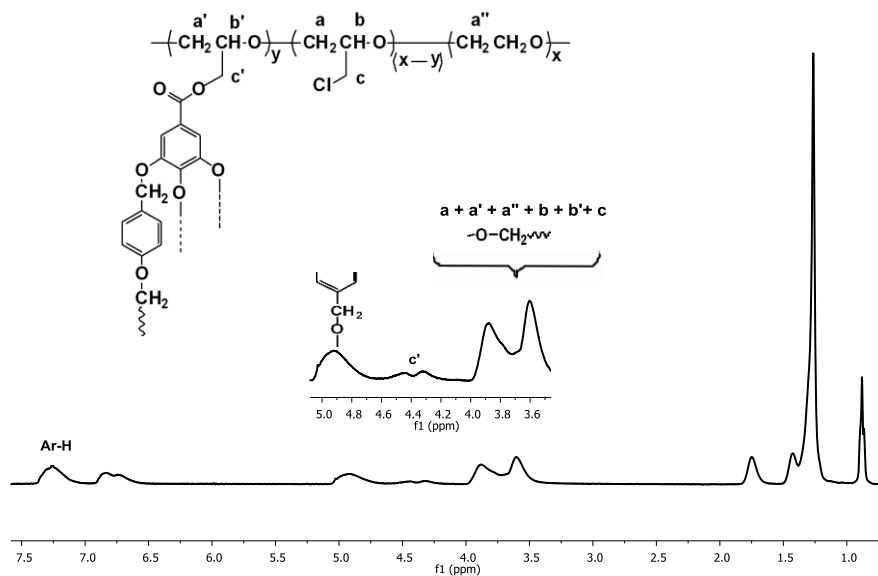


**Figure 2.1.** <sup>1</sup>H NMR spectrum of copolymer CP1 in CDCl<sub>3</sub>

**Figure 2.2** shows the <sup>13</sup>C NMR spectrum of copolymer CP1 with the corresponding assignments. The aromatic carbons and the carbonyl of the benzoate moiety introduced appear between 166 and 108 ppm, whereas carbons 2–12 of the aliphatic alkyl chains appear at the expected displacements in the region between 32 and 14 ppm. The carbons of the main chain units appear in the central region of the spectra. The methine and side methylenic carbons of the modified and unmodified monomeric units appear at different chemical shifts. Therefore, **b** and **b'** appear at 78.6 and 77.4 ppm, respectively, and **c** and **c'**

appear at 43.5 and 63.8 ppm.

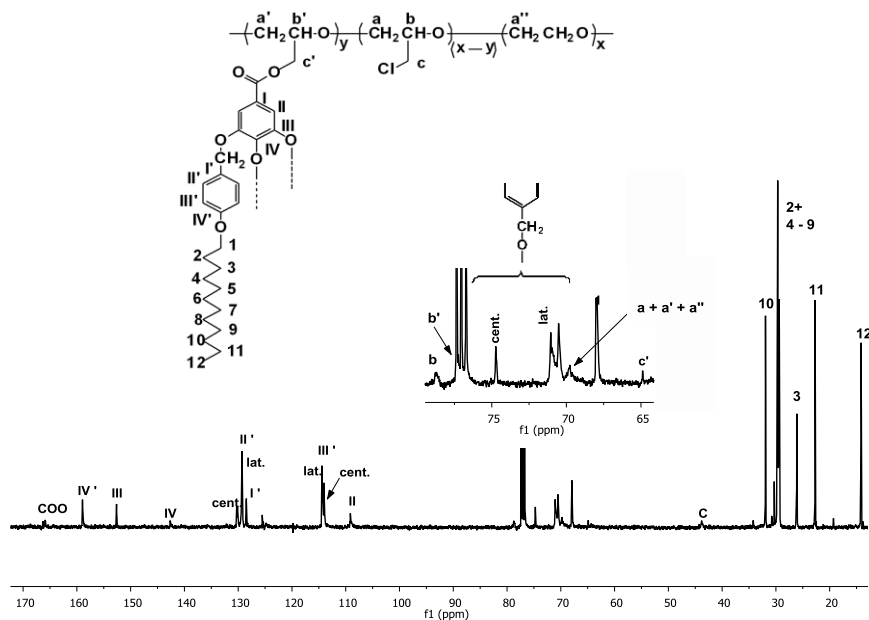


**Figure 2.2.** <sup>13</sup>C NMR spectrum of copolymer CP1 in CDCl<sub>3</sub>

The chemical shift of **b'** was deduced from reported spectra of modified PECH in TCE-d<sub>2</sub><sup>14</sup>, since in our case it appears overlapped with the CDCl<sub>3</sub> signal. The carbons **a**, **a'** and **a''** appear as a broad signal at 69.2 ppm. Carbon 1 of the alkyl chains appears as a wide peak at 67.8 ppm. The chemical shifts of the benzylic methylenes depend on their relative position in the aromatic ring. Those in position 3 and 5 appear at 70.7 ppm, whereas the same carbon in position 4 appears downfield at 74.7 ppm. Neither <sup>1</sup>H NMR nor <sup>13</sup>C NMR spectra showed detectable amounts of any of the signals corresponding to unsaturated vinyl ether units<sup>23</sup>. This indicates that the dehydrohalogenation reaction does not take place under our experimental conditions. The copolymer composition was calculated by NMR spectroscopy because this methodology gave accurate results (as compared with elemental chlorine analysis) in previous studies. Quantification was carried out from the <sup>1</sup>H NMR spectra by comparing the areas of the aromatic peaks between 7.4 and 6.8 ppm, the benzylic proton signal at 4.8 ppm, and the methylenic protons **c'** at 4.4 ppm with the broad signal between 4.0 and 3.5 ppm (**Figure 2.2**). The results agreed with those of the comparative elemental

analysis.

The characterization of the mesomorphic phases was performed on the basis of DSC, POM, and X-ray diffraction experiments. **Table 2.6** shows the results of POM and DSC characterization. Before DSC and POM experiments, all copolymers were annealed for 2 hours in between  $T_g$  and clearing temperature (**Table 2.6**).  $T_g$  was estimated from the second heating on DSC scans in case of all copolymers and ranged between -12 and 3 °C.

In all copolymers, DSC analysis put into evidence an endotherm which ranged between 26 and 50 °C, which suggested the existence of a crystalline portion in the modified copolymers. However, XRD experiments performed at room temperature did not put into evidence any peaks attributable to crystallinity in the samples.

**Table 2.6. Phase transitions and annealing temperature of the copolymers CP1–CP5**

Sample	Modification (%)	$T_g$ (°C) <sup>a</sup>	$T_m$ (°C) <sup>a</sup>	Annealing temperature (°C)	$T_c$ (°C) <sup>b</sup>
CP1	69	-12	50	100	115-118
CP2	59	2	34	70	85-90
CP3	65	0	27	90	95-100
CP4	62	3	26	80	100-115
CP5	57	3	29	70	87-90

<sup>a</sup> Determined by DSC from the second heating scan.

<sup>b</sup> Clearing range determined by POM.

Nevertheless, we performed HR-MAS NMR experiments on CP2 copolymer at 20 and 50 °C, that is, below and above the transition detected by DSC. HR-MAS <sup>13</sup>C NMR spectra of CP2 are reported in **Figure 2.3 a-b**. We focused our attention on the following peaks:

- 43.5 ppm, corresponding to the side methylenic carbon (c) of the unmodified unit;
- 63.8 ppm, corresponding to the side methylenic carbon (c') of the

modified unit;

- 78.6 ppm, corresponding to the methine (b) of the unmodified unit.

We did not take into account the peak at 77.4 ppm, corresponding to the methine (b') of the modified unit, because it was partially overlapped with the chloroform signal.

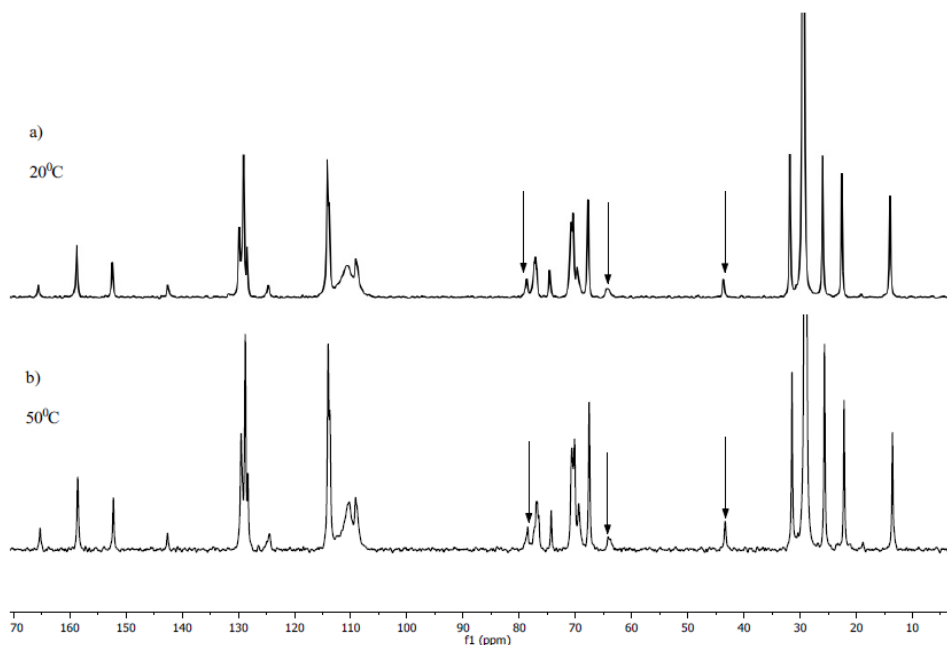


**Figure 2.3.** HR-MAS  $^{13}\text{C}$  spectra of CP2 copolymer at: a) 20°C; b) 50°C. The arrows indicate the peaks considered for  $T_{1\text{C}}$ 's calculation, located at 43.5, 63.8 and 78.6 ppm

We therefore determined  $T_{1\text{C}}$ 's by the inversion-recovery pulse sequence as described in the Experimental part. The results are reported in **Table 2.7**.

**Table 2.7. Carbon spin-lattice relaxation times of selected peaks of CP2 copolymer at 20°C and 50°C**

Peak (ppm)	$T_{1C}$ at 20°C (s)	$T_{1C}$ at 50°C (s)
43.5	1.75± 0.09	0.30± 0.02
63.8	0.39± 0.01, 1.4± 0.4	0.22± 0.01
78.6	0.70± 0.01	0.57± 0.03

In the case of the methylene of the modified unit (63.8 ppm), two components of  $T_{1C}$  were found at 20 °C, which reduced to one when temperature was raised to 50 °C. In the case of methylene and methine of the unmodified units, only one component was found at 20 °C, whose value also decreased on increasing the temperature. In semi-crystalline polymers, double exponential have been observed and they are commonly interpreted by assigning one relaxation process to the crystalline domains and the other relaxation process to the amorphous portion. The longer  $T_{1C}$  value found for c' corresponded to 1.4 s. For the crystalline phase of PEO at room temperature,  $T_{1C}$ 's of 14-16 s were reported<sup>24</sup>, which are considerably longer than in our case. Taking into consideration that a strict similarity between PEO and CP2 structures should not be sought, there are also several aspects which could further justify such differences in the  $T_{1C}$ 's: first, the  $T_{1C}$ 's reported for PEO refer to methylene and methine in the main chain, while in our case the relaxation time refers to a side methylene; second, they were determined about 40° below melting temperature, while in our case the relaxation experiment was performed only 14° below the observed transition; third, given the XRD results, in our case it is reasonable to suppose that the amount of crystalline portion in CP2 is quite low when compared to PEO samples reported in the literature. This could also affect the value of  $T_{1C}$ , as explained below. Therefore, we attributed the two components of  $T_{1C}$  to the presence of amorphous and crystalline portions in copolymer CP2. Finally, we concluded that the endotherms centered round 40 °C could be attributed to main-chain crystallinity for the whole set of polymers. As an approximation, under this assumption, we roughly estimated the degree of crystallinity  $X_c$  in our modified copolymers from the experimental melting enthalpy value and taking as a reference the reported melting enthalpy for 100%



crystalline PEO<sup>25</sup>. The obtained values, together with melting temperatures and melting entropies, are reported in **Table 2.8**.

**Table 2.8. Characteristics of the crystalline phase of copolymers CP1-CP5**

Sample	Modification degree (%)	Melting temperature (°C)	Melting enthalpy <sup>a</sup> (kJ/mol)	Melting entropy <sup>a</sup> (J/K·mol)	X <sub>c</sub> <sup>b</sup> (%)
PEO	-	62	8.67	25.8	100
CP1	69	50	0.32	0.99	3.7
CP2	59	34	0.16	0.50	1.8
CP3	65	27	0.16	0.42	1.8
CP4	62	26	0.16	0.55	1.8
CP5	57	29	0.15	0.49	1.7

<sup>a</sup>Per mol repetitive unit

<sup>b</sup>Degree of crystallinity calculated with respect to 100% crystalline PEO.

As expected, X<sub>c</sub> values resulted extremely low, being 1.7-1.8 %; in the case of CP1, which has the highest modification degree (i.e. 69%), higher melting temperature, melting entropy and crystallinity degree were found. This suggests that the presence of the side dendrons, which are responsible for the mesogenic columnar ordering, is also able to induce some crystalline order in the copolymer main chain. In all cases, such low values of X<sub>c</sub> presumably correspond to a great contact surface between the crystalline and amorphous regions, which determines that the crystal carbons can migrate quickly into the non-crystalline regions and relax. This could explain the short relaxation time found for the crystalline component of methylene c'.

All copolymers exhibited liquid-crystalline behavior, as shown by POM and confirmed by XRD. By DSC, we could evaluate neither the clearing temperature nor the clearing enthalpy, since only a very small variation of heat flow signal with respect to the baseline could be observed, even after annealing. The clearing temperature ranges were therefore determined by POM: they were found to depend on the modification degree achieved, as expected, but were all around 90-100°C. For instance, the change in the optical texture of CP1 in the

clearing range, is shown in **Figure 2.4 a-c**.

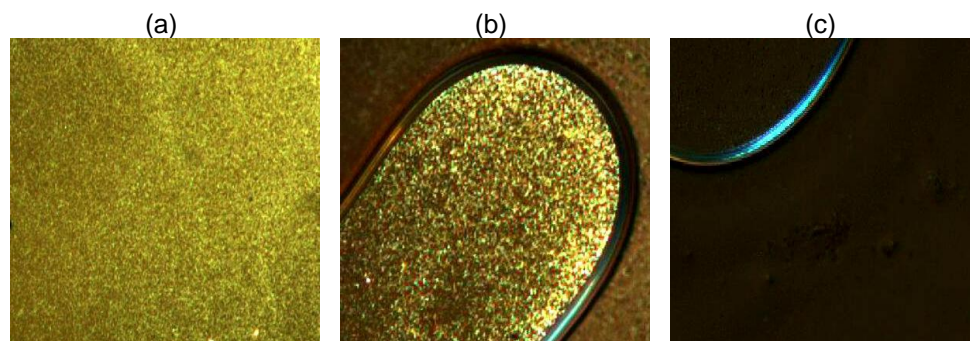


**Figure 2.4.** Optical micrographics between crossed polars of CP1 at: (a) 110°C (b) 115°C (c) 120°C

**Table 2.9.** X-ray patterns of oriented samples of copolymers CP1–CP5 at room temperature

Polymer	Modification (%)	$d_{100}^a$ (Å)	$d_{001}^b$ (Å)	$a^c$ (Å)	$\mu^d$	$\delta^e$
CP1	69	42	4.7	49	15	5.1
CP2	59	45	4.7	52	20	6.0
CP3	65	46	4.7	53	19	6.0
CP4	62	47	4.7	54	20	6.4
CP5	57	45	4.7	53	20	6.0

<sup>a, b</sup> Experimental planes spacings

<sup>c</sup> Dimension of the hexagonal unit cell

<sup>d</sup> Repeating units of polymer per unit cell

<sup>e</sup> Number of disks per unit cell

**Table 2.9** shows the results of X-ray diffraction experiments performed at room temperature on the samples oriented by shearing in the rubbery state. As an example, **Figure 2.5** shows the X-ray diffraction pattern of CP5 in the low  $2\theta$  range ( $0.9 - 9.2^\circ$ ) (a) and in the medium  $2\theta$  range ( $3 - 25.5^\circ$ ) (b).

In all cases, the XRD pattern showed a sharp reflection at  $2\theta$  approximately  $2.0^\circ$ , and a broad halo at  $2\theta$  approximately  $20^\circ$ .

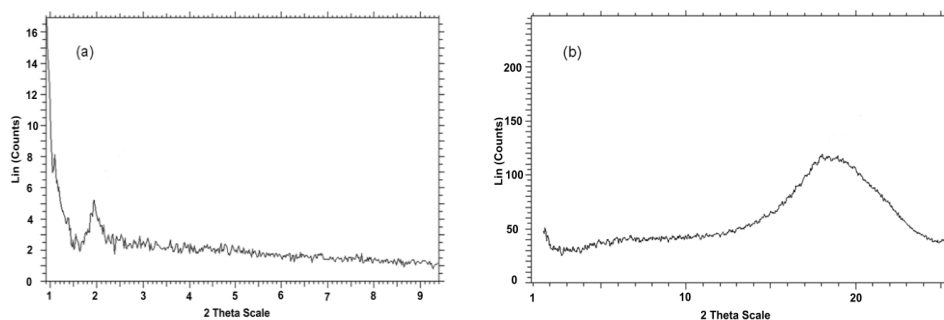


**Figure 2.5. X-ray diffraction pattern of CP5 in the low  $2\theta$  range (0.9–9.28) (a) and in the medium  $2\theta$  range (3–25.58) (b)**

This diffractogram is compatible with a columnar mesophase, the lower spacing corresponding to the planar distance between disks and the higher one corresponding to the lateral distance between columns. The former  $2\theta$  value corresponded to the  $d_{100}$  plane of a columnar phase and allowed to calculate the dimensions of the unit cell, while the latter corresponded to  $d_{001}$  plane and could be referred to the distance between dendrons<sup>15</sup>.

For a hexagonal mesophase, and given the experimental densities  $\rho$ , we can calculate the number of repeat units of polymer  $\mu$  that are present in a hexagonal prism layer of height  $c$  from the following equation:

$$\rho = \frac{2\mu M}{\sqrt{3}N_A a^2 c} \quad (2.2)$$

where  $M$  is the molecular weight of the repeat unit,  $N_A$  is Avogadro's number,  $a = 2 (d_{100})/\sqrt{3}$  is the dimension of the hexagonal unit cell, and  $c = d_{001}\cos \chi$ , and  $\chi$  are the angles between the prism height and the distance between disks calculated from the XRD pattern of oriented samples. The same calculation can also be applied to columnar samples because geometrical considerations make it possible to assume that in a columnar mesophase the columns self-assemble in a compact hexagonal packing where statistical fluctuations in the column positions do not produce any of the additional

reflections that are expected in a  $Col_h$  phase: that is, the instantaneous positions of the columns fit a hexagonal organization even if the average positions do not<sup>14</sup>.

**Figure 2.6** shows the XRD pattern on flat film of an oriented CP5 sample, in the low  $2\theta$  range ( $0.9 - 9.2^\circ$ ) (a) and in the medium  $2\theta$  range ( $3 - 25.5^\circ$ ) (b). It can be seen that the reflection at  $2\theta = 1.9^\circ$ , corresponding to the  $d_{100}$  plane, is polarized in the meridian, while the halo at approximately  $2\theta = 20^\circ$ , corresponding to  $d_{001}$  plane, exhibits polarization at the equator. This experimental evidence showed that dendrons are approximately perpendicular to the column axis and was found in the XRD pattern of oriented samples of the whole copolymer series CP1–CP5.

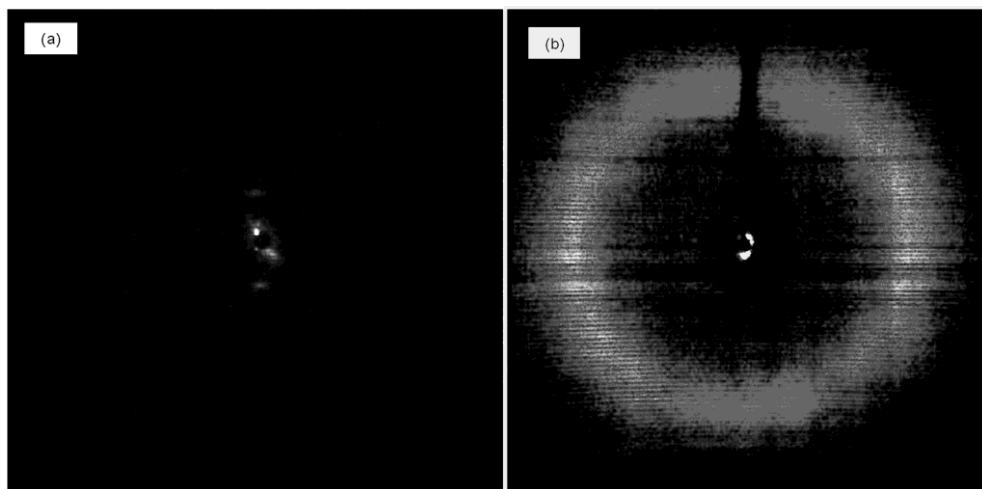


**Figure 2.6.** XRD pattern on flat film of an oriented CP5 sample, in the low  $2\theta$  range ( $0.9-9.2^\circ$ ) (a) and in the medium  $2\theta$  range ( $3-25.5^\circ$ ) (b)

The estimated average number of dendrons per unit cell ranged from 5 to 6. The self-assembling of CP1–CP5 copolymers into columns is schematized in **Figure 2.7**.

In the case of the copolymers obtained by chemical modification of

PECH<sup>15</sup> with the same dendron, the unit cell had dimensions in the same range, but it was found that the number of dendrons contained in a unit cell ranged between 3 and 6, with a tilt angle comprised between 23° and 45°. This difference can be ascribed to the higher flexibility of the ethylene oxide unit, which allowed the unit cell to accommodate more dendrons in the case of these copolymers.

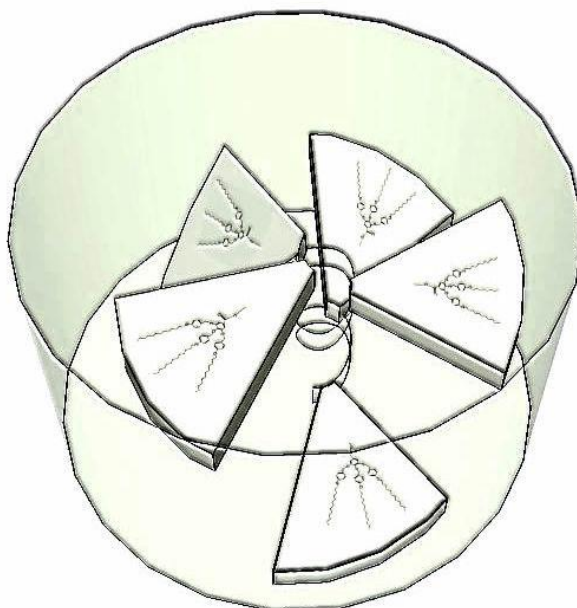


**Figure 2.7.** Schematic representation of columnar structure of CPn copolymers

## 2.5 Conclusions

SCLC polyethers were obtained by a chemical modification of PECH and P(ECH-co-EO) with the dendron potassium 3,4,5-tris[4-(*n*-dodecan-1-yloxy)-benzyloxy] benzoate. The modification degree was found to reach a plateau value around 80%, in case of PECH, and 69%, in case of P(ECH-co-EO). NMR characterization indicated that side reactions, such as dehydrohalogenation, did not take place under our experimental conditions. All modified homopolymers and copolymers exhibited liquid-crystalline columnar behavior, as shown by POM and confirmed by XRD. Moreover, in case of P(ECH-co-EO), DSC analysis and HR-MAS experiments suggested that the presence of the side dendrons, which are responsible for the mesogenic columnar ordering, is also able to induce small crystalline order in the copolymer main chain. The clearing temperature ranges were determined with the help of DSC and POM: they depended on the modification degree, as expected, and were all around 80-140 °C in case of PECH and 90-100 °C in case of P(ECH-co-EO). For P(ECH-co-EO), X-ray diffraction experiments on oriented samples showed that the dendrons are approximately perpendicular to the column axis and that their average number per unit cell ranged from 5 to 6. Therefore, these copolymers can be used to prepare oriented membranes for small cation transport, in agreement with the results that we obtained by using PECH modified with dendrons. In the case of the membranes based on modified P(ECH-co-EO), the higher flexibility of the EO moiety and the different modification degrees achieved, could vary the characteristics of the ion channel in the inner part of the columns.

For this reasons, both families of modified polymers have been used to prepare oriented membranes, as described in chapter number 4.

## 2.6 References

1. Finkelmann, H.; Ringsdorf, H.; Siol, W.; Wendorff, J. H., Synthesis of cholesteric liquid crystalline polymers. Polyreactions in ordered systems, 15. *Die Makromolekulare Chemie* **1978**, 179 (3), 829-832.
2. Brecl, M.; Žigon, M.; Malavašič, T., Side chain liquid crystal polyurethanes with azobenzene mesogenic moieties: Influence of spacer length on hydrogen bonding at different temperatures. *Journal of Polymer Science Part A: Polymer Chemistry* **1998**, 36 (12), 2135-2146.
3. Lacoudre, N.; Le Borgne, A.; Spassky, N.; Vairon, J.-P.; Le Barny, P.; Dubois, J.-C.; Esselin, S.; Friedrich, C.; Noël, C., Synthesis and Characterization of Some Terminally Cyano-Substituted Side-Chain Liquid Crystalline Polyacrylates. *Molecular Crystals and Liquid Crystals Incorporating Nonlinear Optics* **1988**, 155 (1), 113-127.
4. Percec, V.; Lee, M., Molecular engineering of liquid-crystal polymers by living polymerization. 3. Influence of molecular weight on the phase transitions of poly{8-[(4-cyano-4'-biphenyl)oxy]octyl vinyl ether} and of poly{6-[4-cyano-4'-biphenyl)oxy]hexyl vinyl ether}. *Macromolecules* **1991**, 24 (5), 1017-1024.
5. Craig, A. A.; Winchester, I.; Madden, P. C.; Larcey, P.; Hamley, I. W.; Imrie, C. T., Synthesis, thermal characterization and rheological properties of a homologous series of polymethacrylate-based side-chain liquid crystal polymers. *Polymer* **1998**, 39 (5), 1197-1205.
6. Mirčeva, A.; Žigon, M., Synthesis of side-chain liquid crystalline polyurethanes via ester type attachment. *Polymer Bulletin* **1998**, 41 (4), 447-453.
7. Imrie, C. T.; Karasz, F. E.; Attard, G. S., Side-Chain Liquid-Crystalline Copolymers. 2. Polystyrene-Based Side-Chain Polymers Containing Nitroazobenzene. *Macromolecules* **1994**, 27 (6), 1578-1581.
8. (a) Percec, V.; Glodde, M.; Bera, T. K.; Miura, Y.; Shiyonovskaya, I.; Singer, K. D.; Balagurusamy, V. S. K.; Heiney, P. A.; Schnell, I.; Rapp, A.; Spiess, H.-W.; Hudson, S. D.; H. Duan 2002, 384., *Nature* **2002**, 417, 384; (b) Percec, V.; Schlueter, D.; Ungar, G.; Cheng, S. Z. D.; A. Zhang 1998, 1745., *Macromolecules* **1998**, 31, 1745; (c) Percec, V.; Ahn, C.-H.-.; Ungar, G.; Yeardley, D. J. P.; Möller, M.; Sheiko, S., *Nature* **1998**, 391, 161; (d) Jung, H.-T.; Kim, S. O.; Ko, Y. K.; Yoon, D. K.; Hudson, S. D.; Percec, V.; Holerca, M. N.;

Cho, W.-D.; Mosier, P. E., *Macromolecules* **2002**, *35*, 3717-3721; (e) Percec, V.; Holerca, M. N.; Uchida, S.; Yeardley, D. J. P.; Ungar, G., *Biomacromolecules* **2001**, *2*, 729-740.

9. Pugh, C.; Percec, V., Functional polymers and sequential copolymers by phase transfer catalysis. *Polymer Bulletin* **1986**, *16* (6), 521-527.

10. Ujiie, S.; Iimura, K., Thermal properties and orientational behavior of nematic comb-like polyether. *Polymer Journal* **1992**, *24* (5), 427-431.

11. Millán, J.-L.; Martínez, G.; Mijangos, C.; Gómez-Elvira, J. M., Configurational and conformational control of chemical modification and thermal degradation of poly(vinyl chloride). *Makromolekulare Chemie. Macromolecular Symposia* **1989**, *29* (1), 185-196.

12. N'Guyen, T. D.; Deffieux, A.; Boileau, S., Phase-transfer catalysis in the chemical modification of polymers: 1. *Polymer* **1978**, *19* (4), 423-426.

13. Iizawa, T.; Nishikubo, T.; Ichikawa, M.; Sugawara, Y.; Okawara, M., Substitution and elimination reactions of poly(epichlorohydrin) and poly(2-chloroethyl vinyl ether) using phase transfer catalysis. *Journal of Polymer Science: Polymer Chemistry Edition* **1985**, *23* (7), 1893-1906.

14. Ronda, J. C.; Reina, J. A.; Cádiz, V.; Giamberini, M.; Nicolais, L., Self-organized liquid-crystalline polyethers obtained by grafting tapered mesogenic groups onto poly(epichlorohydrin): Toward biomimetic ion channels. *Journal of Polymer Science Part A: Polymer Chemistry* **2003**, *41* (19), 2918-2929.

15. Ronda, J. C.; Reina, J. A.; Giamberini, M., Self-organized liquid-crystalline polyethers obtained by grafting tapered mesogenic groups onto poly(epichlorohydrin): Toward biomimetic ion channels 2. *Journal of Polymer Science Part A: Polymer Chemistry* **2004**, *42* (2), 326-340.

16. Giamberini, M.; Ronda, J. C.; Reina, J. A., Poly(epichlorohydrin) modified with 3,4,5-tris(dodecyloxy)benzoate: The structure and dynamics of the aliphatic side chains in the columnar mesophase. *Journal of Polymer Science Part A: Polymer Chemistry* **2005**, *43* (10), 2099-2111.

17. Bhosale, S. V.; Rasool, M. A.; Reina, J. A.; Giamberini, M., New liquid crystalline columnar poly(epichlorohydrin-co-ethylene oxide) derivatives leading to biomimetic ion channels. *Polymer Engineering & Science* **2013**, *53* (1), 159-167.



18. Percec, V.; Heck, J., Liquid crystalline polymers containing mesogenic units based on half-disc and rod-like moieties. I. Synthesis and characterization of 4-(11-undecan-1-yloxy)-4'-[3,4,5-tri(p-n-dodecan-1-yloxybenzyloxy)benzoate]biphenyl side groups. *Journal of Polymer Science Part A: Polymer Chemistry* **1991**, 29 (4), 591-597.
19. Bovey, F. A.; Mirau, P. A., *NMR of Polymers*. Academic Press: San Diego, USA, 1996.
20. Pérez, M.; Reina, J. A.; Serra, A.; Ronda, J. C., Chemical modification of poly(epichlorohydrin) with phenolate. Studies of the side reactions. *Acta Polymerica* **1998**, 49 (6), 312-318.
21. (a) Reina, J. A.; Cádiz, V.; Mantecón, A.; Serra, A., *Angew Makromol Chem.* **1993**, 209, 95; (b) Pérez, M.; Ronda, J. C.; Reina, J. A.; Serra, A., *Polymer* **2001**, 42, 1.
22. Pugh, C.; Percec, V., American Chemical Society: Washington D.C., 1988; Vol. 364.
23. Montornés, J. M.; Ronda, J. C.; Reina, J. A., *J. Polym. Sci. Part A: Polym. Chem.* **2004**, 42, 3002-3012.
24. Dechter, J. J., *J. Polym. Sci. – Polym. Lett.* **1985**, 23, 261.
25. Buckley, C. P.; Kovacs, A. J., *Prog. Colloid Polym. Sci.* **1975**, 58 44–52.

## *Chapter 3*

---

### *Side-Chain Liquid Crystalline Polymers Based On Chemical Modification Of Polyglycidol*

UNIVERSITAT ROVIRA I VIRGILI

PROTON-EXCHANGE BIOMIMETIC MEMBRANES BASED ON COLUMNAR SIDE-CHAIN LIQUID-CRYSTALLINE POLYETHERS

Suryakant Bhosale

Dipòsit Legal: T.188-2014

### 3.1 Introduction

In chapter 2, we discussed about the modification of chlorinated linear polyethers using the dendrimer, potassium 3,4,5-tris[4-(*n*-dodecan-1-yloxy)benzyloxy]benzoate]. This gave rise to a liquid crystalline material with columnar hexagonal mesophase having central helical polymer backbone and hydrophobic dendrimers. A continuous ion channel along the column axis possibly forms due to this stable columnar mesophase.

The main purpose of this study is to modify polyethers with tapered group, to get well organised hexagonal columnar mesophase which is a key to get efficient proton transporting ion channels. As explained in main introduction of the thesis, these columns consist of outer hydrophobic part made up of tapered group and inner hydrophilic part made up of polyether backbone leading to the proton transport. Likewise, polyol like linear polyglycidol (LPG) can be another suitable polyether candidate which can be modified with 3,4,5-tris[4-(*n*-dodecan-1-yloxy)benzyloxy]benzoic acid (**2**) in order to obtain liquid crystalline columnar polyethers. In this chapter we investigated the modification of LPG by **2** using carbodiimide mediated Steglich esterification between free hydroxyl groups of the linear polyglycidol and carboxylic groups of **2** under different conditions. A degree of modification ranging from 8 to 43% was achieved. The upper value seems to be an apparent plateau. Modified LPGs were subsequently studied in terms of liquid crystalline behaviour. It has been revealed that modified LPGs are showing different mesophases like nematic, distorted hexagonal and hexagonal columnar depending on the degree of modification. Hence, modified linear polyglycidol can be also a suitable candidate for the preparation of cation transporting membranes.

The introduction of mesogenic groups at the external surface of dendrimers has been established as a strategy for the preparation of liquid crystals.<sup>1-3</sup> In most cases the mesogenic groups have been primarily attached covalently at the surface groups of dendrimers. The same strategy has been employed for the preparation of hyperbranched liquid crystalline polymers.<sup>4</sup>

Percec and co-workers for the first time reported the synthesis of thermotropic hyperbranched polyethers with hexagonal columnar phase and nematic phases<sup>5-7</sup>. More recently, Felekis et al,<sup>8</sup> synthesised liquid crystals derived from hydrogen-bonded supramolecular complexes of pyridinylated hyperbranched polyglycerol and cholesterol-based carboxylic acids. A hyperbranched polyether-polyol was reacted with isonicotinoyl chloride hydrochloride for the introduction of the pyridinyl moiety at the external surface. This pyridinylated hyperbranched polymer was subsequently interacted with cholesterol-based carboxylic acids for the formation of the corresponding hydrogen-bonded supramolecular complexes. The materials obtained exhibited smectic A liquid crystalline phases over a broad thermal range from room temperature up to above 170 °C. Therefore, apart from the linear, the hyperbranched polyglycidol (HPG) can be also of interest in terms of chemical modification to achieve liquid crystalline behavior.

Sunder et al<sup>9</sup> have developed a synthetic strategy based on the ring-opening multibranching polymerization (ROMBP) of glycidol (2,3-epoxy-1-propanol), leading to hyperbranched polyglycerols. By using this approach, we synthesized hyperbranched polyglycidol bearing 95 hydroxy end groups per molecule was synthesized in our group. Herein we used these aliphatic polyether-polyols to be modified with **2** using Steglich esterification as used in case of LPG. Further, modified HPG was studied in terms of liquid crystalline behavior.

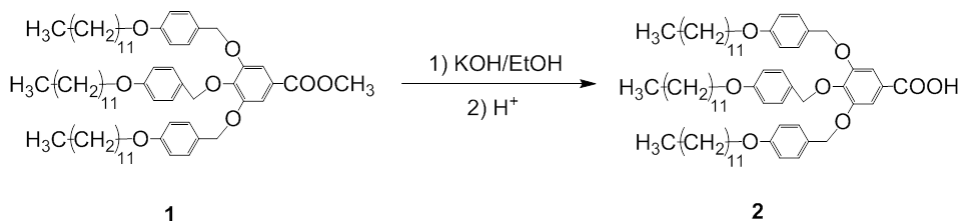
## 3.2 Experimental

### 3.2.1 Materials

All the chemicals were purchased from Sigma–Aldrich, while all solvents were purchased from Scharlab. Diglyme (bis(2-methoxyethyl) ether), *p*-toluenesulfonic acid monohydrate (*p*-TsOH, 98.5%), potassium tert-butoxide (1M solution in THF), *N,N'*-Dicyclohexylcarbodiimide (DCC, 99%), 4-dimethylaminopyridine (DMAP, ≥99%) were used as received. Glycidol (96%) was distilled under reduced pressure and stored over molecular sieves at 2-5 °C. Dimethylformamide (DMF, 99%) was dried<sup>10</sup> and used.

### 3.2.2 Synthesis of 3,4,5-tris[4-(*n*-dodecan-1-yloxy)benzyloxy]benzoic acid (**2**)

As explained in Chapter 2, methyl 3,4,5-tris[4-(*n*-dodecan-1-yloxy)benzyloxy] benzoate (**1**) was prepared as reported literature<sup>11</sup>. Further it converted to **2** by procedure as given below (**Scheme 3.1**).



**Scheme 3.1.** Synthesis of 3,4,5-tris[4-(*n*-dodecan-1-yloxy)benzyloxy] benzoic acid

Potassium hydroxide (5 g, 0.08 mol) in 20 ml of water was added dropwise to a solution of **1** (30.2 g, 0.0299 mol) in a mixture of 400 ml of ethanol and 100 ml of THF. The reaction mixture was refluxed and monitored by TLC (benzene/acetone 9:1). After 2 h it was acidified carefully with concentrated hydrochloric acid (60 ml) and refluxed for an additional 15-min period. The

reaction mixture was poured into 2 l of ice-water and the precipitate was filtered off, washed several times with water, and recrystallized twice from isopropyl alcohol (using active charcoal). Structure of the obtained product characterized by  $^1\text{H}$  (**Figure 3.1**) and  $^{13}\text{C}$  (**Figure 3.2**) NMR techniques. Yield:93%

$^1\text{H}$  NMR ( $\text{CDCl}_3/\text{TMS}$ ):  $\delta$  (ppm) = 7.43 (s, 2H Ar-H-COOH),  $\delta$  (ppm) = 7.34 (d, 4H, -O-Ar-H- $\text{CH}_2$ -O-Ar-COOH from 2 and 6 positions of the external benzylic units),  $\delta$  (ppm) = 7.26 (d, 2H, -O-Ar-H- $\text{CH}_2$ -O-Ar-COOH from 2 and 6 positions of the internal benzylic units),  $\delta$  (ppm) = 6.89 (d, 4H, -O-Ar-H- $\text{CH}_2$ -O-Ar-COOH from 3 and 5 positions of external benzylic units),  $\delta$  (ppm) = 6.76 (d, 2H, -O-Ar-H- $\text{CH}_2$ -O-Ar-COOH from 3 and 5 positions of central benzylic units),  $\delta$  (ppm) = 5.06 (s, 4H, - $\text{CH}_2$ -O-Ar-COOH from 3 and 5 positions of benzoic group),  $\delta$  (ppm) = 5.04 (s, 2H, - $\text{CH}_2$ -O-Ar-COOH from para position of benzoic group),  $\delta$  (ppm) = 3.94 (two overlapped t, 6H, - $\text{CH}_2$ -O-Ar),  $\delta$  (ppm) = 1.79 (m, 6H, - $\text{CH}_2$ - $\text{CH}_2$ -O-Ar),  $\delta$  (ppm) = 1.45 (m, 6H, - $\text{CH}_2$ ( $\text{CH}_2$ ) $_2$ -O-Ar),  $\delta$  (ppm) = 1.27 (m, 48H, -( $\text{CH}_2$ ) $_8$ -),  $\delta$  (ppm) = 0.88 (t, 9H, - $\text{CH}_3$ ).

$^{13}\text{C}$  NMR ( $\text{CDCl}_3/\text{TMS}$ ):  $\delta$  (ppm) = 171.8 (-COOH),  $\delta$  (ppm) = 159.1 (ArC-O-( $\text{CH}_2$ ) $_{10}$ - $\text{CH}_3$  in lateral benzylic unit),  $\delta$  (ppm) = 159.1 (ArC-O-( $\text{CH}_2$ ) $_{10}$ - $\text{CH}_3$  in central benzylic unit),  $\delta$  (ppm) = 152.8 (ArC meta to -COOH),  $\delta$  (ppm) = 143.2 (ArC para to -COOH),  $\delta$  (ppm) = 130.5 (ArC meta to -O-( $\text{CH}_2$ ) $_{11}$ - $\text{CH}_3$  in lateral benzylic units),  $\delta$  (ppm) = 129.4 (ArC meta to ArC-O-( $\text{CH}_2$ ) $_{11}$ - $\text{CH}_3$  in central benzylic unit),  $\delta$  (ppm) = 128.6 (ArC- $\text{CH}_2$ -O-Ar-COOH),  $\delta$  (ppm) = 124.1 (ArC-COOH),  $\delta$  (ppm) = 114.6 (ArC ortho to -O-( $\text{CH}_2$ ) $_{11}$ - $\text{CH}_3$  in lateral benzylic units),  $\delta$  (ppm) = 114.3 (ArC ortho to -O-( $\text{CH}_2$ ) $_{11}$ - $\text{CH}_3$  in central benzylic units),  $\delta$  (ppm) = 109.7 (ArC ortho to COOH),  $\delta$  (ppm) = 74.8 (- $\text{CH}_2$ -O-Ar-COOH in central benzylic unit),  $\delta$  (ppm) = 71.1 (- $\text{CH}_2$ -O-Ar-COOH in lateral benzylic unit),  $\delta$  (ppm) = 68.2 (- $\text{CH}_2$ -O-( $\text{CH}_2$ ) $_{10}$ - $\text{CH}_3$  in lateral benzylic unit),  $\delta$  (ppm) = 68.1 (- $\text{CH}_2$ -O-( $\text{CH}_2$ ) $_{10}$ - $\text{CH}_3$  in central benzylic unit),  $\delta$  (ppm) = 32.4 (- $\text{CH}_2$ - $\text{CH}_2$ - $\text{CH}_3$ ),  $\delta$  (ppm) = 29.8-29.4 (-( $\text{CH}_2$ ) $_6$ -),  $\delta$  (ppm) = 26.2 (- $\text{CH}_2$ -( $\text{CH}_2$ ) $_8$ - $\text{CH}_3$ ),  $\delta$  (ppm) = 22.8 (- $\text{CH}_2$ - $\text{CH}_3$ ),  $\delta$  (ppm) = 14.3 (- $\text{CH}_2\text{CH}_3$ )

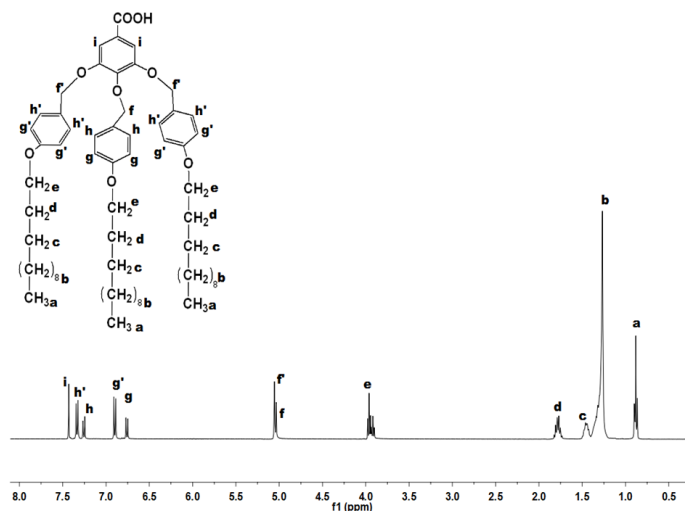


Figure 3.1.  $^1\text{H}$  NMR spectrum of 3,4,5-tris[4-(n-dodecan-1-yloxy)benzyloxy] benzoic acid in  $\text{CDCl}_3$

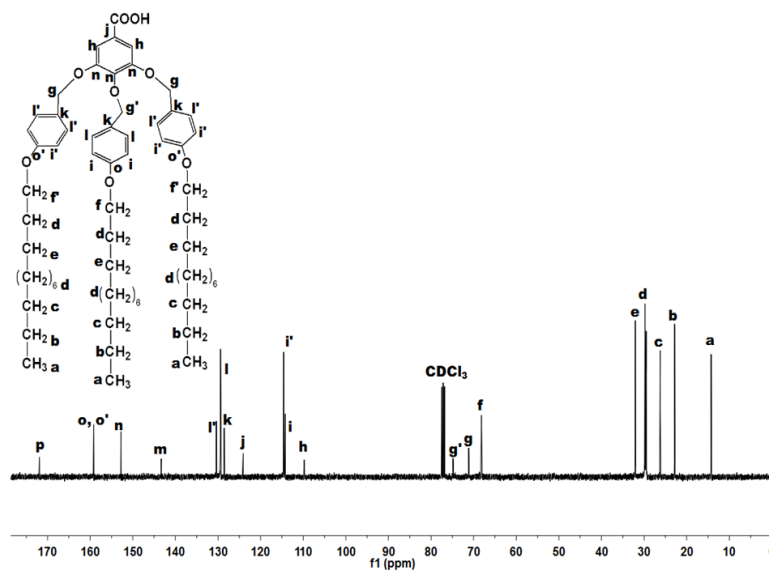
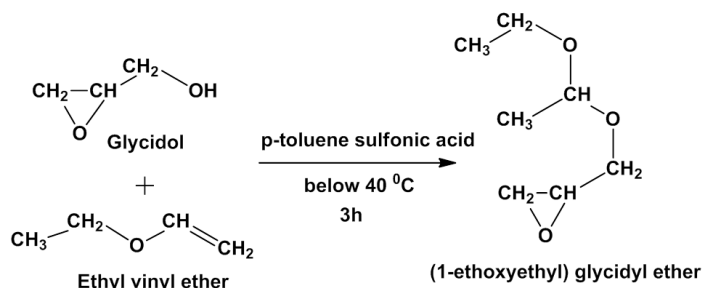


Figure 3.2.  $^{13}\text{C}$  NMR spectrum of 3,4,5-tris[4-(n-dodecan-1-yloxy)benzyloxy] benzoic acid in  $\text{CDCl}_3$



### 3.2.3 Synthesis of linear polyglycidol (LPG)

Synthesis of (1-ethoxyethyl) glycidyl ether (**Scheme 3.2**):



**Scheme 3.2. Synthesis of (1-ethoxyethyl)glycidyl ether**

To a magnetically stirred solution of glycidol (40 g, 0.54 mol) in ethyl vinyl ether (200 mL) is added TsOH (1 g) portionwise, keeping the temperature below 40 °C. The mixture is stirred for 3 h and saturated aqueous NaHCO<sub>3</sub> (100 mL) is then added. The organic layer is separated, dried and evaporated under reduced pressure. Distillation of residue gives a colourless liquid which is (1-ethoxyethyl) glycidyl ether. Structure of the obtained product characterized by <sup>1</sup>H (**Figure 3.3**) and <sup>13</sup>C (**Figure 3.4**) NMR techniques. Yield:70%.

<sup>1</sup>H NMR (CDCl<sub>3</sub>/TMS): δ (ppm) = 4.7- 4.6 (q, 1H), δ (ppm) = 3.7 - 3.2 (m, 4H), δ (ppm) = 3.1 - 3 (m,1H), δ (ppm) = 2.7 - 2.4 (m, 2H), δ (ppm) = 1.3 - 1 (m, 6H)

<sup>13</sup>C NMR (CDCl<sub>3</sub>/TMS): δ (ppm) = 100 (OCHCH<sub>3</sub>O), δ (ppm) = 65 (OCH<sub>2</sub>CH), δ (ppm) = 61.1 (CH<sub>3</sub>CH<sub>2</sub>O), δ (ppm) = 51.2 (CH<sub>2</sub>CHOCH<sub>2</sub>), δ (ppm) = 44.3 (CH<sub>2</sub>OCH), δ (ppm) = 19.4 (CH<sub>3</sub>CH), δ (ppm) = 15 (CH<sub>3</sub>CH<sub>2</sub>)

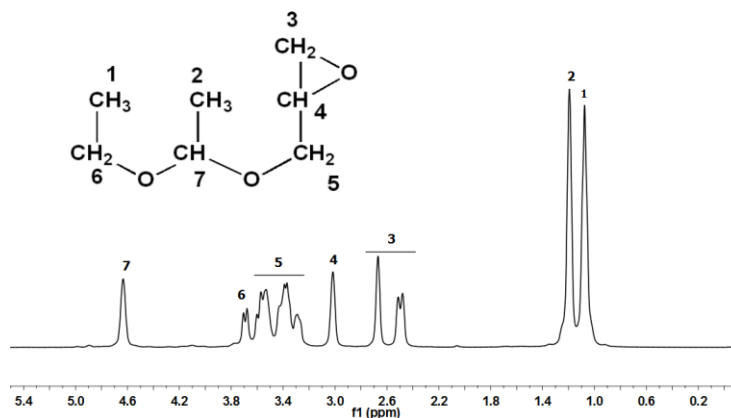


Figure 3.3. <sup>1</sup>H NMR spectrum of (1-ethoxyethyl)glycidyl ether in CDCl<sub>3</sub>

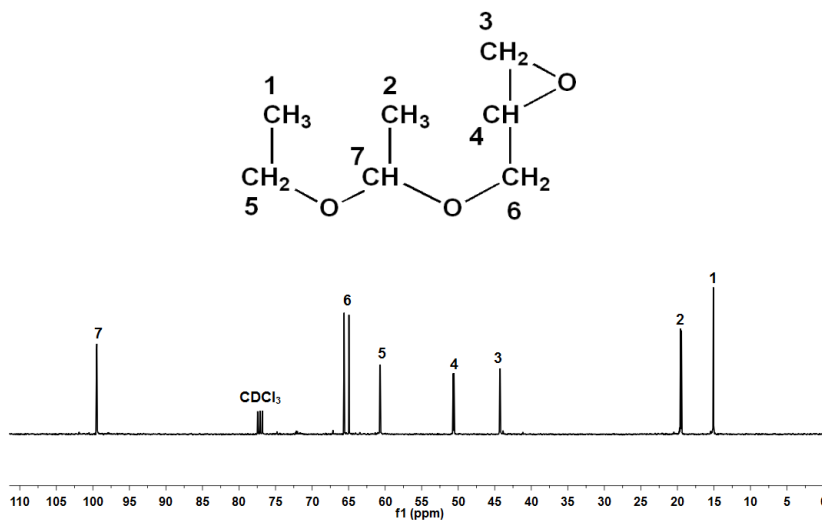
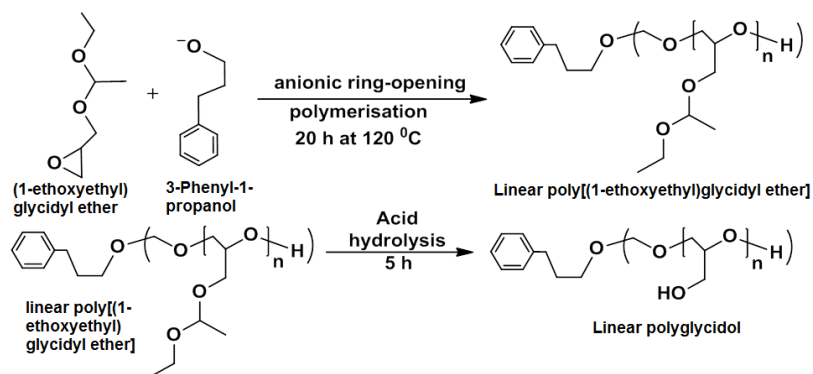


Figure 3.4. <sup>13</sup>C NMR spectrum of (1-ethoxyethyl)glycidyl ether in CDCl<sub>3</sub>

Synthesis of linear poly[(1-ethoxyethyl) glycidyl ether] (**Scheme 3.3**):



**Scheme 3.3. Synthesis of linear polyglycidol**

3-Phenyl-1-propanol (0.27 g, 1.9 mmol) was dissolved in diglyme (7 mL) and potassium tert-butoxide (0.20 mL of a 1 M solution in THF, 0.20 mmol) was added. The formed tert-butyl alcohol was removed by vacuum distillation. (1-ethoxyethyl) glycidyl ether (6.98 g, 47.8 mmol) was added and the mixture was magnetically stirred for 20 h at 120 °C. The solvent was under vacuum removed at 80 °C and linear poly[(1-ethoxyethyl) glycidyl ether] was obtained as a viscous liquid. Structure of the obtained product characterized by  $^1\text{H}$  (**Figure 3.5**) and  $^{13}\text{C}$  (**Figure 3.6**) NMR techniques. Yield: 91%

$^1\text{H}$  NMR ( $\text{CDCl}_3/\text{TMS}$ ):  $\delta$  (ppm) = 7.3-7.1 (m, 3H),  $\delta$  (ppm) = 4.7 - 4.6 (m, 1H),  $\delta$  (ppm) = 3.7 - 3.3 (m, 9H),  $\delta$  (ppm) = 2.7 (t, 2H),  $\delta$  (ppm) = 1.8 (qui, 2H),  $\delta$  (ppm) = 1.3 - 1.1 (m, 6H).

$^{13}\text{C}$  NMR ( $\text{CDCl}_3/\text{TMS}$ ):  $\delta$  (ppm) = 145-125 (Aryl),  $\delta$  (ppm) = 100 ( $\text{OCH}_2\text{OCH}_3$ ),  $\delta$  (ppm) = 79.6,  $\delta$  (ppm) = ( $\text{CH}_2\text{CHOCH}_2$ ),  $\delta$  (ppm) = 74-70 ( $\text{ArCH}_2\text{CH}_2\text{CH}_2$ ,  $\text{CHOCH}_2\text{CH}$ ,  $\text{OCH}_2\text{CHOH}$ ),  $\delta$  (ppm) = 67-64 ( $\text{CHCH}_2\text{OH}$ ,  $\text{OCH}_2\text{CH}_3$ ),  $\delta$  (ppm) = 61.1 ( $\text{OCH}_2\text{CHCH}_2\text{O}$ ),  $\delta$  (ppm) = 32-31 ( $\text{ArCH}_2\text{CH}_2$ ,  $\text{ArCH}_2\text{CH}_2$ ),  $\delta$  (ppm) = 20.1 ( $\text{CHCH}_3$ ),  $\delta$  (ppm) = 14.8 ( $\text{OCH}_2\text{CH}_3$ )

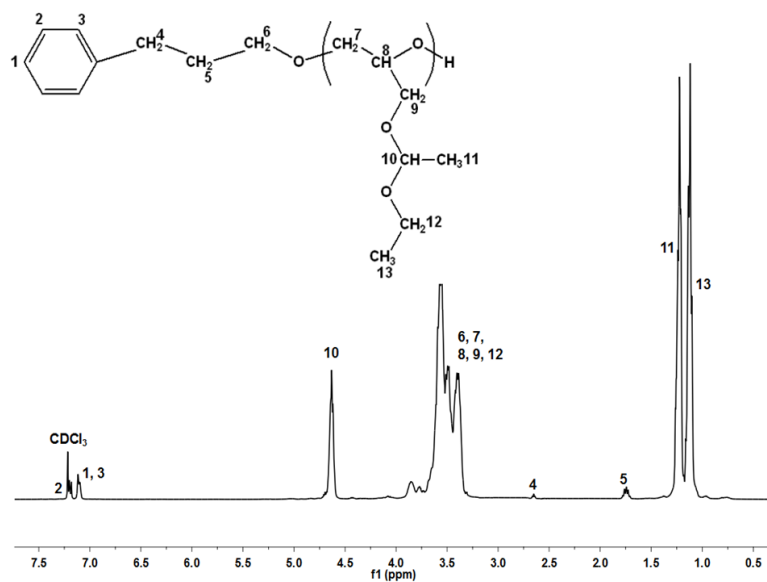


Figure 3.5.  $^1\text{H}$  NMR spectrum of linear poly[(1-ethoxyethyl)glycidyl ether] in  $\text{CDCl}_3$

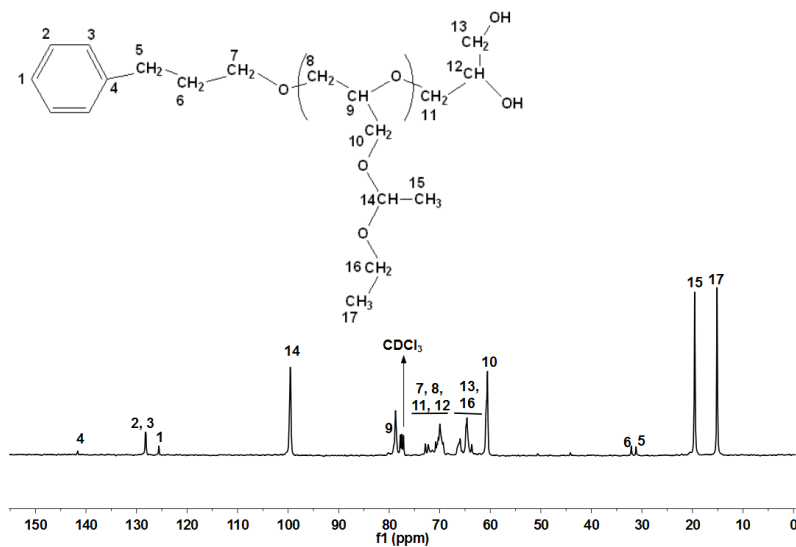


Figure 3.6.  $^{13}\text{C}$  NMR spectrum of linear poly[(1-ethoxyethyl)glycidyl ether] in  $\text{CDCl}_3$

Synthesis of linear polyglycidol (**Scheme 3.3**):

The linear poly[(1-ethoxyethyl) glycidyl ether] (10.0 g, 3.03 mmol of repeat unit) was dissolved in THF (1000 mL), and aqueous 37% HCl (59 g) was added. After 5 h, the polyglycidol was precipitated as an oil. The solvent was removed by decantation and the polyglycidol was dried in vacuum at 80 °C. Structure of the obtained product characterized by  $^1\text{H}$  (**Figure 3.7**) and  $^{13}\text{C}$  (**Figure 3.8**) NMR techniques. Yield:78%

$^1\text{H}$  NMR (deuterated-DMSO/TMS):  $\delta$  (ppm) = 7.3-7.1 (m, 3H),  $\delta$  (ppm) = 4.5 (s, 1H),  $\delta$  (ppm) = 3.7-3.3 (m, 7H),  $\delta$  (ppm) = 2.6 (t, 2H),  $\delta$  (ppm) = 1.7 (qui, 2H).

$^{13}\text{C}$  NMR (deuterated-DMSO/TMS):  $\delta$  (ppm) = 145-125 (Aryl),  $\delta$  (ppm) = 81.1 ( $\text{CH}_2\text{CHOCH}_2$ ),  $\delta$  (ppm) = 74-70 ( $\text{ArCH}_2\text{CH}_2\text{CH}_2$ ,  $\text{CH}_2\text{OCH}_2\text{CH}$ ,  $\text{OCH}_2\text{CHOH}$ ),  $\delta$  (ppm) = 64.8 ( $\text{CHCH}_2\text{OH}$ ),  $\delta$  (ppm) = 61.1 ( $\text{OCH}_2\text{CHOCH}_2\text{OH}$ ),  $\delta$  (ppm) = 32-31 ( $\text{ArCH}_2\text{CH}_2$ ,  $\text{ArCH}_2\text{CH}_2$ ).

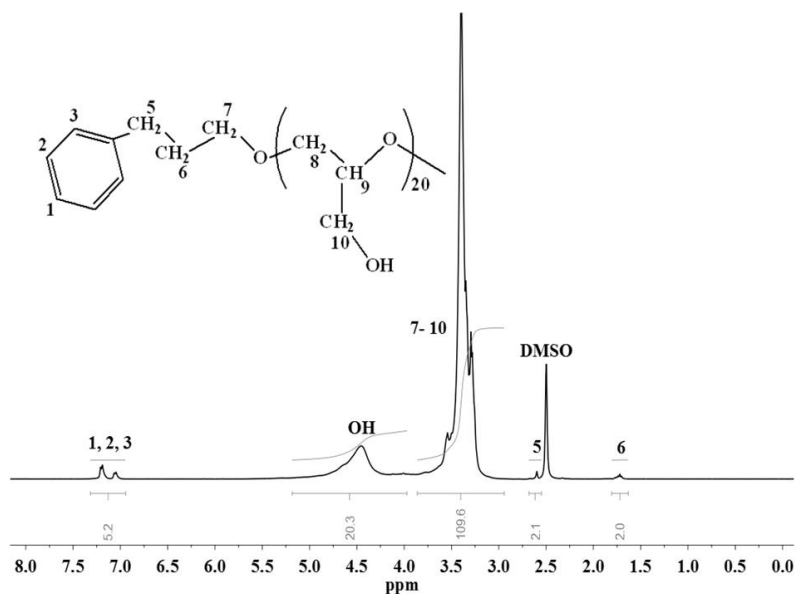


Figure 3.7.  $^1\text{H}$  NMR spectrum of linear polyglycidol in deuterated DMSO

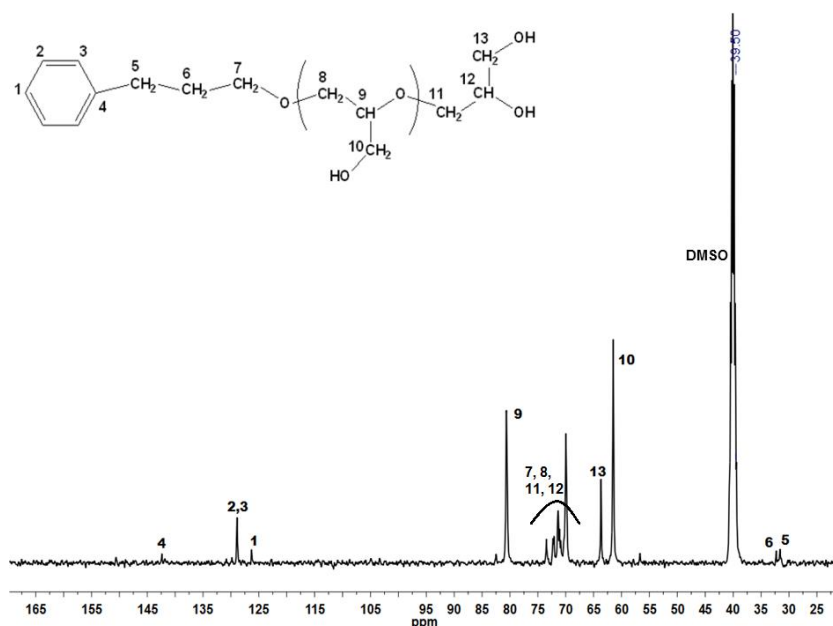


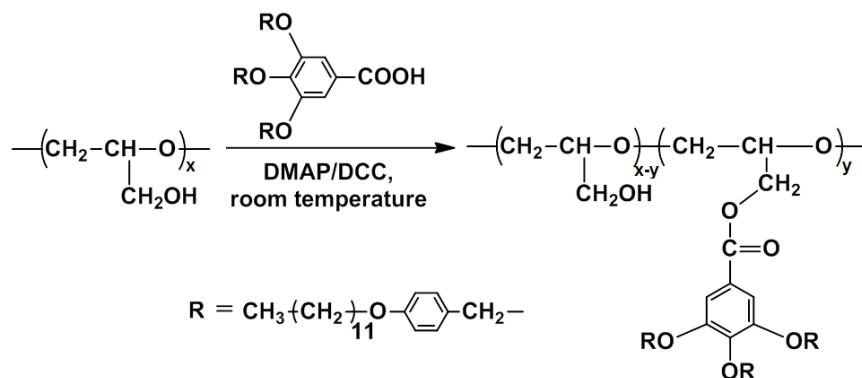
Figure 3.8.  $^{13}\text{C}$  NMR spectrum of linear polyglycidol in deuterated DMSO

### 3.2.4 Synthesis of hyperbranched polyglycidol

HBP,  $M_n$  7,030 g/mol (as determined by  $^1\text{H}$  NMR) with an average of 95 hydroxyl group per molecule was borrowed from the research group of Dr. Angels Serra, Department of Analytical and Organic Chemistry, Universitat Rovira I Virgili, Tarragona, Spain which had been already prepared according to reported procedure<sup>9</sup>.

### 3.2.5 Modification of linear polyglycidol (Scheme 3.4)

The linear polyglycidol has been successfully modified by **2** using carbodiimide mediated Steglich esterification between the free hydroxyl groups of the linear polyglycidol and carboxylic group of **2**.



### Scheme 3.4. Chemical modification of linear polyglycidol

In a three necked round bottomed flask, solution of **2** (2 g, 2 mmol) was prepared by dissolving into dry DMF (5 mL). Stoichiometric amounts of DCC and DMAP were added at 0 °C and the mixture was allowed to stir for 30 min in Ar atmosphere. The necessary amount of linear polyglycidol was dissolved into dry DMF (5 ml) and added dropwise to the above reaction mixture. The reaction mixture was allowed to stir for 2 days at room temperature under Ar atmosphere. Then, precipitated into 500 ml of methanol. Precipitated product was dissolved in THF and reprecipitated into 500 ml methanol. This reprecipitation was repeated for 5 times, in order to remove DCC, DMAP, free acid and other impurities. After precipitation, the modified polymer was collected and dried at 40 °C *in vacuo* for 48 hours. The degree of modifications achieved and corresponding yields are given in **Table 3.1**.

### 3.2.6 Modification of hyperbranched polyglycidol

Similar procedure to LPG modification was used to modify HPG considering 1:1 molar ratio of HPG and **2**.

**Table 3.1** The modification degree and yield obtained in modification of LPG

Sample	RCOOH (mmol) <sup>a</sup>	-OH/ROOH	Time (days)	T (°C)	Modification degree (%) <sup>b</sup>	Yield (%)	
c {	LPG1	2	1:0.3	2	-	8	61
	LPG2	2	1:0.5	2	-	23	70
	LPG3	2	1:0.7	2	-	27	68
	LPG4	2	1:1	2	-	39	81
	LPG5	2	1:1.25	2	-	43	87
d {	LPG6	2	1:1	7	-	42	79
	LPG7	2	1:1	2	40	40	75
	LPG8	2	1:1	2	80	11	65

<sup>a</sup> Stoichiometric amounts of DCC and DMAP in each case

<sup>b</sup> Average value determined by <sup>1</sup>H NMR

<sup>c</sup> Series 1

<sup>d</sup> Series 2



### 3.3 Characterization and Measurements

$^1\text{H}$  and  $^{13}\text{C}$  NMR spectra were recorded at 400 and 100.4 MHz, respectively, on a Varian Gemini 400 spectrometer with proton noise decoupling for  $^{13}\text{C}$  NMR. The  $^{13}\text{C}$  NMR spectra of the polymers were recorded at 30 °C, with a flip angle of 45°, and the number of transients ranged from 20,000 to 40,000 with 10–20% (w/v) sample solutions in  $\text{CDCl}_3$ . The central peak of  $\text{CDCl}_3$  was taken as the reference, and the chemical shifts were given in parts per million from TMS (tetramethyl silane).

Thermal transitions were detected with a Mettler–Toledo differential scanning calorimeter mod. 822 in dynamic mode at a heating or cooling rate of 10 °C/min. Nitrogen was used as the purge gas. The calorimeter was calibrated with an indium standard (heat flow calibration) and an indium–lead–zinc standard (temperature calibration).

Clearing temperatures were roughly estimated using polarized optical microscopy (POM); textures of the samples were observed with an Axiolab Zeiss optical microscope equipped with a Linkam TP92 hot stage.

Densities were determined by gas pycnometry using Micromeritics AccuPyc 1330 device at 30 °C.

Average molecular weights were determined by size exclusion chromatography (SEC); analyses were carried out with an Agilent 1200 series system with PLgel 3  $\mu\text{m}$  MIXED-E, PLgel 5  $\mu\text{m}$  MIXED-D, and PLgel 20  $\mu\text{m}$  MIXED-A columns in series, and equipped with an Agilent 1100 series refractive-index detector. Calibration curves were based on polystyrene standards having low polydispersities. THF was used as an eluent at a flow rate of 1.0  $\text{mL min}^{-1}$ , the sample concentrations were 5–10  $\text{mg mL}^{-1}$ , and injection volumes of 100  $\mu\text{L}$  were used.

For X-ray diffraction experiments, the polymer films were prepared on a glass plate by heating to isotropic melt and cooling slowly down to room temperature at  $10^{\circ}\text{C}/\text{min}$ . Measurements were made using a Bruker-AXS D8-Discover diffractometer equipped with parallel incident beam (Göbel mirror), vertical  $\theta$ - $\theta$  goniometer and XYZ motorized stage. The GADDS detector was a HI-STAR (multiwire proportional counter of  $30 \times 30 \text{ cm}$  with a  $1024 \times 1024$  pixel). Samples were placed directly on the sample holder for transmission mode. The X-ray diffractometer was operated at 40 kV and 40 mA to generate  $\text{CuK}\alpha$  radiation. Two analytical conditions were used;

For low  $2\theta$  range: collimator,  $100 \mu\text{m}$ ; distance sample-detector, 30 cm. The collected *frame* (2D XRD pattern) covers a range from  $0.9$  up to  $9.2^{\circ} 2\theta$ . The diffracted X-ray beam travelled through a He filled chamber (SAXS attachment) to reduce the air scattering at low angles. The direct X-ray beam was stopped by a beam stop placed directly on the detector face. The exposition time was 1800s per frame and it was first chi-integrated to generate the conventional  $2\theta$  vs. intensity diffractogram and after it was  $2\theta$ -integrated to generate a Chi vs. intensity diffractogram.

For medium  $2\theta$  range: collimator,  $500 \mu\text{m}$ ; distance sample-detector, 9 cm. The collected *frame* (2D XRD pattern) covers a range from  $3.0$  up to  $25.5^{\circ} 2\theta$ . The direct X-ray beam is stopped by a beam stop placed behind the sample with an aperture of  $4^{\circ}$ . The exposition time was 300s per frame and it was first chi-integrated to generate the conventional  $2\theta$  vs. intensity diffractogram and after it was  $2\theta$ -integrated to generate a Chi vs. intensity diffractogram.

### 3.4. Results and discussion

#### 3.4.1. Synthesis of 3,4,5-tris[4-(n-dodecan-1-yloxy)benzyloxy]benzoic acid

As mentioned previously, the aim of this work was to obtain polyethers like linear and hyperbranched polyglycidols bearing the dendron 3,4,5-tris[4-(n-dodecan-1-yloxy)benzyloxy]benzoate, so that the formation of hexagonal columnar mesophases could be induced. The chemical modification of these polyols was carried out by Steglich esterification using bulky tapered group having  $-\text{COOH}$  as a reacting group.

The necessary compound **2** to be utilised in chemical modification of LPG and HPG was prepared from **1**. The synthesis of **2** is schematically represented in **Scheme 3.1**. Purity and structure of the product was checked with literature<sup>11</sup>. The structure of the **2** was confirmed by  $^1\text{H}$  (**Figure 3.1**) and  $^{13}\text{C}$  (**Figure 3.2**) NMR spectra and compared to literature<sup>12</sup>. As per the literature<sup>12</sup>, **2** itself is a liquid crystalline material showing hexagonal columnar mesophase. According to Percec et al<sup>12</sup>, it is having a melting temperature  $68\text{ }^\circ\text{C}$  and clearing temperature  $145\text{ }^\circ\text{C}$ .

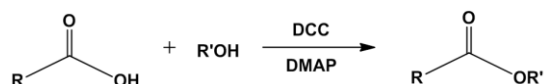
#### 3.4.2. Synthesis of linear polyglycidol

As explained in experimental part and shown in **Scheme 3.2**, (1-ethoxyethyl)glycidyl ether was synthesised from glycidol according to Fitton et al<sup>13</sup>. The structure of the obtained (1-ethoxyethyl)glycidyl ether was confirmed by  $^1\text{H}$  (**Figure 3.3**) and  $^{13}\text{C}$  NMR (**Figure 3.4**). The given structure was also compared to the literature<sup>13</sup>. After synthesis of (1-ethoxyethyl)glycidyl ether, as explained in experimental part, linear poly[(1-ethoxyethyl)glycidyl ether] was prepared from (1-ethoxyethyl)glycidyl ether according to Schmitz et al<sup>14</sup>. Linear polyglycidol was prepared by subsequent removal of the acetal protecting groups of linear poly[(1-ethoxyethyl)glycidyl ether] under acidic hydrolysis conditions (**Scheme 3.3**).

The structure of the obtained linear poly[(1-ethoxyethyl)glycidyl ether] was confirmed by  $^1\text{H}$  (**Figure 3.5**) and  $^{13}\text{C}$  NMR (**Figure 3.6**) and compared to the literature<sup>14</sup>; also the structure of the polyether obtained by deprotection of linear poly[(1-ethoxyethyl) glycidyl ether] was confirmed by  $^1\text{H}$  and  $^{13}\text{C}$  NMR techniques as shown in **Figure 3.7** and **3.8**, respectively. The presence of the aromatic ring as a head group, allowed calculating the degree of polymerization (DP) from  $^1\text{H}$  NMR spectra, by comparing the integrated areas of the peaks coming from aromatic, aliphatic and alcoholic protons as shown in Figure 3.7. DP resulted equal to 20.

### 3.4.3. Chemical modification of linear polyglycidol

The Steglich esterification is a mild reaction, which allows the conversion of sterically hindered alcohols to ester, by use of DCC and DMAP as shown in **Scheme 3.5**. Steglich esterification is usually carried out at room temperature.



**Scheme 3.5. Steglich esterification**

Mechanism of the Steglich Esterification:

DCC and the carboxylic acid are able to form an *O*-acylisourea intermediate, which offers reactivity similar to the corresponding carboxylic acid anhydride. The alcohol may now add to the activated carboxylic acid to form the stable dicyclohexylurea (DHU) and the ester (**Figure 3.9 A**). In practice, the reaction with carboxylic acids, DCC and amines leads to amides without problems, while the addition of DMAP is crucial for the efficient formation of esters (**Figure 3.9 B**).

In this way, we applied Steglich esterification in chemical modification of LPG. It has been observed that these polyols can be modified by carboxylic

group of **2** at room temperature using DCC and DMAP in stoichiometric amounts (**Scheme 3.4**). In case of LPG, we studied this chemical modification under different reaction conditions. These reaction conditions and their corresponding degrees of modification along with product yields are given in **Table 3.1**.

In most cases esterification was carried out at room temperature, since the side product N-acyl urea formation is less likely at lower temperature; in other words, high temperatures favour the formation of side products and are therefore expected to reduce modification degrees correspondingly. This side-reaction is a 1,3-rearrangement of the O-acyl intermediate to a N-acyl urea which is unable to further react with the alcohol (**Scheme 3.6**). N-acyl urea is easy to get washed out during precipitation and causes low degree of modification<sup>17</sup>.

We considered **LPG1** to **LPG5** as series 1 and from **LPG6** to **LPG8** as series 2. In case of series 1, apart from the –OH/ROOH molar ratio, there is no change in reaction time and temperature and it can be seen that in this case the degree of modification increases with increase in molar ratio; finally, we got 43% of degree of modification in case of **LPG5**.

In case of series 2, we studied the effect of increase in reaction time and temperature on degree of modification. According to our previous experience<sup>11,16</sup>, usually reaction time also affects the degree of modification but, as it can be seen in case of **LPG6**, the degree of modification could not be increased on increasing reaction time up to 7 days. As far as reaction temperature is concerned, in case of **LPG7**, an increase in reaction temperature up to 40 °C did not affect the reaction since a degree of modification of 40% was reached. On the other hand, in case of **LPG8**, the degree of modification was significantly decreased up to 11% when the reaction temperature was 80 °C.

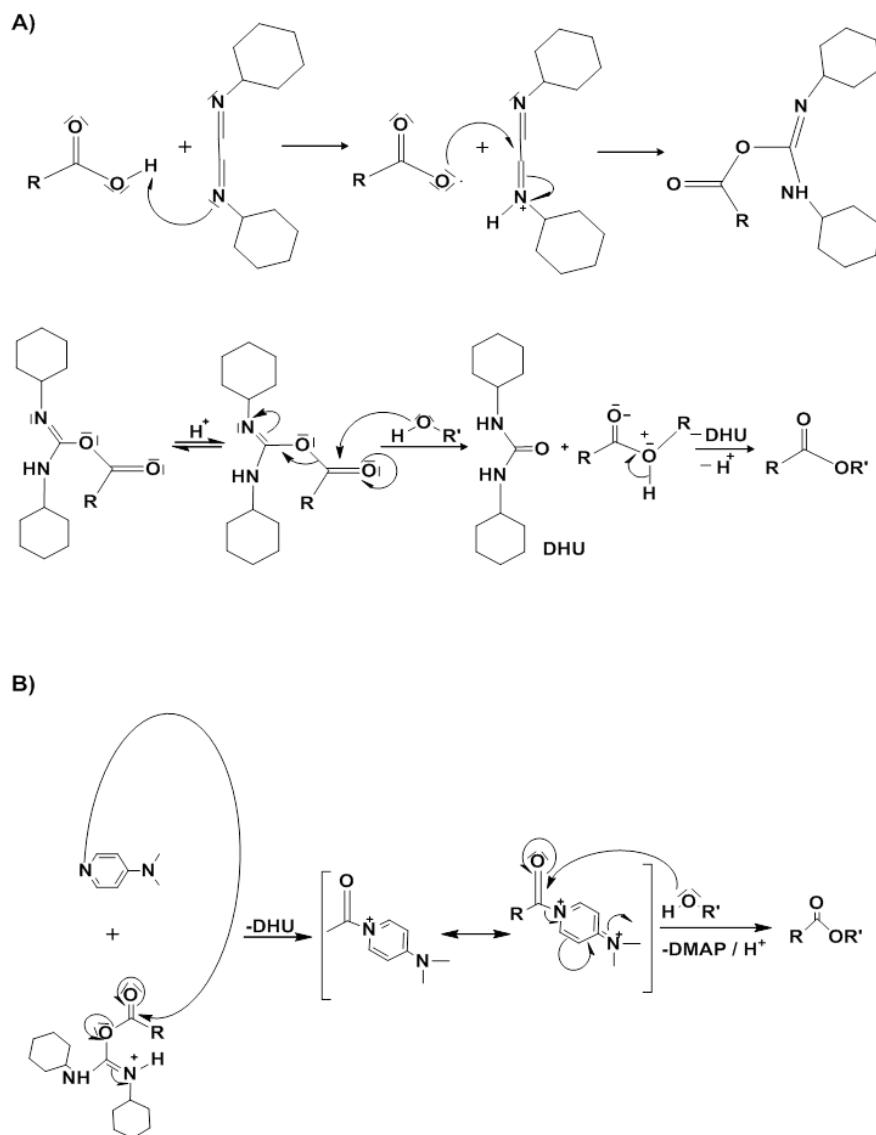


**Figure 3.9. Reaction mechanism of Steglich esterification: A) ester formation by carboxylic acids, DCC and amines B) efficient ester formation by addition of DMAP**



### Scheme 3.6. 1,3-rearrangement of the O-acyl intermediate to a N-acyl urea

After overall effects of molar ratio, time and temperature, we suppose a modification plateau of 43%, which could not be further modified by increasing reaction duration and temperature. Reaction yield could not be improved beyond 87% (**LPG5**); however one should take into account that, in order to get rid of DMAP and DCC several precipitations were required which caused loss of product and turned into low product yield.

The structure of the copolymers was characterized by NMR spectroscopy. **Figure 3.10** reports the  $^1\text{H}$  NMR spectrum of modified **LPG1** as an example. All  $^1\text{H}$  NMR spectra are characterized by broad signals in three regions. The aromatic region shows three signals at 7.2, 6.8, and 6.7 ppm. Considering the relative integration areas and by comparison with the spectrum of methyl 3,4,5-tris(*n*-dodecan-1-yloxy)benzoate, the signal at 7.2 (8H) can be assigned to the protons of the benzoate group plus the aromatic protons ortho to the benzylic carbon  $-\text{CH}_2\text{O}-$ . The signals at 6.8 and 6.6 ppm (4H+2H) correspond to the aromatic protons meta to the benzylic carbon  $-\text{CH}_2\text{O}-$  of the lateral and central alkyloxybenzyloxy substituents respectively. The characteristic signals, corresponding to most protons of the dodecyloxy alkyl chains in the dendron, can be observed in the high-field region at 1.7, 1.4, 1.3, 1.2, and 0.8 ppm. The most interesting region lies between 5 and 3.4 ppm in which five signals can be observed. The two signals at 4.4 and 4.3 ppm correspond to the methylenic protons **c'** in the modified monomeric unit; in this region also the signals coming from the free  $-\text{OH}$  groups are overlapped. The signal at 3.9 ppm corresponds to the methylene attached to the oxygen in the alkyl chains of the mesogenic unit and methinic proton **b'**. The broad signals between 3.8 and 3.4 ppm correspond

to the methylenic and methinic protons **a**, **a'**, **b**, and **c** in the modified and unmodified monomeric units. Finally, the signal centered at 4.9 ppm can be assigned to the benzylic methylenes of the dodecyloxybenzyloxy substituent.

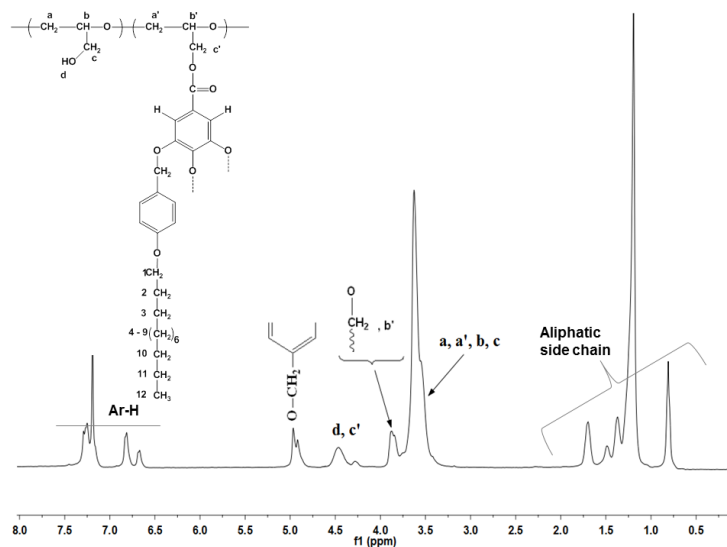


**Figure 3.10.**  $^1\text{H}$  NMR spectrum of modified LPG1 in  $\text{CDCl}_3$

**Figure 3.11** shows the  $^{13}\text{C}$  NMR spectrum of modified **LPG1** with the corresponding assignments. The aromatic carbons and the carbonyl carbon appear between 166 and 108 ppm, whereas carbons 2–12 of the aliphatic alkyl chains appear in the region between 32 and 14 ppm. The carbons of the backbone appear in the central region of the spectrum. The methine and side methylenic carbons of the modified and unmodified monomeric units appear at different chemical shifts. Thus, **b** and **b'** appear at 80.6 and 77.4 ppm, while **c** and **c'** appear at 62.2 and 64.4 ppm respectively. The carbons **a** and **a'** appear overlapped at 69.5 ppm. Carbon 1 of the alkyl chains appears as a sharp at 67.8 ppm. The chemical shifts of the benzylic methylenes depend on their relative position in the benzoate ring. Those in position 3 and 5 appear at 71.1 ppm, whereas the same carbon in position 4 appears overlapped with peaks coming from 1,1,2,2-tetrachloroethane- $d_2$ .



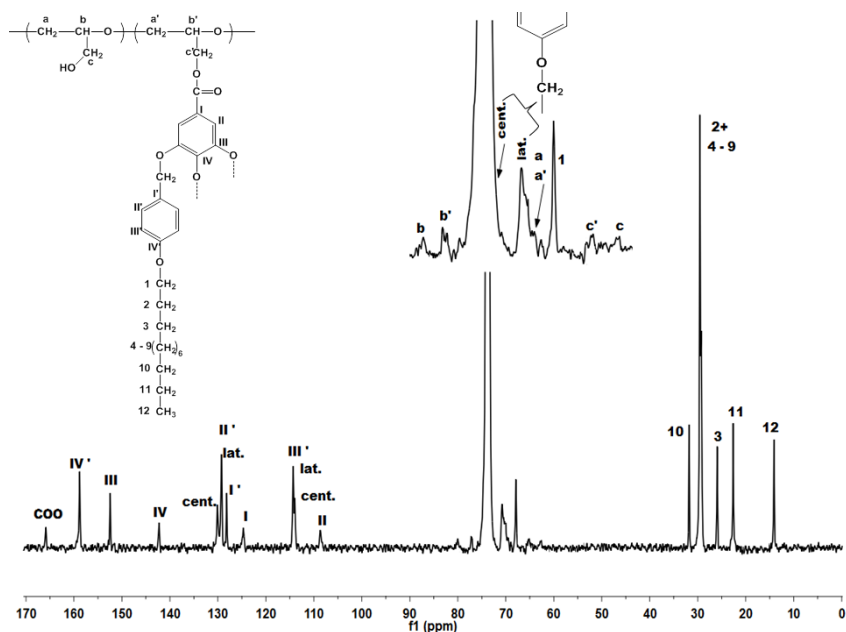


**Figure 3.11.**  $^{13}\text{C}$  NMR spectrum of modified LPG1 in 1,1,2,2-Tetrachloroethane- $d_2$

The degree of modification of modified polymer was calculated by  $^1\text{H}$  NMR spectroscopy because this methodology gave good results in previous studies<sup>11,16</sup>. Quantification was carried out by comparing the areas of the aromatic peaks between 7.4 and 6.6 ppm and the benzylic proton signal at 4.9 ppm with the broad signal between 3.8 and 3.4 ppm.

Molecular weights and polydispersities of LPG derivatives determined by SEC are reported in **Table 3.2**. The introduction of the dendritic groups can lead to significant changes in the hydrodynamic volume with respect to the starting polymer, and can sometimes induce unexpected trends of the molecular weights with the modification degree. However, in this case one can see that molecular weight increases with modification degree, as expected. In general terms, the density values (**Table 3.2**) did not exhibit appreciable variation; slightly higher

values were found in the case of **LPG5-LPG7**, which also showed higher polydispersities.

**Table 3.2 Average molecular weights and densities of the modified LPG**

Sample	Modification degree (%)	$M_n \cdot 10^{-3b}$	$M_w \cdot 10^{-3b}$	$\frac{M_w}{M_n^b}$	$\rho$ (g/cm <sup>3</sup> ) <sup>c</sup>
LPG1	8	2.70	3.19	1.18	1.07
LPG2	23	4.79	6.57	1.37	1.07
LPG3	27	5.16	7.34	1.42	1.08
LPG4	39	7.36	10.87	1.47	1.08
LPG5	43	7.62	12.76	1.62	1.17
LPG6	42	7.52	11.46	1.52	1.17
LPG7	40	7.11	10.93	1.53	1.17
LPG8	11	2.93	3.57	1.21	1.07
LPG <sup>a</sup>	-	-	1.48 <sup>d</sup>	-	1.02

<sup>a</sup> Unmodified linear polyglycidol.

<sup>b</sup> Determined by SEC

<sup>c</sup> Determined at 30°C. Error: ± 3%

The mesomorphic phases were investigated by the Differential Scanning Calorimetric (DSC), Polarised Optical Microscopy (POM) and confirmed by X-ray diffraction (XRD).

DSC and POM were used to investigate the clearing temperature of modified LPG. **Table 3.3** shows the clearing temperature ranges and the glass transition temperatures of the whole LPG series.

**Table 3.3 Clearing temperature ranges and glass transition temperatures of the modified LPG**

Sample	Modification degree (%)	$T_g$ (°C) <sup>a</sup>	$T_c$ (°C) <sup>b</sup>
<b>LPG</b>	-	-10	-
<b>LPG1</b>	8	-10	32-35
<b>LPG2</b>	23	-30	71-75
<b>LPG3</b>	27	-32	79-84
<b>LPG4</b>	39	-27	97-101
<b>LPG5</b>	43	-16	116-120
<b>LPG6</b>	42	-21	95-98
<b>LPG7</b>	40	-13	95-99
<b>LPG8</b>	11	-20	49-52

<sup>a</sup> Determined by DSC second heating scan

<sup>b</sup> Determined by DSC second heating scan and POM

The liquid crystalline textures of LPG samples were observed by POM after annealing the samples for two hours at a temperature slightly lower than their respective clearing temperatures, in order to favour the growth of the liquid crystalline domains. POM images of both series are shown in **Figure 3.12**. A typical broken fan-shaped arrangement of hexagonal columnar mesophase can be seen in case of **LPG2-LPG7**, whose modification degrees range approximately between 20 and 40%. At variance, **LPG1** and **LPG8**, with modification degrees around 10%, exhibited different textures by POM.

In order to confirm these mesophases **LPG1**, **LPG2**, **LPG3** and **LPG4** were studied by XRD analysis. **LPG5-LPG7** have modification degrees quite close to **LPG4** and, in the case of **LPG6** and **LPG7**, the clearing range was also similar to **LPG4**. Therefore we considered reasonable to extend the results from XRD experiments on **LPG4** also to **LPG5-LPG7**. For this reason, only samples from **LPG1** to **LPG4** were analysed by XRD technique and the corresponding mesophases are explained in further discussion. In case of **LPG8**, similar

mesomorphic behaviour was observed in DSC and POM to **LPG1**. Therefore we expected alike XRD results.

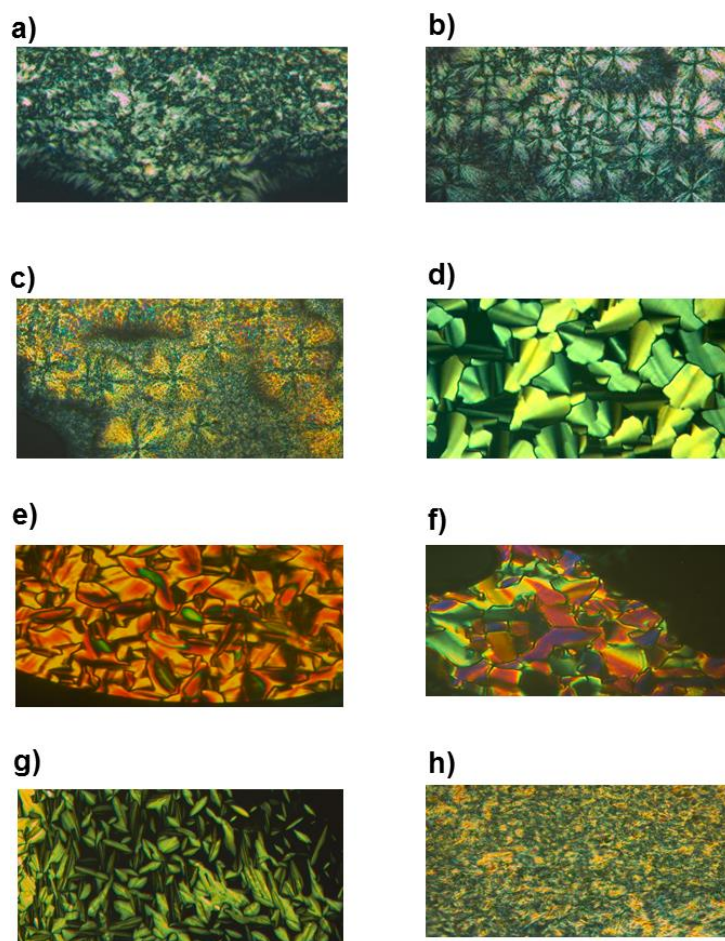


**Figure 3.12.** Optical micrographics between crossed polars of a) LPG1, 30 °C b) LPG2, 69 °C c) LPG3, 79 °C d) LPG4, 97 °C e) LPG5, 116 °C f) LPG6, 94 °C g) LPG7, 93 °C and f) LPG8, 47 °C

The intensity vs  $2\theta$  graph of **LPG1** at room temperature after slow cooling from isotropic melt is shown in **Figure 3.13**. It shows only two signals, a sharp reflection at  $2\theta$  around  $2.1^\circ$ , corresponding to a d-spacing of 42.0 Å, and a broad halo at  $2\theta$  around  $20^\circ$ , giving a d-spacing of 4.5 Å. From our previous experience, the sharp reflection could correspond to  $d_{100}$ , of a columnar

mesophase ( $Co$ ), while the halo to  $d_{001}$  (lateral distance between adjacent dendrons on the column).

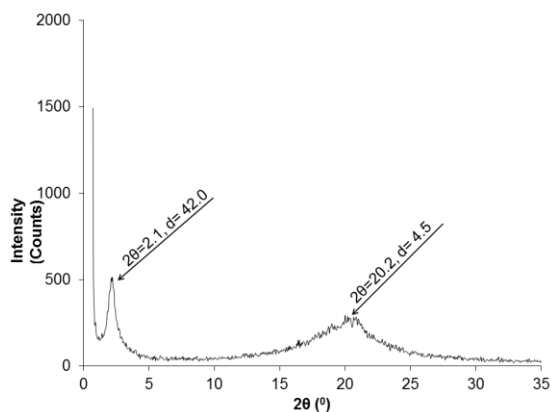


**Figure 3.13.** X-ray diffraction pattern of LPG1 at room temperature after cooling down from isotropic melt

Intensity vs  $2\theta$  graphs at room temperature after slow cooling from isotropic melt of samples **LPG2** and **LPG3** are shown in **Figure 3.14** and **Figure 3.15** respectively.

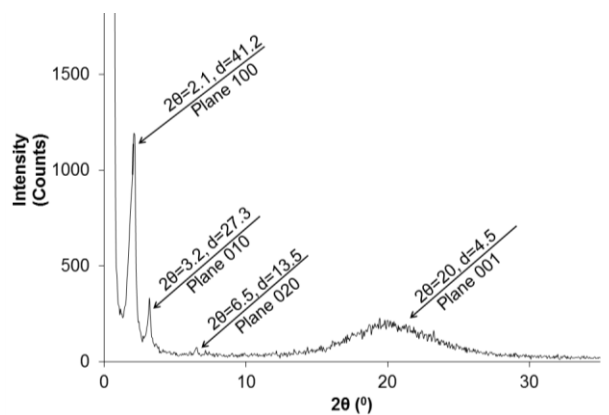


**Figure 3.14.** X-ray diffraction pattern of LPG2 at room temperature after cooling down from isotropic melt

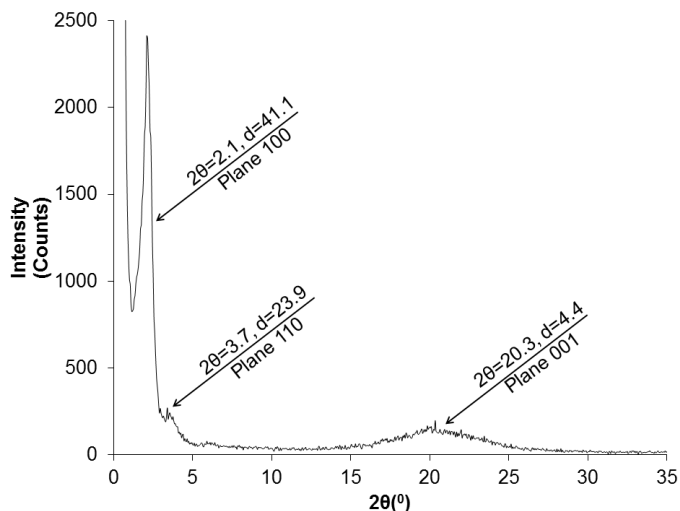


**Figure 3.15.** X-ray diffraction pattern of **LPG3** at room temperature after cooling down from isotropic melt

**LPG2** shows three sharp  $2\theta$  reflections at  $2.1^\circ$ ,  $3.2^\circ$  and  $6.5^\circ$  corresponding to  $d = 41.2 \text{ \AA}$ ,  $d = 27.3 \text{ \AA}$  and  $d = 13.5 \text{ \AA}$  respectively, and a diffuse halo centered around  $2\theta = 20^\circ$  giving  $d$ -spacing about  $4.5 \text{ \AA}$ . **LPG3** shows two sharp  $2\theta$  reflections at  $2.1^\circ$  and  $3.7^\circ$  corresponding to  $d = 41.1 \text{ \AA}$  and  $d = 23.9 \text{ \AA}$  respectively, and a diffuse halo centered around  $2\theta = 20^\circ$  giving  $d = 4.4 \text{ \AA}$ .

In general, the  $d$ -spacings of sharp reflections in the ratio of  $1:1/\sqrt{3}:1/2$  and a diffuse halo given at high angle confirm the presence of a hexagonal columnar mesophase ( $Col_h$ ): The first three sharp reflections corresponds to the planes  $d_{100}$ ,  $d_{110}$ ,  $d_{200}$  respectively, while the broad halo is related to  $d_{001}$ . This is the case of the polymer **LPG3**, although the usually less intense (200) reflections, could not be seen in this case. On the other hand, the X-ray diffraction pattern of polymer **LPG2** is in agreement with the less-symmetrical rectangular columnar mesophase ( $Col_r$ ). In this case, the sharp reflections at  $41.2$ ,  $27.3$  and  $13.5 \text{ \AA}$  can be assigned to (100), (010) and (020) planes, respectively. It must be noted, that the occurrence of a rectangular columnar

mesophase is also compatible with the broken fan shaped texture as observed by POM (**Figure 3.12**).

The X-ray diffraction pattern of sample **LPG4** (recorded at room temperature) shows three sharp reflections at  $2\theta = 1.9^\circ$ ,  $3.3^\circ$  and  $3.7^\circ$ , which correspond to  $d = 46.4 \text{ \AA}$ ,  $d = 26.4 \text{ \AA}$  and  $d = 23.5 \text{ \AA}$  respectively, and a diffuse halo centered around  $2\theta = 19^\circ$  giving  $d = 4.7 \text{ \AA}$ . The d-spacings of the sharp reflections are in the ratio  $1:1/\sqrt{3}:1/2$ , confirming the presence of hexagonal columnar mesophase ( $CoI_h$ ). Intensity vs  $2\theta$  graph at room temperature after slow cooling from isotropic melt is shown in **Figure 3.16**.

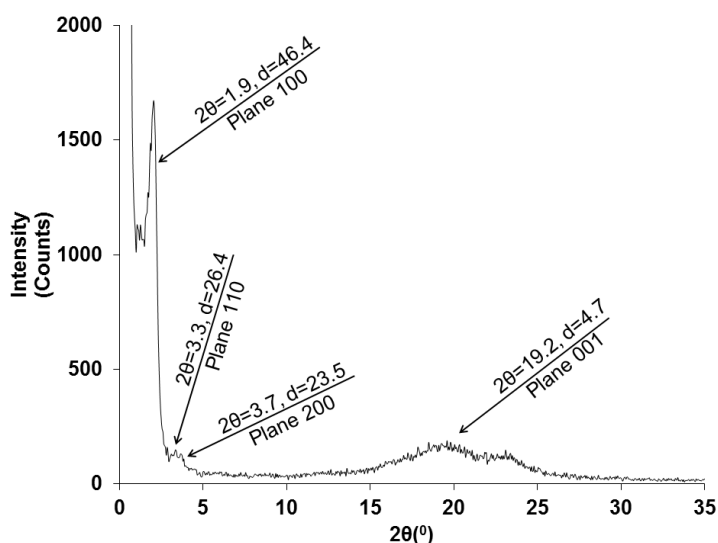


**Figure 3.16.** X-ray diffraction pattern of LPG4 at room temperature after cooling down from isotropic melt.

**Table 3.4** summarises the results of X-ray diffraction experiments of polymers **LPG1** to **LPG4** performed at room temperature.

**Table 3.4. X-ray diffraction data of modified LPG at room temperature**

Sample	Modification degree (%)	$d_{100}$ (Å)	$d_{010}$ (Å)	$d_{001}$ (Å)	$a^a$ (Å)	$\mu^b$	$\delta^c$	Mesophase <sup>d</sup>
LPG1	8	42.0	-	4.5	-	-	-	<i>Col</i>
LPG2	23	41.2	27.3	4.5	-	-	-	<i>Col<sub>r</sub></i>
LPG3	27	41.1	-	4.4	47.4	8	2.1	<i>Col<sub>h</sub></i>
LPG4	39	46.4	-	4.7	53.6	9	3.4	<i>Col<sub>h</sub></i>

<sup>a</sup> Dimension of the hexagonal unit cell

<sup>b</sup> Repeat units of polymer per unit cell

<sup>c</sup> Number of dendrons per unit cell

<sup>d</sup> *Col*: columnar, *Col<sub>r</sub>*: rectangular columnar, *Col<sub>h</sub>*: hexagonal columnar

As explained in chapter 2, knowing the experimental densities  $\rho$ , we can calculate the number of repeat units of polymer  $\mu$  that are present in a hexagonal prism layer of height  $c$  from the following equation:

$$\rho = \frac{2\mu M}{\sqrt{3}N_A a^2 c} \quad (4.1)$$

where  $M$  is the molecular weight of the repeat unit,  $N_A$  is Avogadro's number,  $a = 2(d_{100})/\sqrt{3}$  is the dimension of the hexagonal unit cell, and  $c = d_{001}\cos\chi$ , where  $\chi$  is the angle between the column axis and dendrons; if we assume that dendrons are perpendicular to the column axis,  $c = d_{100}$  and  $\mu$  can be calculated. By considering the experimental modification degree of the polymer  $\alpha$ , we can finally find the number of dendrons contained in a unit cell,  $\delta = \mu \times \alpha$ . According to the calculations, the average number of dendrons per unit cell of samples **LPG3** and **LPG4** is 2.1 and 3.4 respectively.



### 3.4.4. Chemical modification of hyperbranched polyglycidol

Sunder et al<sup>9</sup> described the controlled anionic ring opening polymerization of glycidol, making use of a partially deprotonated triol as alkoxide initiator. Also, demonstrated that anionic polymerization with rapid cation-exchange equilibrium, using slow monomer addition conditions can be employed to obtain hyperbranched polyols with polyether structure in a controlled manner. A simplified structure of HPG is shown in **Figure 3.17**.

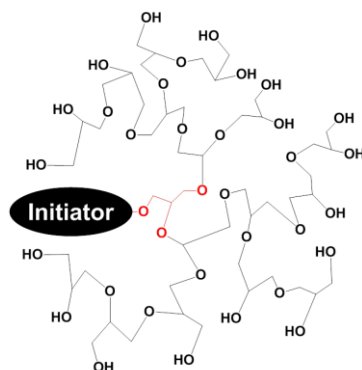


**Figure 3.17. Schematic structure of hyperbranched polyglycidol (HPG)**

Hyperbranched polyglycidol (HPG) was prepared according to this procedure. This synthesized hyperbranched polyglycidol bears 95 hydroxy end groups per molecule calculated by <sup>1</sup>H NMR. Its structure was confirmed by <sup>1</sup>H and <sup>13</sup>C NMR spectra shown in **Figure 3.18** and **3.19**, respectively, which were compared to the literature<sup>9</sup>: In <sup>1</sup>H NMR, chemical shifts at 4.9–4.4 ppm are assigned to OH, while a broad signal at 3.8–3.2 ppm to all CH and CH<sub>2</sub> of HPG. In <sup>13</sup>C NMR, chemical shift at 80.5–75.5 ppm is assigned to non-hydroxylated CH, while 74–67 ppm to CHOH, -CH<sub>2</sub>- and non-hydroxylated CH. Region between 63.9–61.0 ppm can be assigned to CH<sub>2</sub>OH.

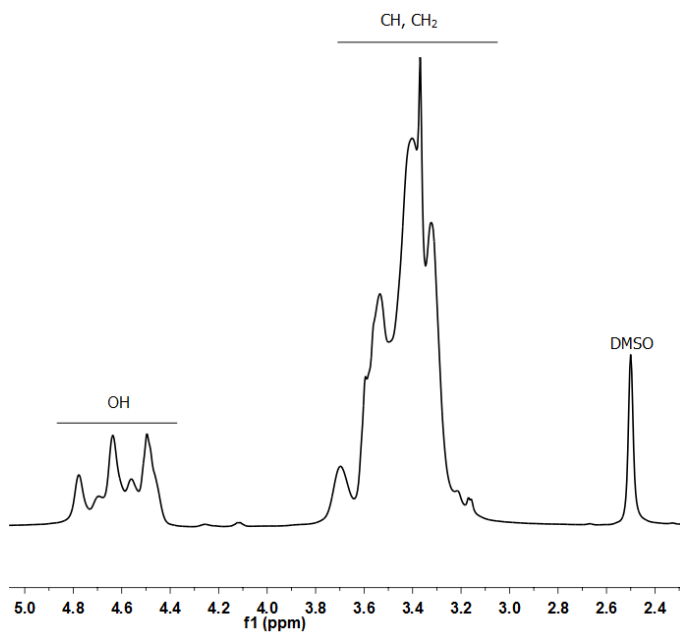


Figure 3.18.  $^1\text{H}$  NMR spectrum of HPG in deuterated DMSO

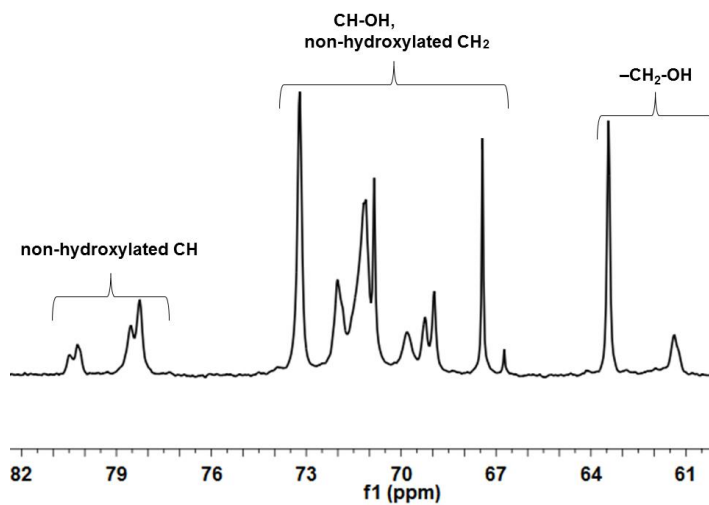


Figure 3.19.  $^{13}\text{C}$  NMR spectrum of HPG in deuterated DMSO

Once we have HPG, we proceed with its chemical modification through Steglich esterification with carboxylic acid **2**. In this case, we tested only the stoichiometric OH/RCOOH molar ratio 1:1. The reaction was performed at room temperature for two days. The structure of the modified HPG was confirmed by  $^1\text{H}$  and  $^{13}\text{C}$  NMR techniques.

$^1\text{H}$  NMR spectrum (**Figure 3.20**) of modified HPG is very similar to the one recorded to modified **LPG1** (**Figure 3.10**). For instance, shifts coming from aromatic, benzylic and dodecyloxy alkyl chains protons are appearing exactly at the same chemical shift than in case of modified **LPG1**. Also, in this case, the most interesting region lies between 5 and 3.4 ppm in which four signals can be observed. The signals at 4.6-4.2 ppm region correspond to the methylenic protons **c'** in the modified monomeric units; also in this region, signals coming from the free  $-\text{OH}$  are overlapped. The signal centered at 4.9 ppm can be assigned to the benzylic methylenes and methinic protons **c''** coming from modification of secondary alcohols in HPG. The signals at 3.9-3.4 ppm region correspond to methylene attached to the oxygen in the alkyl chains of the mesogenic unit and to all other CH and  $\text{CH}_2$  in the HPG backbone.

**Figure 3.21** shows the  $^{13}\text{C}$  NMR spectrum of modified HPG with the corresponding assignments. The carbonyl, aromatic carbons and carbons of aliphatic alkyl chains are appear approximately at the same chemical shifts than in case of modified **LPG1**. Signals due to all carbons located in the hyperbranched polyglycidol backbone appear at 82–60 ppm region. The peaks in the region between 78 to 81 ppm can be assigned to the non-hydroxylated CH carbons. Signals observed at 61 and 64 ppm can be assigned to the unmodified  $-\text{CH}_2\text{OH}$  and modified **c'** primary alcohol carbon, respectively. All other carbons located in the hyperbranched backbone give rise to the signals in the region 76–68 ppm; in this region also signals due to benzylic methylene carbons appear.

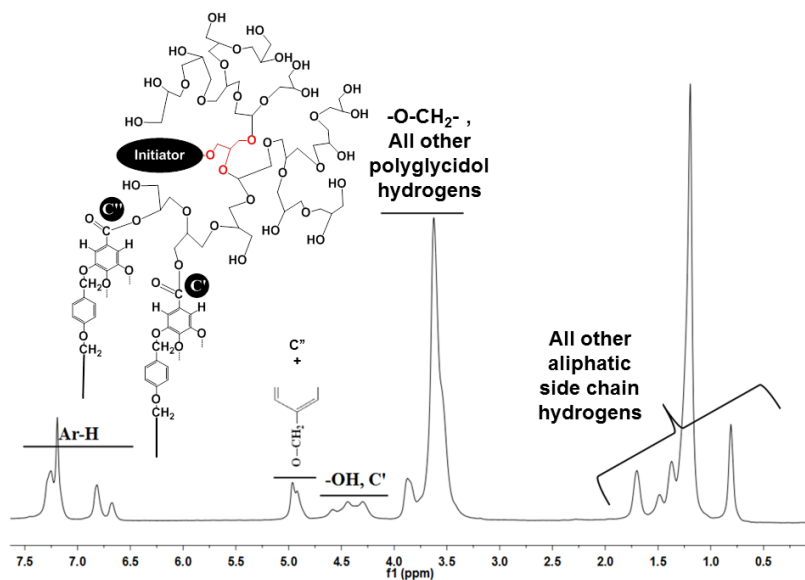


Figure 3.20.  $^1\text{H}$  NMR spectrum of modified HPG in deuterated  $\text{CDCl}_3$

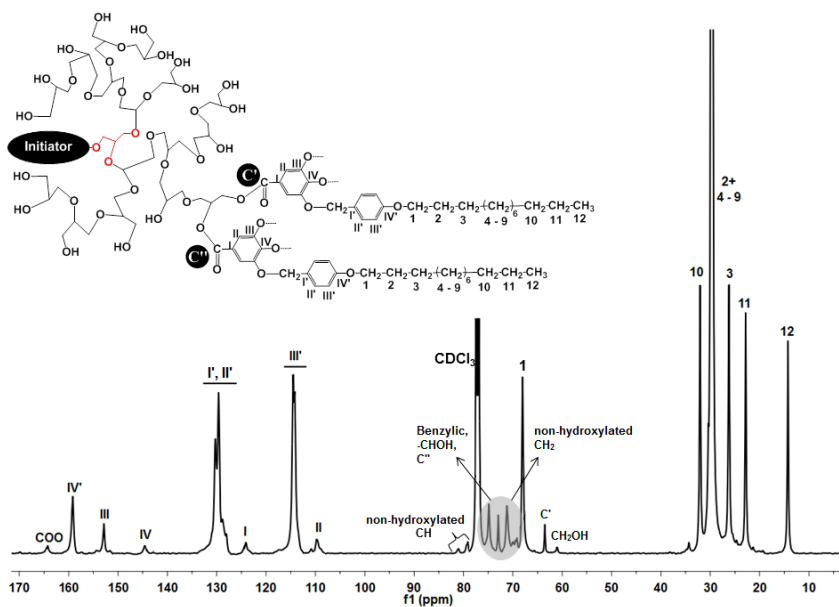


Figure 3.21.  $^{13}\text{C}$  NMR spectrum of modified HPG in deuterated  $\text{CDCl}_3$

The degree of modification was calculated by  $^1\text{H}$  NMR spectra. Integrated area between 7.5-6.5 ppm region corresponding to aromatic region compared with integrated area between 4.0-3.4 ppm region corresponding to -O-CH<sub>2</sub>- and all other polyglycidol hydrogens. Of course, this quantification was not easy since HPG itself is having complicated structure. Considering primary and secondary alcohols, it is unpredictable to know the modified alcohols whether they are primary or secondary, still we calculated degree of modification by considering both cases, that is, only all primary alcohols are modified and in another case only all secondary alcohols are modified. Degree of modification lies in the range of 11 to 12% with the yield of 68%. HPG exhibited no liquid crystalline behaviour as observed by POM and DSC. This can be ascribed to the very low modification degree of this sample, which is not sufficient to prompt LC behaviour; moreover, hyperbranched structures limits conformational freedom and, therefore, difficult the mesogens to interact to each other and give rise to the mesophase.

### 3.5 Conclusions

A new family of side-chain liquid-crystalline polyethers based on chemical modification of LPG was synthesized by Steglich esterification. Subsequently, chemical modification of HPG was also tested by considering only one modification of OH/RCOOH molar ratio 1:1. In case of chemical modification of LPG, it is found that effective modification occurs at room temperature. A plateau seems to be achieved for a degree of modifications of about 40%. Liquid crystalline properties of modified LPG and HPG were studied by POM and DSC. All modified LPG samples show liquid crystallinity and corresponding mesophases were further recognised by XRD. No liquid crystalline behavior was observed for modified HPG. Samples with lower degree of modification (**LPG1** and **LPG2**) show columnar and rectangular columnar mesophases, respectively, while samples with higher degree of modification (**LPG3** and **LPG4**) show hexagonal columnar mesophases.

### 3.6 References

1. Cameron, J. H.; Facher, A.; Lattermann, G.; Diele, S., Poly(propyleneimine) dendromesogens with hexagonal columnar mesophase. *Advanced Materials* **1997**, *9* (5), 398-403.
2. Baars, M. W. P. L.; Söntjens, S. H. M.; Fischer, H. M.; Peerlings, H. W. I.; Meijer, E. W., Liquid-Crystalline Properties of Poly(propylene imine) Dendrimers Functionalized with Cyanobiphenyl Mesogens at the Periphery. *Chemistry – A European Journal* **1998**, *4* (12), 2456-2466.
3. Tsiourvas, D.; Felekis, T.; Sideratou, Z.; Paleos, C. M., Liquid Crystals Derived from Cholesterol Functionalized Poly(propylene imine) Dendrimers. *Macromolecules* **2002**, *35* (16), 6466-6469.
4. Sunder, A.; Quincy, M.-F.; Mülhaupt, R.; Frey, H., Hyperbranched Polyether Polyols with Liquid Crystalline Properties. *Angewandte Chemie International Edition* **1999**, *38* (19), 2928-2930.
5. Percec, V.; Kawasumi, M., Synthesis and characterization of a thermotropic nematic liquid crystalline dendrimeric polymer. *Macromolecules* **1992**, *25* (15), 3843-3850.
6. Percec, V.; Chu, P.; Kawasumi, M., Toward "Willowlike" Thermotropic Dendrimers. *Macromolecules* **1994**, *27* (16), 4441-4453.
7. Ropponen, J.; Tuuttila, T.; Lahtinen, M.; Nummelin, S.; Rissanen, K., Thermal and X-ray powder diffraction studies of aliphatic polyester dendrimers. *Journal of Polymer Science Part A: Polymer Chemistry* **2004**, *42* (22), 5574-5586.
8. Felekis, T.; Tziveleka, L.; Tsiourvas, D.; Paleos, C. M., Liquid Crystals Derived from Hydrogen-Bonded Supramolecular Complexes of Pyridinylated Hyperbranched Polyglycerol and Cholesterol-Based Carboxylic Acids. *Macromolecules* **2005**, *38* (5), 1705-1710.
9. Sunder, A.; Hanselmann, R.; Frey, H.; Mülhaupt, R., Controlled Synthesis of Hyperbranched Polyglycerols by Ring-Opening Multibranching Polymerization. *Macromolecules* **1999**, *32* (13), 4240-4246.
10. Santiago, D.; Morell, M.; Fernández-Francos, X.; Serra, À.; Salla, J. M.; Ramis, X., Influence of the end groups of hyperbranched poly(glycidol) on the

cationic curing and morphology of diglycidylether of bisfenol A thermosets. *Reactive and Functional Polymers* **2011**, 71 (4), 380-389.

11. Ronda, J. C.; Reina, J. A.; Giamberini, M., Self-organized liquid-crystalline polyethers obtained by grafting tapered mesogenic groups onto poly(epichlorohydrin): Toward biomimetic ion channels 2. *Journal of Polymer Science Part A: Polymer Chemistry* **2004**, 42 (2), 326-340.

12. Percec, V.; Cho, W. D.; Mosier, P. E.; Ungar, G.; Yearley, D. J. P., Structural Analysis of Cylindrical and Spherical Supramolecular Dendrimers Quantifies the Concept of Monodendron Shape Control by Generation Number. *Journal of the American Chemical Society* **1998**, 120 (43), 11061-11070.

13. Fitton, A. O.; Hill, J.; Jane, D. E.; Millar, R., Synthesis of Simple Oxetanes Carrying Reactive 2-Substituents. *Synthesis* **1987**, 1987 (12), 1140-1142.

14. Schmitz, C.; Keul, H.; Möller, M., Synthesis of multi-arm-star polyglycidols of different architecture grafted with polyacrylate side arms. *European Polymer Journal* **2009**, 45 (9), 2529-2539.

15. Kohler, J.; Keul, H.; Moller, M., Post-polymerization functionalization of linear polyglycidol with diethyl vinylphosphonate. *Chemical Communications* **2011**, 47 (28), 8148-8150.

16. Bhosale, S. V.; Rasool, M. A.; Reina, J. A.; Giamberini, M., New liquid crystalline columnar poly(epichlorohydrin-co-ethylene oxide) derivatives leading to biomimetic ion channels. *Polymer Engineering & Science* **2013**, 53 (1), 159-167.

17. Goodman, M.; Felix, A.; Moroder, L.; Toniolo, C., *Synthesis of Peptides and Peptidomimetics*. Thieme Medical Publishers, Incorporated: 2002.





## *Chapter 4*

---

# *Preparation And Assessment Of Proton- Conducting Membranes Based On Homeotropically Aligned Side-Chain Liquid Crystalline Polyethers*

UNIVERSITAT ROVIRA I VIRGILI

PROTON-EXCHANGE BIOMIMETIC MEMBRANES BASED ON COLUMNAR SIDE-CHAIN LIQUID-CRYSTALLINE POLYETHERS

Suryakant Bhosale

Dipòsit Legal: T.188-2014

## 4.1 Introduction

During last three decades of intensive membrane preparation research, different techniques have been proposed to generate selective, permeable films, that is a membrane. "A membrane is a selective barrier between two phases"<sup>1</sup>. A membrane should always be associated with its application according to this definition. These applications can range from desalination, dialysis, filtration to gas separation. Depending on the desired application, different membrane morphologies may be sought. Basically, according to their morphology, membranes could be classified as dense or porous. Dense and porous membranes are distinct from each other based on the size of separated molecules. Dense membrane is usually a thin layer of dense matrix utilized in the separation process of small molecules (usually in gas or liquid phase) and transport occurs through this dense matrix due to different phenomena like, driving force of pressure, concentration or electrical potential gradient, reverse osmosis etc. Porous membranes are intended on separation of larger molecules such as solid colloidal particles, large biomolecules, etc., and in this case transport occurs through the pores. Mostly, porous membranes are distinguished into symmetric and asymmetric membranes (**Figure 4.1**). In symmetric membranes the diameter of pores is constant throughout the cross-section of the membrane. The pore size of asymmetric membranes are different in size.

The most used and thus important class of techniques for membrane preparation is called phase inversion.<sup>2</sup> These processes rely on the phase separation of polymer solutions producing porous polymer films. Often these structures can act as a membrane. Phase separation mechanisms can generally be subdivided in three main categories depending on the factor that induce demixing of polymer solution and non-solvent (a species not miscible with the polymer). By a change in this factor, asymmetric morphologies are posed on the polymer film<sup>3</sup>. Phase separation can be induced by different methods, for instance, temperature, chemical reactions and diffusion. By changing the temperature at the interface of the polymer solution, heat will be exchanged and demixing can be induced (temperature induced phase separation or TIPS). The

original polymer solution can also be subjected to a reaction which causes phase separation (reaction induced phase separation or RIPS).

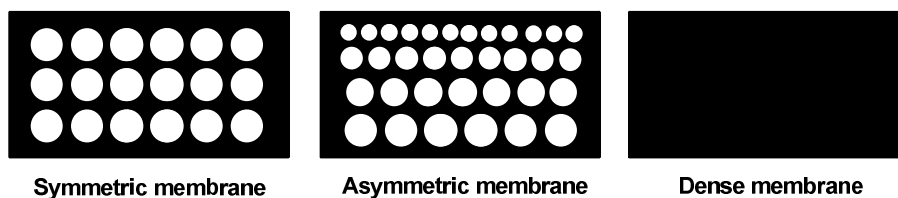


**Figure 4.1. Schematic representation of membrane morphologies**

By contacting a polymer solution to a liquid or vapor, diffusional mass exchange will lead to a change in the local composition of the polymer film and demixing can be induced (diffusion induced phase separation or DIPS).

The most used technique is diffusion induced phase separation, that is DIPS, as well TIPS and RIPS which actually were not used in our case. Membranes based on SCLCPs were preferentially synthesized by DIPS method.

Three types of techniques were developed to reach DIPS:

1. *Vapor precipitation*

Membrane formation by evaporation (porous structures) uses polymer solutions containing a volatile solvent, a less volatile non-solvent and a polymer. Preferential loss of solvent will generate meta- or unstable compositions and phase separation will be induced at this point.

2. *Evaporation*

When a polymer is subjected to a vapor containing a non-solvent, often symmetric structures are generated.

3. *Immersion precipitation*

Immersion precipitation is achieved by diffusion of non-solvent from a coagulation bath into the polymer solution in the form of film and diffusion of solvent from the polymer solution into the non-solvent bath. These techniques are schematically represented in **Figure 4.2**.

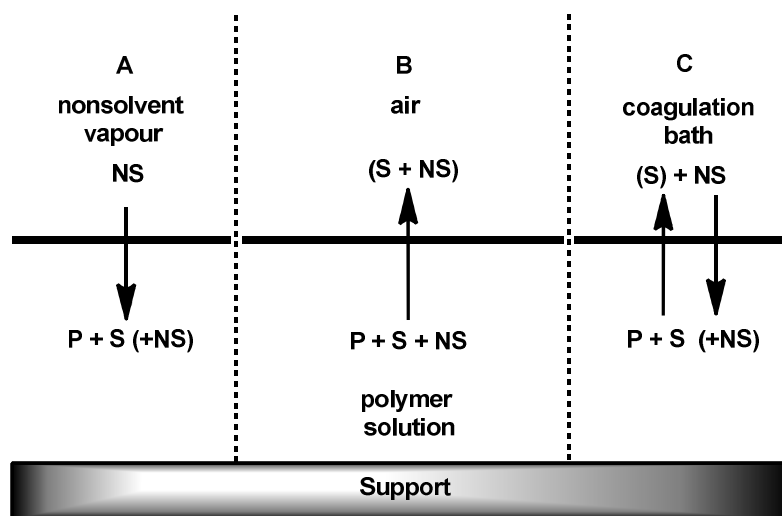


**Figure 4.2.** Schematic representation of three DIPS processes: A) precipitation with non-solvent vapor, B) evaporation of solvent, C) immersion precipitation. Main direction of diffusion of the different species is indicated by arrows. Polymer, solvent and non-solvent are represented with P, S and NS respectively. Components which are not necessary to be present in the original polymer solution and coagulation bath are put between brackets.

As explained in the main introduction of this thesis, our membrane system is based on SCLC polyethers having hydrophilic ether linkage that would be used for the proton transport. For this effective proton transport, these SCLC polyethers need to be homeotropically oriented. The direction along which the molecules of a liquid crystal prefer to orient is called the director. Basically, there are three main types of the LC director ( $n$ ) alignment near solid wall or at the free surface. These are homeotropic, planar, and tilted orientations (**Figure 4.3**). The surface, which is in a contact with mesophase is usually considered to be flat on

the microscopic scale, and the position of the director near it is determined by polar  $\theta$  and azimuthal  $\varphi$  angles (**Figure 4.4**).

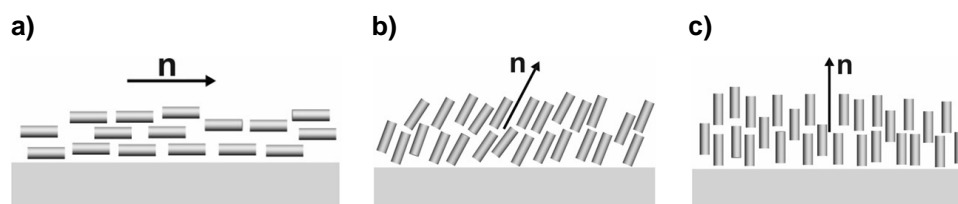


**Figure 4.3.** Types of liquid crystals orientation near surface where  $n$  is director: a) planar b) tilted and c) homeotropic

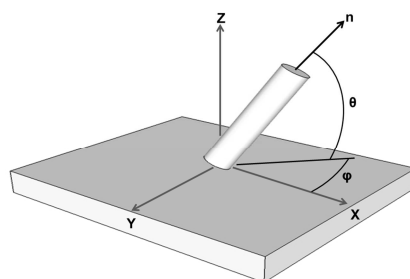


**Figure 4.4.** Position of director  $n$  near surface is determined by polar  $\theta$  and azimuthal  $\varphi$  angles

The director with planar orientation lies in the plane of the surface or phase separation border and in case of tilted orientation  $\theta$  is fixed and  $\varphi$  is arbitrary, while when the director  $n$  is oriented homeotropically, the polar angle  $\theta = 90^\circ$  (**Figure 4.4**). Thus, both planar and tilted orientation are not really useful in our case but homeotropic orientation is a significant orientation for actual proton transport through the membrane, to make the transport path as short as possible.

Tylkowski et al<sup>4</sup>, described the preparation of proton transport membranes based on a SCLCPs, which exhibited a columnar structure, obtained by chemically modifying poly(epichlorohydrin) (PECH) with a tapered group. The columns were homeotropically oriented, by casting and taking advantage of

surface interactions between the polymer and hydrophilic substrates. The oriented membranes exhibited proton transport comparable to Nafion<sup>®</sup>117. Out of three techniques of DIPS, oriented membranes were prepared by evaporation method as shown in **Figure 4.5** below: in a glass beaker (internal diameter: 2.7 cm), 5 g of a 4 wt.% polymer solution in chloroform was added dropwise to 3 g distilled water at room temperature. After a short time, the polymeric solution had moved to the bottom of the glass container and two liquid layers (organic at the bottom and aqueous on the top) could be clearly distinguished. Afterward, the two liquid phases were evaporated at 40 °C in an oven and membranes about 200 µm thick were obtained. Membranes were then dried at room temperature overnight. Thicker membranes could be obtained by increasing concentration of the polymer solution or by decreasing the beaker size. When a more concentrated polymer solution was used (i.e. 5 wt.%) or the contact areas between organic and aqueous phases were reduced (i.e. using a beaker with an internal diameter of 2.1 cm), thicker membranes (about 300 µm) with lower orientation were obtained. The same procedure was applied to obtain PECH membranes. The columns were successfully oriented in a homeotropic fashion as confirmed by X-ray diffraction (XRD), Environmental scanning electron microscope (ESEM) and Polarised optical microscope (POM).

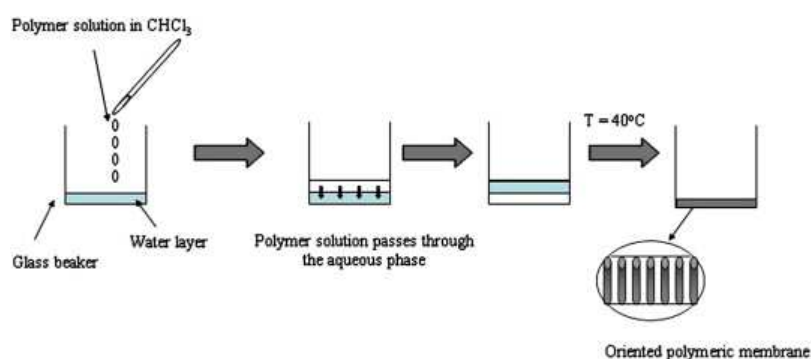


**Figure 4.5. Procedure for preparation of oriented membranes<sup>4</sup>**

The presence of oriented channels in the polymeric membrane resulted in remarkable proton permeability, around  $2 \cdot 10^{-6} \text{ cm}^2 \text{ s}^{-1}$ , comparable to that of Nafion<sup>®</sup> N117. The comparison between Na<sup>+</sup> concentration in the feed solution,



and the simultaneous pH variation in the stripping, suggested proton/cation antiport in the transport mechanism: that is, when protons move through the membrane, the cations move in the opposite direction as counter ions. On the other hand, poor proton transport could be detected on unoriented membranes based on the same SCLCPs or on unmodified PECH. But, the main drawback of this work is the limited reproducibility of the procedure used to prepare the oriented membranes.

After failure in reproducibility of this method, we started to look for other approaches. We tried different approaches of membrane preparation considering all technical and morphological aspects of the desired membrane, for instance, other two techniques of DIPS, that is immerse precipitation and vapor precipitation. Unfortunately, both these types of DIPS techniques failed to produce homeotropic orientation leading to look for other alternative methods. After reviewing the literature<sup>5,6</sup> about homeotropic orientation of SCLCPs, we developed a novel methodology and named it as Baking Process. In short, baking process is a method of obtaining SCLC polymeric film by cooling down to room temperature from its isotropic melt at a very slow cooling rate, for instance, 5 °C/min, while laying on an adequate support. Both hydrophilic glass and hydrophobic thin teflon sheet (approximately 150 µm thick) substrates were used to study the baking process on previously synthesized SCLCPs. These procedures resulted successful due to their reproducibility to organize ion conducting paths in a homeotropic fashion. This method opened a wide window to use previously synthesized SCLCPs, PECH and P(ECH-co-EO) to prepare homeotropically oriented polyether membranes based on SCLCPs leading to efficient proton transport. Apart from these methods, shear oriented membranes producing planar orientation were also prepared to compare with homeotropically oriented membranes.

As a last step, the assessment of the membranes which were successfully homeotropically oriented was performed to check proton transport by means of conductivity measurements. We measured proton conductivity of these oriented polyether films using AC four-probe EIS over a frequency range of 10<sup>7</sup> to 1 Hz.

## 4.2 Experimental

### 4.2.1 Materials

All chemical reagents and organic solvents were obtained from commercial sources and used without any further purification. As described in Chapter 2, all modified polyether samples were obtained by chemical modification of commercial PECH and (P(ECH-co-EO)) with potassium 3,4,5-tris[4-(n-dodecan-1-yloxy)benzyloxy] benzoate (HP and CP family, respectively). Two modifications from each family were selected: 63% modified **HP2** and 80% modified **HP3** were selected from PECH family, while 69% modified **CP1** and 59% modified **CP2** were selected from P(ECH-co-CO) family.

### 4.2.2 Preparation of hydrophilic glass substrate

Hydrophilic glass was prepared by using an ordinary glass plate by the procedure reported elsewhere<sup>7</sup>. Glass to be treated, was immersed in piranha solution (3:7 by volume of 30% H<sub>2</sub>O<sub>2</sub> and H<sub>2</sub>SO<sub>4</sub>) for 5 min. at room temperature to generate hydroxyl groups as well as to clean the surfaces. These substrates were washed with H<sub>2</sub>O, acetone, and MeOH, and dried. Hydrophilicity of the treated glass was confirmed by contact angle measurement.

### 4.2.3 Preparation of membranes based on SCLCPS by immersion precipitation

A casting solution 30% (w/w) was prepared by dissolving the polymer THF, then used a casting machine to spread the casting solution onto a treated glass surface or teflon sheet with a controlled thickness. The support with a wet film on top was then immersed in a bath of Milli-Q water (non-solvent). The solvent diffused into the precipitation bath, while the non-solvent diffused into the cast film. After a time in which the solvent and the non-solvent were exchanged, the polymer solution (wet film) became thermodynamically unstable and demixing took place. Finally, a solid polymer membrane was formed with an asymmetric structure, which could be peeled off from the glass. The overall

process of membrane preparation by immersion precipitation is shown in **Figure 4.6**.

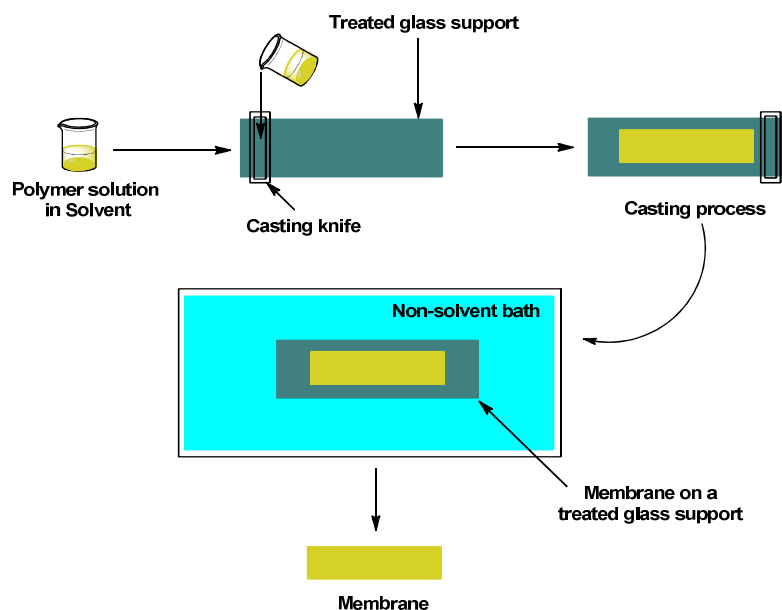


**Figure 4.6. Process of immersion precipitation**

#### 4.2.4 Preparation of membranes based on SCLCPS by vapor precipitation

In this process, membranes based on SCLCPs were obtained by putting in contact a polymeric solution with a non-solvent vapor, that is water vapor. It was crucial to design the system where the polymeric solution could get in contact with the water vapor. The overall system was prepared as shown in **Figure 4.7**. For achieving a highly humid atmosphere inside the glass container, a compressed air flow was forced to pass through two bubble bottles connected in series. The bubble bottles contained distilled water and, in addition, one of them was heated to 80°C in a water bath, in order to increase water content in the air flow. The conditions found within the container were 20 °C and 95% relative humidity. Inside this container, a membrane prepared by a casting machine from a solution 30% (w/w) on a treated glass support was kept until it gets precipitated into a polymer film.

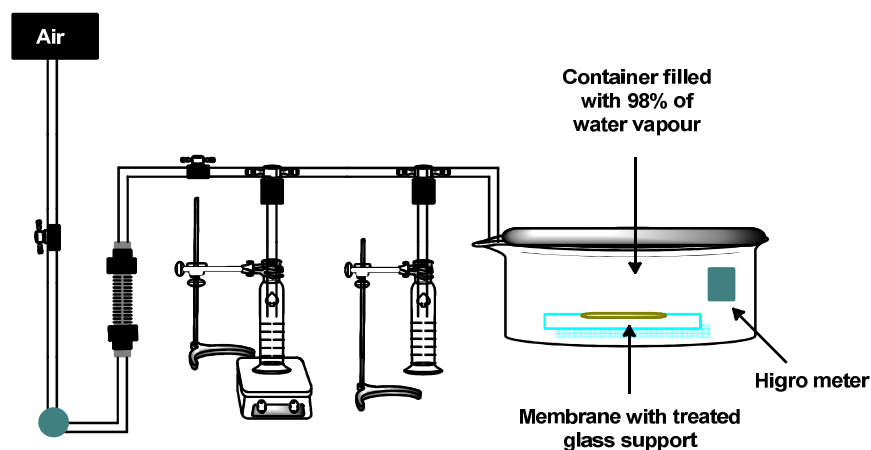


Figure 4.7. Process of vapor precipitation

#### 4.2.5 Membrane orientation by baking process

Membranes based on SCLCPs of thickness around 200  $\mu\text{m}$  were prepared by immersion precipitation on a teflon sheet as described in 4.2.3, dried overnight at room temperature in ambient condition and subsequently used for baking process. The polymer membrane (apprx. 2 cm diameter) along with teflon sheet was mounted on a hot stage of POM and it was heated above the isotropization temperature; then it was allowed to cool slowly (5  $^{\circ}\text{C}/\text{min.}$ ) down to room temperature. After baking process, the membrane was kept at room temperature for approximately 1 hour and then it was easily separated from the teflon sheet and obtained as an intact, uniform membrane (**Figure 4.8**). The appearance of the membrane is shown in **Figure 4.9**. As well this process was tested on hydrophilic substrate, that is, treated glass.

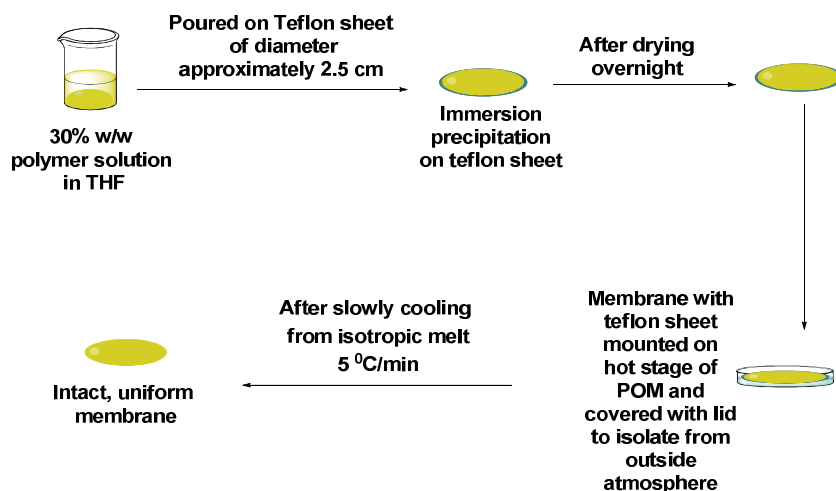


Figure 4.8. Baking process

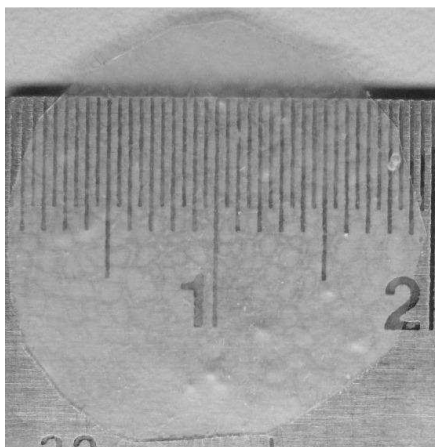


Figure 4.9. Oriented membrane of approximately 2 cm diameter obtained by baking process

#### 4.2.6 Preparation of membranes based on SCLCPs by shearing process

The polymers were mechanically oriented by shearing at temperatures slightly below the melting temperatures of the corresponding polymers on a silicon single crystal wafer surface cut parallel to the plane (510).

### 4.3 Characterisation techniques

Optical microscopy between crossed polars was performed at different temperatures depending on clearing temperatures of SCLCPs, with an Axiolab Zeiss optical microscope equipped with hot stage (LINKAM TP 92)

XRD patterns were obtained by using a Bruker-AXS D8-Discover diffractometer equipped with parallel incident beam (Göbel mirror), vertical  $\theta$ - $\theta$  goniometer, XYZ motorized stage and with a GADDS (General Area Diffraction Detector System). Samples were placed directly on the sample holder for reflection mode. An X-ray collimator system close-to-the-sample allows to analyze areas of 500  $\mu\text{m}$ . The X-ray diffractometer was operated at 40 kV and 30 mA to generate  $\text{CuK}_\alpha$  radiation. The GADDS detector was 30 x 30 cm with a 1024 x 1024 pixel CCD sensor placed at 30 cm from the sample. The collected frame (2D XRD pattern) covers at such distance a range from 0.9 up to 9.2<sup>o</sup> 2 $\theta$ . The diffracted X-ray beam travels through a He beam path (SAXS attachment) to reduce the air scattering at low angles. The exposition time was of 900s per frame.

The cross-sections and surface morphologies of the polymeric membranes were characterized by ESEM (Quanta 600, FEI). Cross-sections were prepared by fracturing the membranes in liquid nitrogen. When ESEM experiments were performed in high vacuum, samples were coated with a gold layer before observation.

The surface morphology of the oriented membranes was detected by atomic force microscopy (AFM) (Pico+, 5500, Agilent Technologies). The surface area of the topographical images was 1 x 1  $\mu\text{m}$ . A very thin cantilever tip (1 nm) AHR150-15 from Budget Sensors having resonance frequency of 150 kHz was used to investigate surface morphology of membranes in tapping mode.

The RMS roughness (root-mean-squared roughness) was calculated according to the equation given by Boussu et al<sup>8</sup>. The  $R_{\text{rms}}$  is given by the standard deviation of the data,

$$R_{rms} = \sqrt{\frac{\sum_{n=1}^N (Z_n - \bar{Z})^2}{N - 1}} \quad (4.1)$$

where,  $Z$  is the surface height,  $\bar{Z}$  is the average of the  $Z$  values within the given area,  $Z_n$  is the current  $Z$  value, and  $N$  is the number of data points within the given area.

The thickness of the membranes was measured using a micrometer with a sensitivity of 2  $\mu\text{m}$ . The measurements were carried out at various points, and the membranes were found to have constant thickness.

Static contact angles of deionized (DI) water on the substrates were measured using OCA15EC instrument which is equipped with DropImage Standard software. Measurements were made by delivering a 3  $\mu\text{L}$  drop of Milli-Q water from a microsyringe onto the surface of the sample mounted on an illuminated horizontal stage.

The integral electric resistance of the sample was measured by using a simple sensitive Ohm-meter of Keithley: 199 system DMM/Scanner.

The proton conductivity of membranes was measured using four-point probe conductivity cell (lab-made conductivity cell was used which was prepared in Centre For Surface Chemistry And Catalysis, Katholieke Universiteit Leuven, Belgium) at RH 5%, 50% and 100% at different temperatures range. In case of HPs, conductivities were measured at 30  $^{\circ}\text{C}$ , 50  $^{\circ}\text{C}$  and 70  $^{\circ}\text{C}$ , while in case of CPs, at 30  $^{\circ}\text{C}$  and 50  $^{\circ}\text{C}$ . Membrane impedance was determined using a  $M^2$  Materials Mate's 7260 Impedance Analyser. The impedance analyzer was worked in galvanostatic mode over frequency range from 1 Hz to  $10^7$  Hz by Nyquist method<sup>9</sup> using Zscore software. Each sample was cut in 3.14  $\text{cm}^2$  prior to mounting on the cell. The proton conductivity ( $\sigma$ ) was obtained by following formula :

$$\sigma = l/RS \quad (4.2)$$

where  $\sigma$  is the proton conductivity (S/cm), and  $l$  is the thickness of the membrane (cm).  $R$  is the membrane impedance ( $\Omega$ ) and  $S$  is the surface area for ion to penetrate the membrane ( $\text{cm}^2$ ). The impedance of each sample was measured five times to ensure data reproducibility and calculate standard deviations.



#### 4.4 Results and discussion

As explained before, our system consist of ion conducting paths having hydrophobic mesogenic side chains and hydrophilic ether linkages in polymer backbone. In the beginning, the idea was to use DIPS techniques to obtain oriented membranes: the anchoring of hydrophilic ether linkage to hydrophilic substrate would take place, while the mesogenic part would try to minimize the contact with hydrophilic non-solvent which in this case is water. In this way, considering this possibility, initially HP2 polymer was used to prepare membranes by immersion and vapor precipitation methods as explained in experimental part.

Hydrophilic glass substrate to be used for the membrane preparation by immersion and vapor precipitation was prepared as explained in the experimental part. The hydrophilicity of the glass was confirmed by contact angle measurements. **Figure 4.10** below shows the comparison between the contact angles of the untreated and treated glass. Contact angle of glass before treatment was  $49^{\circ}$  which was found to be decreased after treatment, as expected for more hydrophilic glass.

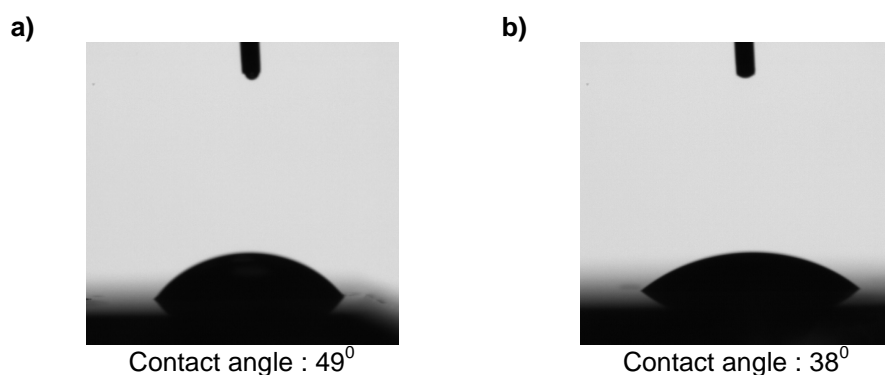


**Figure 4.10. Comparison of contact angles a) untreated glass and b) treated glass**

After membranes preparation by phase inversion, XRD technique was used to study their orientation. In XRD analysis, samples were analysed in

reflection mode as previously explained. Reflection mode is an effective and advanced mode to analyse thin film morphology compared to transmission mode. In transmission mode, which is a conventional method, X-ray radiation has a large penetration depth into any matter and, due to this property, X-ray diffraction is not surface sensitive; reflection mode is the technique to overcome this restriction since it is performed at a very low incident angle to maximize the signal from the thin layers. The stationary incident beam makes a very small angle with the sample surface, typically  $0.3$  to  $3^\circ$ , which increases the path length of the X-ray beam through the film. This helps to increase the diffracted intensity, while at the same time, reduces the diffracted intensity from the substrate. Overall, there is a dramatic increase in the film signal to background ratio. Since the path length increases when reflection mode is used, the diffracting volume increases proportionally. This is the reason for the increased signal strength.

As shown in **Figure 4.11** below, unfortunately both immersion and vapor precipitation techniques failed to get homeotropic orientation since, negligible orientation of Debye ring could be seen.

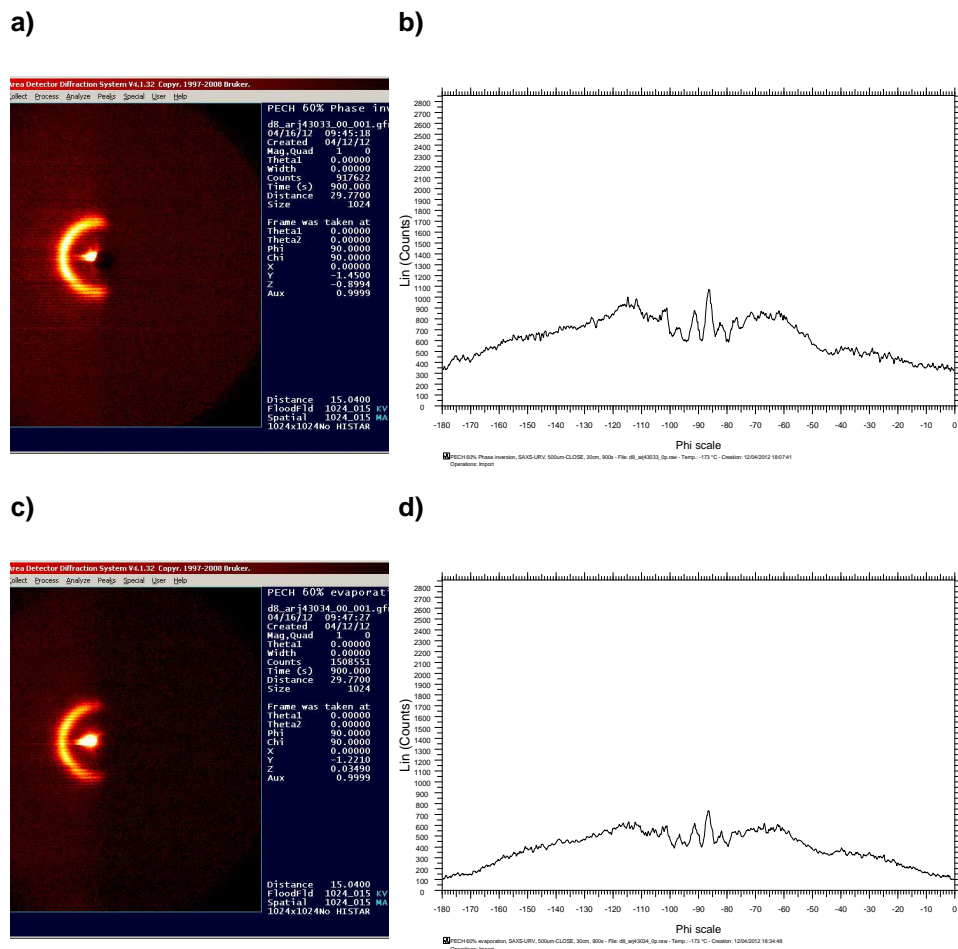


**Figure 4.11.** XRD analysis of membranes prepared from HP2 : a) Debye ring pattern and b) Phi diffractogram from azimuthal scan on the reflection at  $2\theta = 2.1^\circ$  of membrane prepared by immerse precipitation method; c) Debye ring pattern and d) Phi diffractogram from azimuthal scan on the reflection at  $2\theta = 2.2^\circ$  of membrane prepared by vapor precipitation method respectively

After a literature study about SCLCPs, we found very interesting information about homeotropic orientation of these kind of materials. Rapp et al reported<sup>5</sup> that local interactions, structure-directing elements, and order phenomena all together determine the self-assembly process of supramolecular

systems and how this assembly with its local molecular packing and dynamics is influenced by:

- (i) the polymer backbone,
- (ii) the generation of dendritic side groups, or
- (iii) the type and size of linkers.

For instance, the polymer poly(3',4',5'-tris[4''-(*n*-dodecyl-1-oxy)benzyloxy] benzylmethacrylate) referred as **G1-PMA**, was used to investigate self-assembly in a columnar fashion, which is well organized below as well as above  $T_g$ . According to this research, polymer backbone does not have a significant influence on the structure adopted by the system. Rather, the aromatic moieties in the dendrons are producing driving forces in self-assembly process, inducing a helical arrangement. On the basis of the high degree of local order found within the dendrons, they are identified as the structure-directing moieties of the columnar architecture. The inner aromatic ring of the dendrons is fully immobile, while the outer ones are significantly mobile. The aliphatic region is dominated by the dodecyl chains of the dendron. However, this region is not of major interest, as the aliphatic side chains do not play a significant role in the self-assembling process of the dendritic polymer. In self-assembly, aliphatic tails of one column interpenetrate to the adjacent column. This was also shown by Giamberini et al<sup>10</sup>, who investigated the dynamics and structure of the aliphatic side chains of a randomly grafted copolymer, obtained through the chemical modification of poly(epichlorohydrin) with potassium 3,4,5-tris(dodecyloxy)benzoate, with variable-temperature solid-state <sup>13</sup>C NMR.

For the structure and, in particular, the molecular dynamics of the dendritic side groups, the OCH<sub>2</sub> units play a central role, as they link the different moieties as shown in **Figure 4.12**.

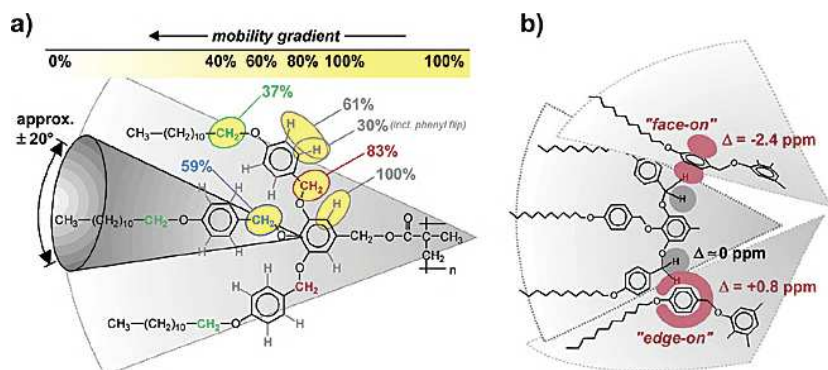


**Figure 4.12. Characteristic features of the molecular dynamics and packing of the dendrons in G1-PMA. (a) A mobility gradient of the dendrons. On the basis of order parameter  $S \approx 60\%$ , the motion of the three linear chains occurs within a cone with an opening angle of approximately  $\pm 20^\circ$ .<sup>23</sup> (b) From the  $^1\text{H}$  chemical-shift effects observed for the 3,5- $\text{OCH}_2\text{Ph}$  groups, “face-on” and “edge-on” types of contacts between dendrons can be derived. The figure should only be taken as a schematic visualization of principal structural features rather than a part of the actual structure.<sup>5</sup>**

Also, according to the studies done by Percec et al<sup>6</sup>, it has been demonstrated by combination of different techniques including DSC, XRD and POM, how these tapered groups could self-assemble and self-organize into hexagonal columnar and rectangular columnar liquid crystals. Combining the NMR information with the XRD data, it was concluded that this kind of material can be homeotropically oriented when the system is allowed to self-organize during slow cooling on a hydrophobic substrate from the melt into the liquid crystal and glassy hexagonal columnar phases.  $\pi$ - $\pi$  stacking of aromatic moieties is responsible for this homeotropic orientation. In the conclusion, homeotropic orientation is originated by  $\pi$ - $\pi$  stacking of aromatic moieties (as explained by Percec et al<sup>6</sup>) which are producing driving forces in this self-assembly process (as explained by Rapp et al<sup>5</sup>)

All this literature data led to think of another point of view to obtain homeotropic orientation of our SCLCPs that gave birth to the new technique named as a Baking process, which in-short includes heating of the polymer film

to the isotropic melt and cooling down slowly to room temperature at very slow rate. In order to study if this method would be working or not, we used HP2 sample to prepare a membrane. As explained in experimental part, the polymer membrane was prepared by immersion precipitation, submitted to the baking process and investigated by XRD analysis. This method gave satisfactory results on both hydrophilic (treated glass) and hydrophobic (teflon sheet) substrates: the baking process successfully oriented SCLCPs in a homeotropic manner. As shown in **Figure 4.13** below, the  $2\theta$  reflection at  $2.2^\circ$  lies in the equator, that means that corresponds to a diffraction in the membrane plane.

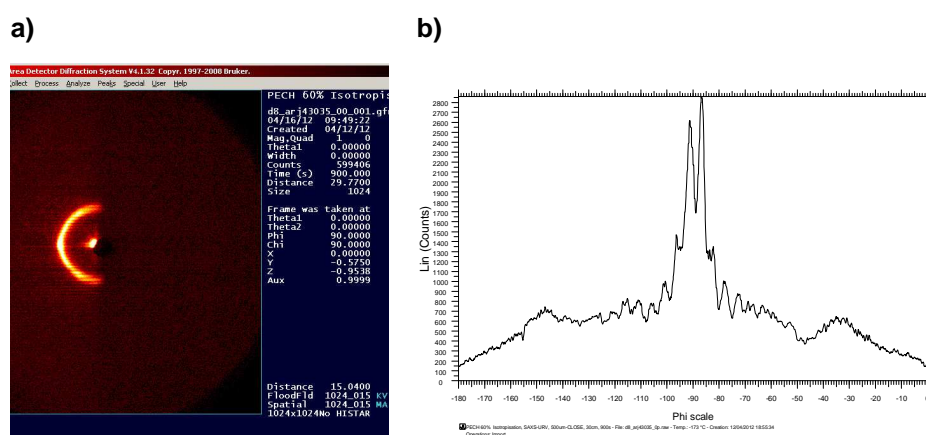


**Figure 4.13.** XRD analysis of HP2 polymer membrane prepared by baking process on a teflon sheet: a) Debye ring pattern b) Phi diffractogram from azimuthal scan on the reflection at  $2\theta = 2.2^\circ$

After getting successfully homeotropic orientation of HP2 based membranes, new membranes out of HP3, CP1 and CP2 were prepared by baking process on teflon support and analysed by XRD technique. Teflon support was selected, as it was easier to peel off the membrane compared to glass plate. As shown in **Figure 4.14** below, in all cases we found homeotropic orientation.

**Table 4.1** shows the calculated values of peak sharpness in terms of peak width at half of the height and angle of orientation with respect to the meridian, which clearly indicate the achieved homeotropic orientation.

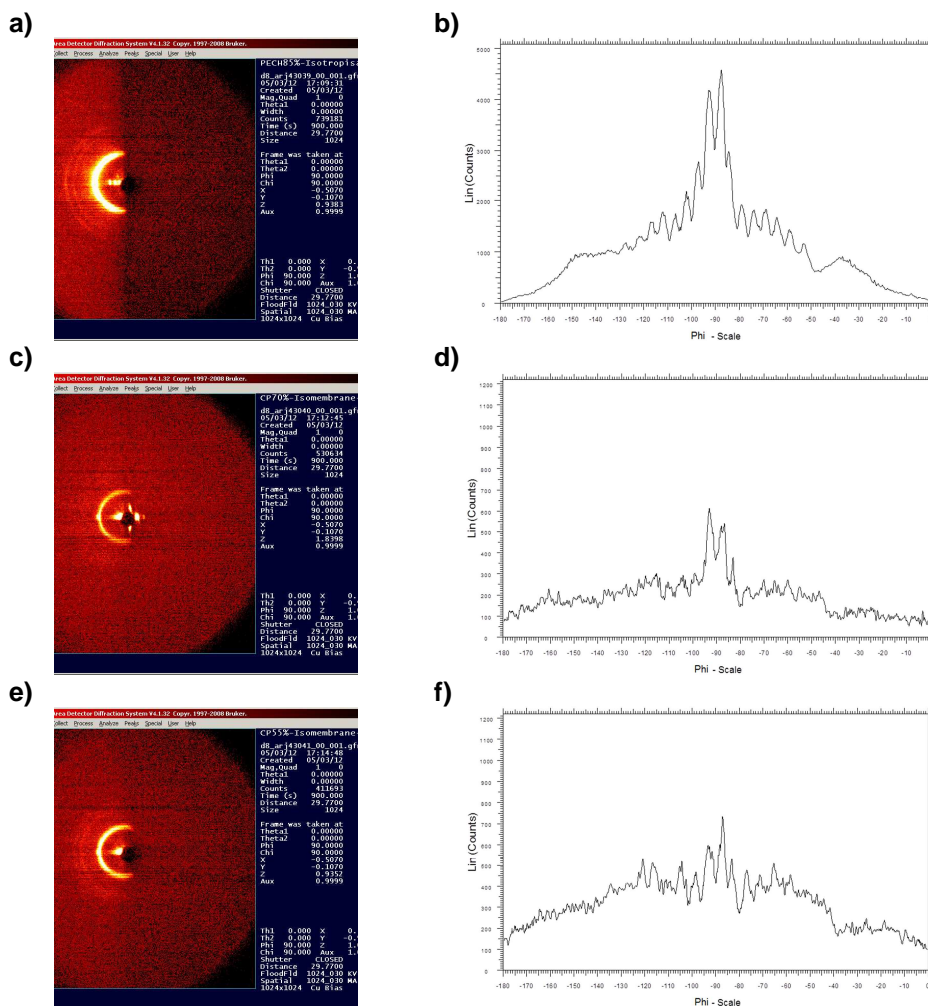


**Figure 4.14.** XRD analysis of membranes prepared by baking process on a teflon sheet: a) and b), Debye ring pattern and Phi diffractogram from azimuthal scan on the reflection at  $2\theta = 2.2^\circ$  of HP3 respectively; c) and d) Debye ring pattern and Phi diffractogram from azimuthal scan on the reflection at  $2\theta = 1.9^\circ$  of CP1 respectively; e) and f), Debye ring pattern and Phi diffractogram from azimuthal scan on the reflection at  $2\theta = 1.9^\circ$  of CP2 respectively

**Table 4.1. Calculated peak width at half of the height and angle of orientation of different membranes prepared by baking process on teflon substrate.**

Sample	Peak width at half of the height ( $^{\circ}$ )	Angle of orientation ( $^{\circ}$ )
HP2	11	89
HP3	12	90
CP1	9	88
CP2	6	91

In this way, all membrane samples prepared by baking process showed homeotropic orientation which is a crucial factor in order to achieve an efficient proton transport.

We could also confirm the effectiveness of studying these membranes by reflection mode XRD, comparing the results obtained on HP2 both in transmission and in reflection modes, as shown in **Figure 4.15**.

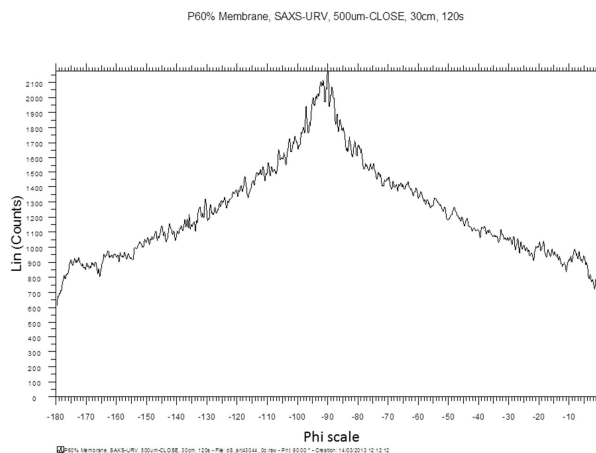
HP2 oriented polymer membranes were also investigated in terms of contact angle measurement by considering teflon-side and air-side, that is, the part which was directly in contact with the teflon support during the baking process, and the other one, on opposite side. The purpose of this investigation was to know, if there is any difference in the polymer arrangement between the two sides. As shown in **Figures 4.16 a)** and **b)**, both sides are hydrophobic having similar contact angles. Hydrophobicity is probably coming from dominating exposition of tapered groups which represent the hydrophobic part of the polymer.

In other words, in case of homeotropic orientation, the membrane surface is hydrophobic because of maximum area occupied by well oriented hydrophobic tapered groups. Differently, in case of unorientation, membrane surface is found hydrophilic with contact angle of  $71^{\circ}$  (**Figure 4.16 c)**, probably



because ionic paths are not well organised and they are randomly oriented in all directions, thus exposing also hydrophilic polymeric portions on the surface.

a)



b)

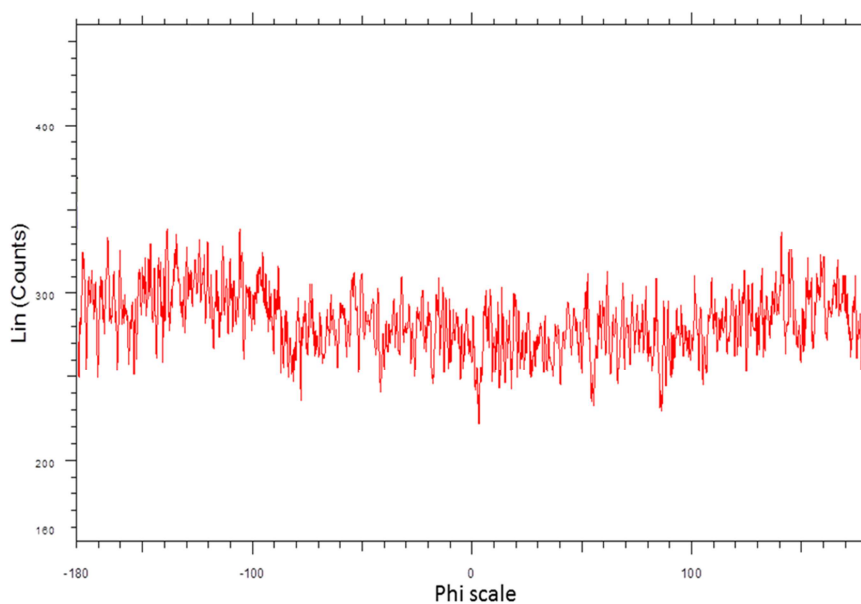


**Figure 4.15. Phi diffractograms from azimuthal scan on the reflection at  $2\theta = 2.1^\circ$  of HP2 polymer membrane prepared by baking process in: a) reflection mode b) transmission mode**

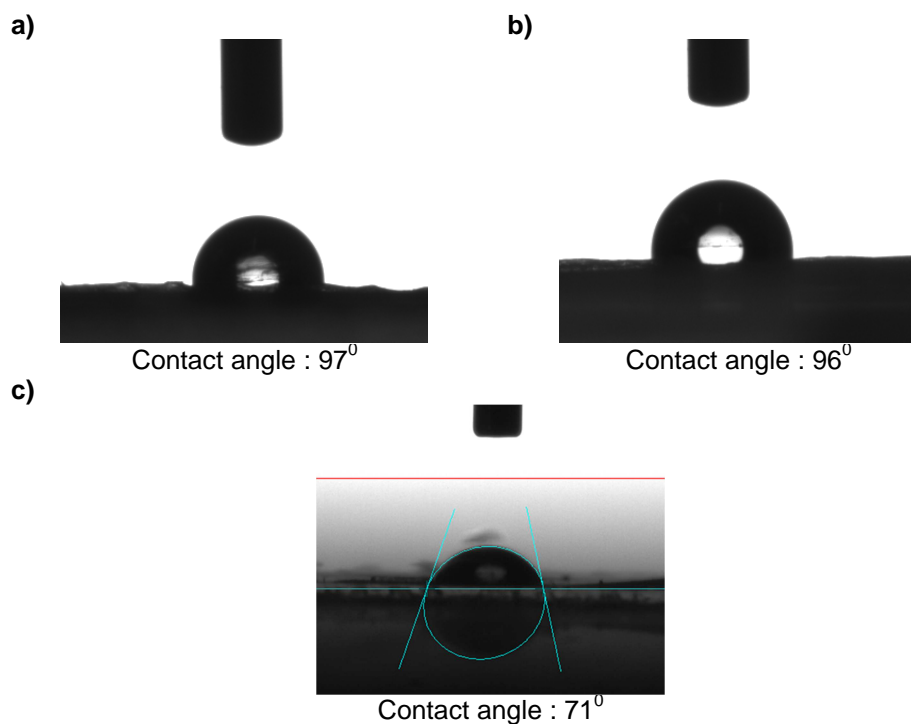


**Figure 4.16. Comparison of hydrophobicity by contact angle method of oriented HP2 polymer membrane a) air-side b) teflon-side and c) unoriented membrane**

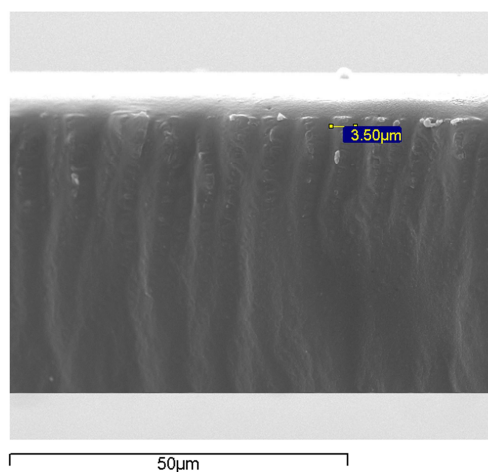


**Figure 4.17. ESEM image of cross-section of oriented HP2 membrane by baking process**

**Figure 4.17** shows the high-vacuum ESEM analysis of freeze-fractured cross-section of oriented HP2 membrane obtained by baking process. The fracture occurs in a direction approximately parallel to the membrane cross-section, and wavy aggregates about 3.5  $\mu\text{m}$  in diameter were observed.

After the cross-sectional morphology, surface morphology of HP2 was also studied by means of AFM technique. Different HP2 membranes were prepared for this investigation: 1. Oriented membranes: oriented on glass (hydrophilic surface) and teflon (hydrophobic surface), 2. Unoriented membrane: prepared by phase inversion method and 3. Shear oriented membrane (prepared as explained in experimental part). As shown in **Figure 4.18**, all oriented membranes exhibited fingerprint-like phase images as seen in case of Rice et al<sup>11</sup>. Apart from glass substrate (**Figure 4.18 a**), this fingerprint-like morphology in phase image was also observed on both sides of teflon substrate, that is teflon side and air side (**Figure 4.18 b and c**). The similar morphology on both sides of membranes supports the fact that, while homeotropic orientation occurs, there are similar effects of heating and cooling on both sides of membrane during baking process. Differently, in case of unoriented and shear oriented membranes this fingerprint-like morphology is not visible in phase images (**Figure 4.19**). From the **Figures 4.18** and **4.19** it seems like baking process prompts the fingerprint-like surface morphology. Also this phenomenon was confirmed in case of oriented CP2 membrane which also showed same surface morphology (**Figure 4.20**). AFM images showed that HP2 exhibited fingerprint-like phase image all over the surface area, while in case of CP2, it seemed like overall surface area was not showing uniform fingerprint-like structure.

Root-Mean-Squared (RMS) roughness was calculated from AFM topographic images of some samples investigated (**Table 4.2**). Roughness is an important membrane property, since it determines characteristics such as wettability. In all cases, the membranes resulted quite smooth, exhibiting RMS roughness values in the range of 1-11 nm.

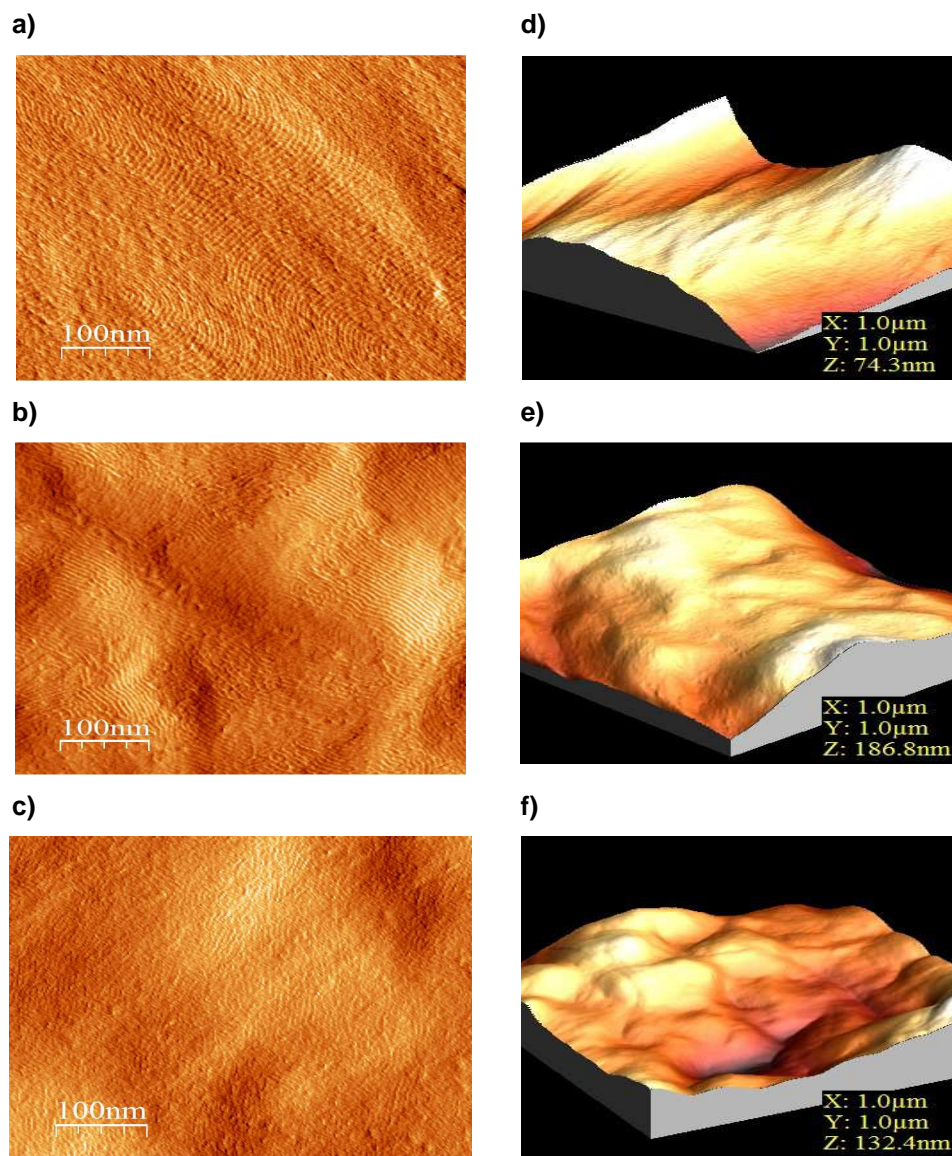


**Figure 4.18. AFM phase image pattern of oriented membranes of HP2: a) on glass surface b) on teflon (air side) c) on teflon (teflon side), and topographic image pattern of oriented membranes of HP2: d) on glass surface e) on teflon (air side) f) on teflon (teflon side)**

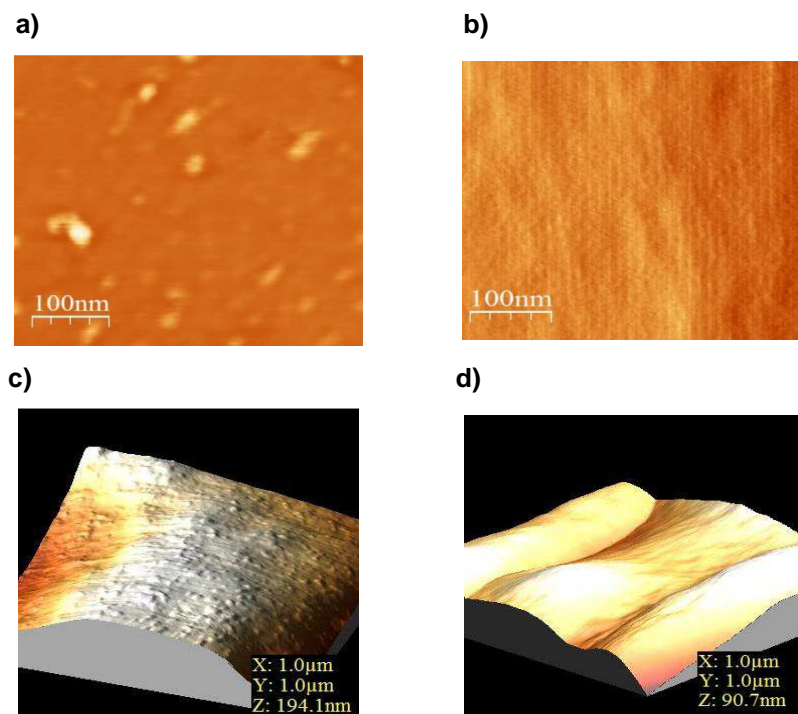


**Figure 4.19. AFM phase image pattern of surface morphology of HP2 membranes: a) unoriented b) shear oriented, and topographic image pattern of surface morphology of HP2 membranes: c) unoriented d) shear oriented**

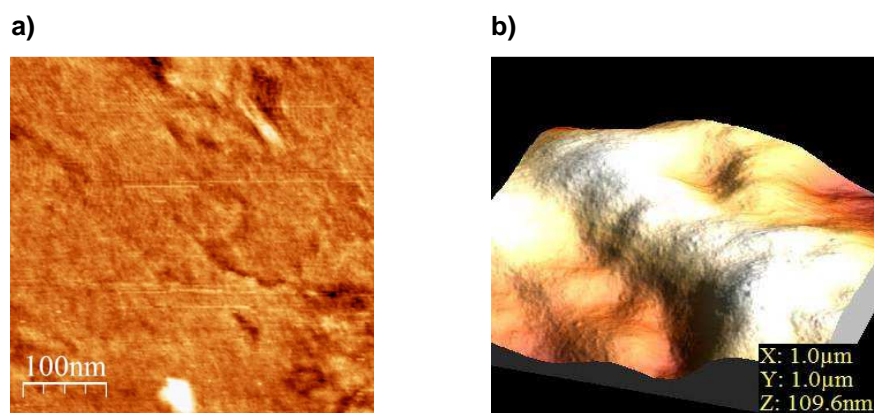


**Figure 4.20. AFM pattern of air side surface morphology of CP2 membrane prepared by baking process a) phase image b) topographic image**

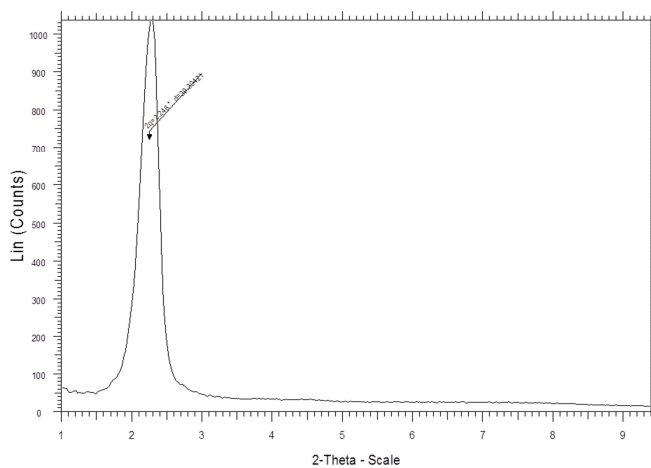
**Table 4.2. RMS roughness values of the samples of HP2 and CP2, as calculated by AFM**

Sample	Teflon oriented-air side of membrane (nm)	Teflon oriented-teflon side of membrane (nm)	Glass oriented-air Side of membrane (nm)	unoriented membrane (nm)	Shear oriented membrane (nm)
HP2	7.6	10.9	1.8	5.5	3.9
CP2	6.8	-	-	-	-

As shown in **Figure 4.21**, the XRD pattern of oriented HP2 shows only a sharp peak  $2\theta$  at  $2.1^\circ$ ,  $d = 39.3 \text{ \AA}$ , while in the case of oriented CP2, three sharp reflections corresponding to  $d_{100}$ ,  $d_{110}$  and  $d_{200}$  of a hexagonal columnar phase were found. This information, combined with AFM results, seems to indicate that, in the case of HP2, the oriented polymer is organized in lamellae aligned perpendicular to the membrane surface, as explained hereinafter. Actually, the lamellar thickness, as measured by AFM (**Figure 4.22**), resulted approximately  $40 \text{ \AA}$ , which is in agreement with the value of the spacing corresponding to  $2\theta$  at  $2.1^\circ$ ,  $d = 39.3 \text{ \AA}$  in the XRD pattern. On the other hand, in the case of CP2, the evidences from XRD and AFM suggest a coexistence of lamellar and columnar structure in the oriented membranes.

As explained before, these systems consist of a hydrophilic polymer backbone and hydrophobic mesogenic side chains. Therefore, they could be regarded as a sort of diblock copolymer. Diblock copolymers display fingerprint-like lamellar morphology on AFM phase image.<sup>12,13</sup> Also Rice et al<sup>11</sup> observed a well defined fingerprint-like lamellar morphology on the surface of ultrathin film of poly(styrene-block-ethylene oxide). In the thin film state, the block copolymer nano-domain formation takes place relative to the surfaces of the film. Segalman et al<sup>13</sup>, explained the orientation of block copolymer domains with respect to the substrate surface. These different types of orientation of block copolymer domains are shown in **Figure 4.23**.

a)



b)

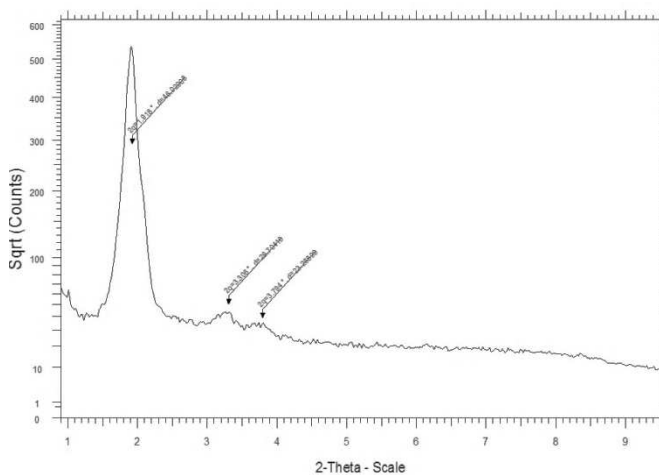


Figure 4.21. XRD diffraction pattern of intensity vs  $2\theta$ : a) oriented HP2 membrane b) oriented CP2 membrane

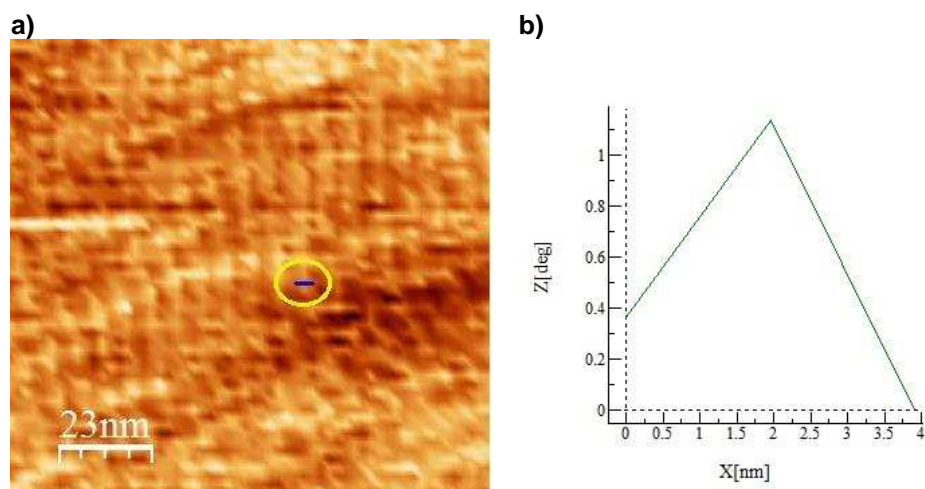


Figure 4.22 a) Measurement of thickness of one lamellar band in AFM phase image b) size of thickness of one lamellar band is approximately 4 nm.

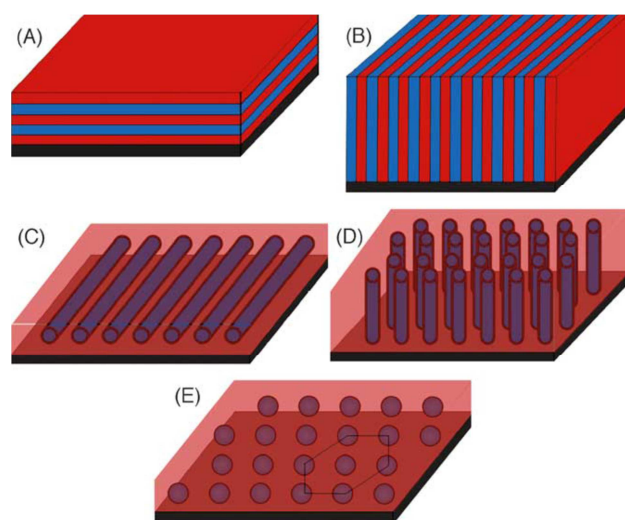
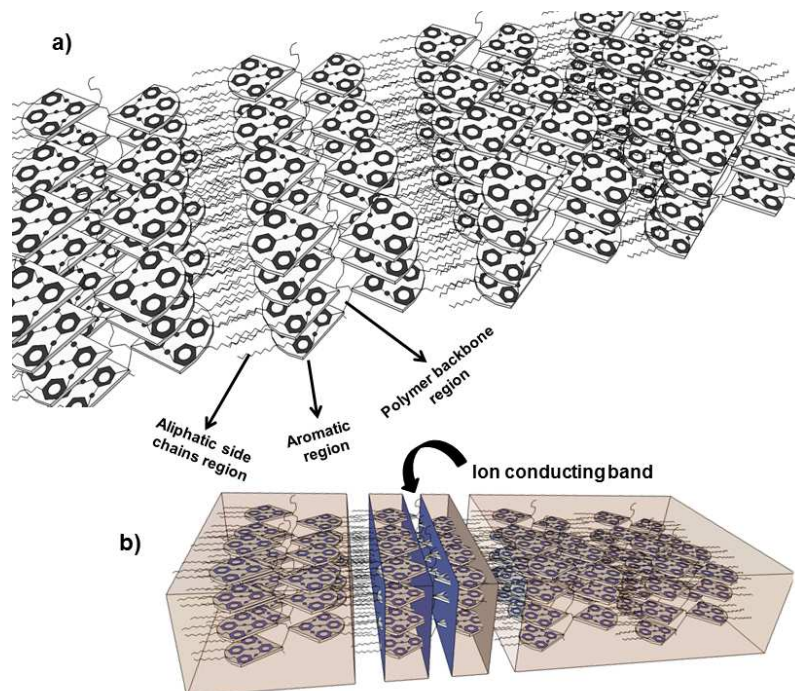


Figure 4.23. The orientation of block copolymer domains with respect to the substrate surface: (A) Lamellae lying parallel to the substrate, (B) lamellae aligned perpendicular, (C) cylinders lying parallel, (D) cylinders perpendicular, and (E) spheres



In case of HP2 there are two possibilities according to AFM results, that is the ion conducting paths might be columns lying parallel to the substrate as shown in **Figure 4.23 (C)** or they might be lamellae aligned perpendicular as shown in **Figure 4.23 (B)**. In the case of oriented HP2 and CP2,  $2\theta$  reflection at approximately  $2^\circ$  from XRD lies in equator, that means that it corresponds to a diffraction in the membrane plane. Thus, both these samples are homeotropically oriented: that is, the presence of columns aligned parallel to the substrate is not compatible with the XRD pattern exhibited by the oriented membranes. Therefore, the findings from AFM must correspond to a lamellar structure, with the lamellae oriented perpendicular to the membrane surface (alike **Figure 4.23 B)**

We schematically represented the hypothesis of formation of fingerprint-like lamellar structure in AFM phase images as shown in **Figure 4.24**. As it can be seen in **Figure 4.24 a**, the helical polymer backbone is stretched to establish preferable lamellar orientation and fingerprint-like structure. This structure might have been assembled due to formation of separate regions corresponding to the aliphatic side chain region, aromatic region and polyether backbone region. That is, they are arranged in separated hydrophilic and hydrophobic regions that could give rise to the fingerprint-like structure in AFM phase image. As shown in **Figure 4.24 b**, the arrangement of the lamellae in perpendicular fashion to the membrane surface will probably give rise to the formation of different bands corresponding to the different regions. Therefore, the region corresponding to the polymer backbone can be considered as an ion conducting band, rather than an ion conducting channel which was expected in the case of a columnar structure. As explained in the main introduction of the thesis, this region is sensitive for the ion conduction due to the polymer backbone having hydrophilic ether linkage.



**Figure 4.24. Schematic representation of the formation of fingerprint-like lamellar structure a) supramolecular self assembly of the lamellar structure showing different regions b) formation of ion conducting band (This image is just a schematic representation and not to the scale)**

Under this hypothesis, proton transport through these bands could occur by a hopping mechanism, that is protons jump from a lone pair of electrons of one oxygen atom of polymer backbone to the next, due to weak coordination. In this case, oxygen atoms from polymer backbone of ion conducting bands are supposed to be used for proton transport and thus water molecules would not be necessary, unlike DuPont's Nafion® membranes, which are the benchmark materials used as a proton transporting electrolyte in direct methanol fuel cells (DMFC).<sup>14</sup> As a matter of fact, no water sorption could be detected on oriented membranes based on PECH modified with potassium 3,4,5-tris[4-(n-dodecan-1-yloxy)benzyloxy] benzoate<sup>4</sup>.

After confirming their homeotropic orientation using XRD and AFM techniques, we used these membranes to check actual proton transport by means of conductivity measurements.

Before conductivity measurements, we evaluated integral electric resistance of the samples by using sensitive Ohm-meter as shown in **Figure 4.25**. For these homeotropically oriented membranes based on SCLC polyethers, no intrinsic electrical conductivity was detected, that is they behave as good dielectrics.



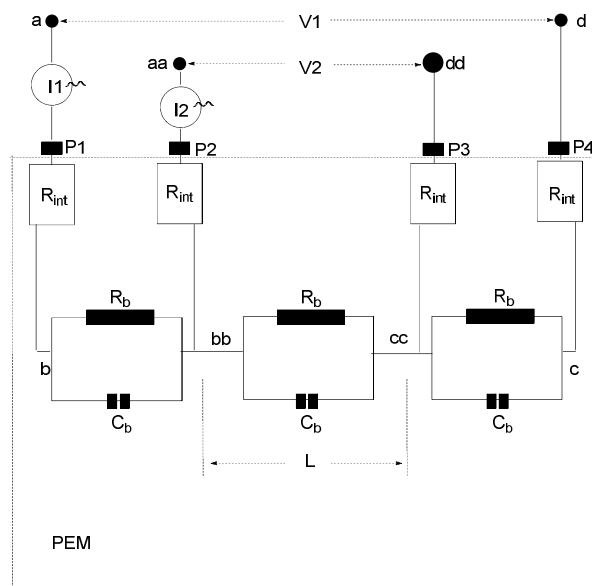
**Figure 4.25. Intrinsic electrical conductivity measurement by sensitive ohm meter**

It means that, at mentioned voltage in ambient conditions and at room temperature no electric charge carriers were present in samples, as expected.

Proton transport mechanism is a very complex-phenomenon in artificial polymer membranes, and, as explained in main introduction of thesis, the vehicle or hopping mechanism is a well-accepted hypothesis for this transport.<sup>15-17</sup> Proton conductivity is generally obtained from the measurement of resistivity of

the proton-conductive membrane against the flow of either alternating current (AC) or direct current (DC). Electrochemical impedance spectroscopy (EIS) is the most widespread method, where analysis of a complex-plane frequency dependent response of a sample may allow estimation of its proton conductivity. As protons are the sole mobile charge, their conductivity can be measured by a DC technique only using the  $H/H^+$  reversible electrodes, which is expensive and too complex for a routine test. An AC technique is commonly considered as the most appropriate for solid electrolytes.

It is generally perceived that four-probe EIS offers an advantage over two-probe EIS because it is believed to eliminate contact impedances. In the two-probe cell configuration, the current-generating electrodes also serve as the voltage-measuring probes, and thus interfacial impedance is expected to dominate in the lower frequency range. It is reported that the membrane ionic resistance can be satisfactorily resolved from interfacial impedance only when the frequency is  $\geq 100$  Hz.<sup>18</sup> In contrast, with a four-probe cell configuration, the voltage measuring probes are connected through a high impedance device so that negligible current flows across these interfaces. Cahan and Wainwright<sup>18</sup> compared two- and four-electrode configurations over the frequency range 1 Hz to 65 kHz, and reported that the four-electrode measurement provided a constant impedance, whereas interfacial impedance dominated the observed frequency response for the two-electrode system. Therefore we measured proton conductivity of these oriented polyether films using AC four-probe EIS over a frequency range of  $10^7$  to 1 Hz. A schematic diagram of the current- and voltage-measuring circuit for 4-probe conductivity cells is shown in **Figure 4.26**.<sup>19</sup> The polymer electrolyte membrane is represented by a bulk resistance,  $R_b$ , and bulk capacitance,  $C_b$ , connected in parallel.  $Z_{int}$  represents the Pt/PEM interfacial impedance. The voltage-sensing probes are separated from the current injectors, and due to the high input impedance of the voltage measuring circuit, negligible current passes through them. The effect of the blocking electrode is diminished and the equivalent circuit simplifies to a single  $R_b C_b$  parallel circuit, which is expected to yield a semicircular impedance response over the entire frequency region.



$R_b, C_b$  : Membrane bulk resistance and bulk capacitor  
 $Z_{int}$ : Pt/membrane interfacial impedance  
 $L$ : Distance of two voltage-sensing probes in 4-probe  
 $I1$ : ac current applied  
 $I2$ : ac current in measuring circuit  
 $V1$ : ac potential applied  
 $V2$ : ac potential measured in measuring circuit  
 $a, b, c, d$ : ac signal applied circuit  
 $aa, bb, cc, dd$ : ac signal measuring circuit  
 $P1, P2, P3$  and  $P4$ : Pt current/voltage probe

**Figure 4.26. Schematic diagram of the AC current and voltage measuring circuit for 4-probe (P1, P2, P3, and P4) configurations<sup>19</sup>**

The conductivity values of HPs and CPs at different temperatures and percentages of relative humidity (RH) are given in **Table 4.3**. 5%, 50% and 100% of RHs were used to study the effect of RH on proton conductivity while, depending on temperature resistivity of the membranes, different temperatures were applied. Although clearing temperatures of HP's and CP's are higher than 100 °C, softening of polymers was the main problem to perform conductivity tests above 100 °C. For instance, in case of HP's, membranes were able to stand up to 70 °C. On the other hand, CP's could not bear temperatures above 50 °C. Above these temperatures, membranes were susceptible to softening and stuck to membrane holder of the conductivity cell. Hence, we carried out conductivity

tests at temperatures 30, 50 and 70 °C in case of HPs, while at 30 and 50 °C in case of CPs.

**Table 4.3. Proton conductivity versus temperature and relative humidity for samples HP2, HP3, CP1 and CP2**

Relative Humidity [%]	Membrane	$\sigma \cdot 10^3$ at 30°C [S/cm]	$\sigma \cdot 10^3$ at 50°C [S/cm]	$\sigma \cdot 10^3$ at 70°C [S/cm]
5	HP2	1.6 (±0.4)	1.9 (±0.4)	2.5 (±0.3)
	HP3	4.1 (±0.8)	4.2 (±0.6)	5.1 (±0.1)
	CP1	8.8 (±0.7)	14 (±1.5)	-
	CP2	3.5 (±0.3)	7.3 (±0.3)	-
50	HP2	1.6 (±0.4)	1.8 (±0.6)	2.5 (±0.3)
	HP3	4.0 (±0.3)	4.4 (±0.7)	5.1 (±0.7)
	CP1	9.2 (±0.4)	13 (±3.1)	-
	CP2	4.3 (±0.6)	6.7 (±0.2)	-
100	HP2	1.6 (±0.6)	1.9 (±0.5)	2.4 (±0.5)
	HP3	4.1 (±0.2)	4.3 (±0.4)	5.0 (±0.2)
	CP1	9.2 (±0.6)	14 (±2.2)	-
	CP2	4.3 (±0.2)	7.3 (±0.2)	-

In these SCLCPs, conductivity increases on increasing the degree of modification. Compared to HPs, CPs shows the highest value of proton conductivity. This could depend on the presence of more flexible ethylene oxide moieties in CPs series, which allows a better orientation of the ionic paths responsible for proton conductivity. Proton conductivity in Nafion<sup>®</sup>117 is 13.3 mS/cm at 30 °C in 100% RH atmosphere. This value decreases with increase in temperature and with RH decrease<sup>20</sup>. On the contrary, in membranes based on SCLCPs, the highest conductivity was found in CP1, 8.8 mS/cm at 30 °C in 5% RH atmosphere and 14 mS/cm at 50 °C in 5% RH atmosphere. It can be noticed that conductivity values of SCLCPs membranes are comparable to Nafion<sup>®</sup>. Also, it must be underlined that they remain constant on increasing percentage of relative humidity, that is, conductivity increases on increasing temperature

without any effect of relative humidity. This clearly indicates that proton conductivity in membranes based on SCLCPs is independent of water content, unlike Nafion<sup>®</sup>.

These results are preliminary. Further insight into the potential applications of reported SCLCPs as proton-conducting materials will be given by a deep elucidation of the proton-transport mechanism through them. Therefore, future work will be focused on proton permeability tests on these oriented membranes, in order to confirm a proton/cation antiport mechanism as it was proposed by Tylkowski et al.<sup>4</sup> In addition, it is crucial to understand how the formation of oriented lamellae occurs during the baking process. For this purpose, different supports as well as different cooling rates should be tested. Also, SCLCPs based on polyamines modified by 3,4,5-tris[4-(n-dodecan-1-yloxy)benzyloxy]benzoic acid will be considered as novel potential proton-conducting materials, due to the presence of the basic nitrogen in their main chain<sup>21</sup>.

## 4.5 Conclusion

Different preparation methods of oriented membranes based on SCLCPs have been investigated, since the method previously reported by Tylkowski et al<sup>4</sup> showed poor reproducibility. Polymer membranes based on SCLCPs were prepared by immersion precipitation, vapor precipitation and baking process on different supports. Immersion and vapor precipitation could not be able to orient polymer in a homeotropic fashion, while baking process has shown effective homeotropic orientation with better reproducibility. This reproducibility was proved by using different polyethers: 63% modified **HP2** and 80% modified **HP3** from PECH family, and 69% modified **CP1** and 59% modified **CP2** from P(ECH-co-CO) family. Homeotropic orientation was investigated by XRD analysis in reflection mode which has demonstrated as a better mode compared to transmission mode. Oriented membranes were found to be hydrophobic on both sides, while unoriented membranes were hydrophilic, as shown by their contact angles. AFM technique showed a fingerprint-like phase image on both sides of the oriented membranes. This evidence, together with XRD results, indicates that the oriented polymers arrange themselves either as lamellae perpendicular to the membrane surface (HPs), or as both lamellae and columns (CPs). These lamellae would correspond to the different polymer regions: in particular, the region corresponding to the polymer backbone could act as ion conducting band. The presence of oriented ion conducting bands in the polymeric membrane resulted in remarkable proton conductivity, in the range of  $10^{-2}$  to  $10^{-3}$  mS/cm, independently from the relative humidity.



## 4.6 References

1. Mulder, M., *Basic Principles of Membrane Technology Second Edition*. Kluwer: 1996.
2. Strathmann, H.; Kock, K., The formation mechanism of phase inversion membranes. *Desalination* **1977**, *21* (3), 241-255.
3. Broens, L.; Altena, F. W.; Smolders, C. A.; Koenhen, D. M., Asymmetric membrane structures as a result of phase separation phenomena. *Desalination* **1980**, *32* (0), 33-45.
4. Tylkowski, B.; Castelao, N.; Giamberini, M.; Garcia-Valls, R.; Reina, J. A.; Gumí, T., The importance of orientation in proton transport of a polymer film based on an oriented self-organized columnar liquid-crystalline polyether. *Materials Science and Engineering: C* **2012**, *32* (2), 105-111.
5. Rapp, A.; Schnell, I.; Sebastiani, D.; Brown, S. P.; Percec, V.; Spiess, H. W., Supramolecular Assembly of Dendritic Polymers Elucidated by <sup>1</sup>H and <sup>13</sup>C Solid-State MAS NMR Spectroscopy. *Journal of the American Chemical Society* **2003**, *125* (43), 13284-13297.
6. Percec, V.; Glodde, M.; Bera, T. K.; Miura, Y.; Shiyonovskaya, I.; Singer, K. D.; Balagurusamy, V. S. K.; Heiney, P. A.; Schnell, I.; Rapp, A.; Spiess, H. W.; Hudson, S. D.; Duan, H., Self-organization of supramolecular helical dendrimers into complex electronic materials. *Nature* **2002**, *417* (6905), 384-387.
7. Yoshio, M.; Kagata, T.; Hoshino, K.; Mukai, T.; Ohno, H.; Kato, T., One-Dimensional Ion-Conductive Polymer Films: Alignment and Fixation of Ionic Channels Formed by Self-Organization of Polymerizable Columnar Liquid Crystals. *Journal of the American Chemical Society* **2006**, *128* (16), 5570-5577.
8. Boussu, K.; Van der Bruggen, B.; Volodin, A.; Snauwaert, J.; Van Haesendonck, C.; Vandecasteele, C., Roughness and hydrophobicity studies of nanofiltration membranes using different modes of AFM. *Journal of Colloid and Interface Science* **2005**, *286* (2), 632-638.
9. Mikhailenko, S. D.; Guiver, M. D.; Kaliaguine, S., Measurements of PEM conductivity by impedance spectroscopy. *Solid State Ionics* **2008**, *179* (17-18), 619-624.
10. Giamberini, M.; Ronda, J. C.; Reina, J. A., Poly(epichlorohydrin) modified with 3,4,5-tris(dodecyloxy)benzoate: The structure and dynamics of the aliphatic

side chains in the columnar mesophase. *Journal of Polymer Science Part A: Polymer Chemistry* **2005**, *43* (10), 2099-2111.

11. Rice, R. H.; Mokarian-Tabari, P.; King, W. P.; Szoszkiewicz, R., Local Thermomechanical Analysis of a Microphase-Separated Thin Lamellar PS-*b*-PEO Film. *Langmuir* **2012**, *28* (37), 13503-13511.

12. Fasolka, M. J.; Banerjee, P.; Mayes, A. M.; Pickett, G.; Balazs, A. C., Morphology of Ultrathin Supported Diblock Copolymer Films: Theory and Experiment. *Macromolecules* **2000**, *33* (15), 5702-5712.

13. Segalman, R. A., Patterning with block copolymer thin films. *Materials Science and Engineering: R: Reports* **2005**, *48* (6), 191-226.

14. Grot, W. G., Perfluorinated ion exchange polymers and their use in research and industry. *Macromolecular Symposia* **1994**, *82* (1), 161-172.

15. Day, T. J. F.; Schmitt, U. W.; Voth, G. A., The Mechanism of Hydrated Proton Transport in Water. *Journal of the American Chemical Society* **2000**, *122* (48), 12027-12028.

16. Eikerling, M.; Kornyshev, A. A.; Kuznetsov, A. M.; Ulstrup, J.; Walbran, S., Mechanisms of Proton Conductance in Polymer Electrolyte Membranes. *The Journal of Physical Chemistry B* **2001**, *105* (17), 3646-3662.

17. Li, T.; Wlaschin, A.; Balbuena, P. B., Theoretical Studies of Proton Transfer in Water and Model Polymer Electrolyte Systems. *Industrial & Engineering Chemistry Research* **2001**, *40* (22), 4789-4800.

18. Cahan, B. D.; Wainright, J. S., AC Impedance Investigations of Proton Conduction in Nafion™. *Journal of The Electrochemical Society* **1993**, *140* (12), L185-L186.

19. Xie, Z.; Song, C.; Andreaus, B.; Navessin, T.; Shi, Z.; Zhang, J.; Holdcroft, S., Discrepancies in the Measurement of Ionic Conductivity of PEMs Using Two- and Four-Probe AC Impedance Spectroscopy. *Journal of The Electrochemical Society* **2006**, *153* (10), E173-E178.

20. Sahu, A. K.; Pitchumani, S.; Sridhar, P.; Shukla, A. K., Nafion and modified-Nafion membranes for polymer electrolyte fuel cells: An overview. *Bull Mater Sci* **2009**, *32* (3), 285-294.

21. Šakalytė, A.; Reina, J. A.; Giamberini, M., Liquid crystalline polyamines containing side dendrons: Toward the building of ion channels based on polyamines. *Polymer* **2013**, *54* (19), 5133-5140.



## *Chapter 5*

---

### *General Conclusions*

UNIVERSITAT ROVIRA I VIRGILI

PROTON-EXCHANGE BIOMIMETIC MEMBRANES BASED ON COLUMNAR SIDE-CHAIN LIQUID-CRYSTALLINE POLYETHERS

Suryakant Bhosale

Dipòsit Legal: T.188-2014

### *General conclusions*

---

- ❖ Novel liquid crystalline columnar polymers could be prepared by chemical modification of: either commercial polyethers like polyepichlorohydrin (PECH) and poly(epichlorohydrin-co-ethylene oxide) [P(ECH-Co-EO)] or polyethers synthesized on purpose, i.e. linear polyglycidol (LPG) with 3,4,5-tris[4-(n-dodecan-1-yloxy)benzyloxy] benzoic acid.
  
- ❖ The modification degree was found to reach a plateau around 80% (in case of PECH), 69% [in case of P(ECH-co-EO)] and 43% (in case of LPG). All modified homopolymers and copolymers exhibited liquid-crystalline columnar behavior, as shown by POM and confirmed by XRD. Moreover, in case of modified LPG samples, we obtained different mesophases like, columnar, rectangular columnar and hexagonal columnar depending on the achieved degree of modification. The clearing temperature ranges were determined with the help of DSC and POM: they depended on the modification degree, as expected, and were in the range 80-140 °C in case of PECH, 90-100 °C in case of P(ECH-co-EO) and 35-105 in case of LPG.
  
- ❖ Apart from the linear polyethers, chemical modification of hyperbranched polyether was also studied by considering only one modification of OH/RCOOH molar ratio 1:1, which gave the degree of modification in the range of 11-12% without liquid crystalline properties.
  
- ❖ A novel method of orientation of ion conducting paths in a homeotropic fashion was developed which has shown effective reproducibility. This reproducibility was proved by using different polyethers: 63% modified HP2 and 80% modified HP3 from PECH family, while 69% modified CP1 and 59% modified CP2 from P(ECH-co-CO) family. Homeotropic orientation investigated by XRD analysis in reflection mode which has demonstrated as a better mode compared to transmission. Oriented membranes were found to be hydrophobic on both sides while, unoriented membranes are hydrophilic as shown by their contact angles. Cross-sectional and surface morphologies were investigated by ESEM

and AFM, respectively. AFM phase images of oriented membranes surface showed a fingerprint-like morphology, which resembles diblock copolymers arranged in lamellar structure. According to this morphology, we concluded that ion conducting bands are formed, rather than ion conducting channels, during orientation process.

- ❖ The assessment of these oriented membranes was performed through proton transport by means of conductivity tests. Oriented membranes prepared from both, HP and CP families were tested. All oriented samples demonstrated proton conductivity at different temperatures and relative humidity conditions. According to the conductivity results, we concluded that there is no effect of relative humidity on proton conduction; on the contrary, it is affected by temperature since it increases with increase in temperature. The presence of oriented ion conducting bands in the polymeric membranes resulted in remarkable proton conductivity, in the range of  $10^{-2}$  to  $10^{-3}$  mS/cm. Therefore, these proton transporting membranes based on side chain liquid-crystalline polyethers seem promising for proton exchange membrane fuel cells (PEMFCs) or in artificial photosynthesis.

## *Appendices*

---



UNIVERSITAT ROVIRA I VIRGILI

PROTON-EXCHANGE BIOMIMETIC MEMBRANES BASED ON COLUMNAR SIDE-CHAIN LIQUID-CRYSTALLINE POLYETHERS

Suryakant Bhosale

Dipòsit Legal: T.188-2014

## **Appendix A: List of figures, schemes and tables**

### **Chapter 1**

#### ***Figures***

- Figure 1.1. General scheme of fuel cell
- Figure 1.2. The working principle of the direct methanol fuel cell
- Figure 1.3. Chemical structure of Nafion®
- Figure 1.4. Schematic representation of the hopping (Grotthus) mechanism
- Figure 1.5. Schematic representation of the vehicular mechanism
- Figure 1.6. Phase separation in membranes : broader (left) and narrower (right) ionic channels for proton transport
- Figure 1.7. Ion transportation through the cell membrane
- Figure 1.8. Ion channels formed by cylindrical packing of crown ether molecules
- Figure 1.9.  $C_2$ -symmetric tetrahydrofuran pentamer prepared in enantiomerically pure form by a convergent synthesis. Compounds of this type are of interest for the construction of synthetic ion channels from polyether helices
- Figure 1.10. Supramolecular self-assembly of TMV into a helical conformation
- Figure 1.11. One-dimensional ion-conductive polymer films containing ion nanochannels
- Figure 1.12. a) Calamitic (rod-like) liquid crystals b) Discotic (disc-like) liquid crystals
- Figure 1.13. Several mesophases shown by discotic liquid crystals.
- Figure 1.14. Schematic representation of a main-chain liquid-crystalline polymer (MCLCP)
- Figure 1.15. Schematic representation of a side-chain liquid-crystal polymer (SCLCP)

#### ***Tables***

- Table 1.1. Classification of fuel cells and their main features

## Chapter 2

### Figures

Figure 2.1.  $^1\text{H}$  NMR spectrum of copolymer CP1 in  $\text{CDCl}_3$

Figure 2.2.  $^{13}\text{C}$  NMR spectrum of copolymer CP1 in  $\text{CDCl}_3$

Figure 2.3. HR-MAS  $^{13}\text{C}$  spectra of CP2 copolymer at: a)  $20^\circ\text{C}$ ; b)  $50^\circ\text{C}$ . The arrows indicate the peaks considered for  $T_{1\rho}$ 's calculation, located at 43.5, 63.8 and 78.6 ppm

Figure 2.4. Optical micrographics between crossed polars of CP1 at: (a)  $110^\circ\text{C}$  (b)  $115^\circ\text{C}$  (c)  $120^\circ\text{C}$

Figure 2.5. X-ray diffraction pattern of CP5 in the low  $2\theta$  range ( $0.9\text{--}9.28$ ) (a) and in the medium  $2\theta$  range ( $3\text{--}25.58$ ) (b)

Figure 2.6. XRD pattern on flat film of an oriented CP5 sample, in the low  $2\theta$  range ( $0.9\text{--}9.2^\circ$ ) (a) and in the medium  $2\theta$  range ( $3\text{--}25.5^\circ$ ) (b)

Figure 2.7. Schematic representation of columnar structure of CPn copolymers

### Schemes

Scheme 2.1. Synthetic path for potassium 3,4,5-tris[4-(n-dodecan-1-yloxy)benzyloxy]benzoate)

Scheme 2.2. Synthetic path for chemical modification of PECH

Scheme 2.3. Synthetic path for chemical modification of P(ECHco-EO)

### Tables

Table 2.1 The modification degree and yield obtained in the modification of PECH

Table 2.2. Clearing temperatures and densities of the modified PECH

Table 2.3. X-ray patterns of samples oriented at room temperature

Table 2.4. The modification degree and copolymer yield obtained in the modification of P(ECH-co-EO)

Table 2.5. Molecular weight and densities of the synthesized copolymers

Table 2.6. Phase transitions and annealing temperature of the copolymers CP1–CP5

Table 2.7. Carbon spin-lattice relaxation times of selected peaks of CP2 copolymer at 20°C and 50°C

Table 2.8. Characteristics of the crystalline phase of copolymers CP1-CP5

Table 2.9. X-ray patterns of oriented samples of copolymers CP1–CP5 at room temperature

### Chapter 3

#### Figures

Figure 3.1.  $^1\text{H}$  NMR spectrum of 3,4,5-tris[4-(n-dodecan-1-yloxy)benzyloxy] benzoic acid in  $\text{CDCl}_3$

Figure 3.2.  $^{13}\text{C}$  NMR spectrum of 3,4,5-tris[4-(n-dodecan-1-yloxy) benzyloxy]benzoic acid in  $\text{CDCl}_3$

Figure 3.3.  $^1\text{H}$  NMR spectrum of (1-ethoxyethyl)glycidyl ether in  $\text{CDCl}_3$

Figure 3.4.  $^{13}\text{C}$  NMR spectrum of (1-ethoxyethyl)glycidyl ether in  $\text{CDCl}_3$

Figure 3.5.  $^1\text{H}$  NMR spectrum of linear poly[(1-ethoxyethyl)glycidyl ether] in  $\text{CDCl}_3$

Figure 3.6.  $^{13}\text{C}$  NMR spectrum of linear poly[(1-ethoxyethyl)glycidyl ether] in  $\text{CDCl}_3$

Figure 3.7.  $^1\text{H}$  NMR spectrum of modified linear polyglycidol in deuterated DMSO

Figure 3.8.  $^{13}\text{C}$  NMR spectrum of linear polyglycidol in deuterated DMSO

Figure 3.9. Reaction mechanism of Steglich esterification: A) ester formation by carboxylic acids, DCC and amines B) efficient ester formation by addition of DMAP

Figure 3.10.  $^1\text{H}$  NMR spectrum of modified LPG1 in  $\text{CDCl}_3$

Figure 3.11.  $^{13}\text{C}$  NMR spectrum of modified LPG1 in 1,1,2,2-Tetrachloro-ethane- $d_2$

Figure 3.12. Optical micrographics between crossed polars of a) LPG1, 30 °C b) LPG2, 69 °C c) LPG3, 79 °C d) LPG4, 97 °C e) LPG5, 116 °C f) LPG6, 94 °C g)

LPG7, 93 °C and f) LPG8, 47 °C

Figure 3.13. X-ray diffraction pattern of LPG1 at room temperature after cooling down from isotropic melt

Figure 3.14. X-ray diffraction pattern of LPG2 at room temperature after cooling down from isotropic melt

Figure 3.15. X-ray diffraction pattern of LPG3 at room temperature after cooling down from isotropic melt

Figure 3.16. X-ray diffraction pattern of LPG4 at room temperature after cooling down from isotropic melt.

Figure 3.17. Schematic structure of hyperbranched polyglycidol (HPG)

Figure 3.18. <sup>1</sup>H NMR spectrum of HPG in deuterated DMSO

Figure 3.19. <sup>13</sup>C spectrum of HPG in deuterated DMSO

Figure 3.20. <sup>1</sup>H NMR spectrum of modified HPG in deuterated CDCl<sub>3</sub>

Figure 3.21. <sup>1</sup>H NMR spectrum of modified HPG in deuterated CDCl<sub>3</sub>

### **Schemes**

Scheme 3.1. Synthesis of 3,4,5-tris[4-(n-dodecan-1-yloxy)benzyloxy]benzoic acid

Scheme 3.2. Synthesis of (1-ethoxyethyl)glycidyl ether

Scheme 3.3. Synthesis of linear polyglycidol

Scheme 3.4. Chemical modification of linear polyglycidol

Scheme 3.5. Steglich esterification

Scheme 3.6. 1,3-rearrangement of the O-acyl intermediate to a N-acyl urea

### **Tables**

Table 3.1 The modification degree and yield obtained in modification of LPG

Table 3.2 Average molecular weights and densities of the modified LPG

Table 3.3 Clearing temperature ranges and glass transition temperatures of the modified LPG

Table 3.4. X-ray diffraction data of modified LPG at room temperature

## Chapter 4

### Figures

Figure 4.1. Schematic representation of membrane morphologies

Figure 4.2. Schematic representation of three DIPS processes: A) precipitation with non solvent vapor, B) evaporation of solvent, C) immersion precipitation. Main direction of diffusion of the different species is indicated by arrows. Polymer, solvent and nonsolvent are represented with P, S and NS respectively. Components which are not necessary to be present in the original polymer solution and coagulation bath are put between brackets.

Figure 4.3. Types of liquid crystals orientation near surface where  $n$  is director: a) planar b) tilted and c) homeotropic

Figure 4.4. Position of director  $n$  near surface is determined by polar  $\theta$  and azimuthal  $\phi$  angles

Figure 4.5. Procedure for preparation of oriented membranes

Figure 4.6. Process of immersion precipitation

Figure 4.7. Process of vapor precipitation

Figure 4.8. Baking process

Figure 4.9. Oriented membrane of approximately 2 cm diameter obtained by baking process

Figure 4.10. Comparison of hydrophilicity of a) untreated glass and b) treated glass by contact angle method

Figure 4.11. XRD analysis of membranes prepared from HP2 : a) Debye ring pattern and b) Phi diffractogram from azimuthal scan on the reflection at  $2\theta = 2.13^\circ$  of membrane prepared by immerse precipitation method respectively; c) Debye ring pattern and d) Phi diffractogram from azimuthal scan on the reflection at  $2\theta = 2.17^\circ$  of membrane prepared by vapor precipitation method respectively

Figure 4.12. Characteristic features of the molecular dynamics and packing of the dendrons in G1-PMA. (a) A mobility gradient along the dendrons is obvious from the local order parameters. On the basis of order of parameter  $S \approx 60\%$ , the motion of the three linear chains occurs within a cone with an opening angle of approximately  $\pm 20^\circ$ . (b) From the  $^1\text{H}$  chemical-shift effects observed for the

3,5-OCH<sub>2</sub>Ph groups, “face-on” and “edge-on” types of contacts between dendrons can be derived. The figure should only be taken as a schematic visualization of principal structural features rather than a part of the actual structure.

Figure 4.13. XRD analysis of HP2 polymer membrane prepared by baking process on a teflon sheet: a) Debye ring pattern b) Phi diffractogram from azimuthal scan on the reflection at  $2\theta = 2.24^\circ$

Figure 4.14. XRD analysis of membranes prepared by baking process on a teflon sheet: a) and b), Debye ring pattern and Phi diffractogram from azimuthal scan on the reflection at  $2\theta = 2.22^\circ$  of HP3 respectively; c) and d) Debye ring pattern and Phi diffractogram from azimuthal scan on the reflection at  $2\theta = 1.90^\circ$  of CP1 respectively; e) and f), Debye ring pattern and Phi diffractogram from azimuthal scan on the reflection at  $2\theta = 1.91^\circ$  of CP2 respectively

Figure 4.15. Phi diffractograms from azimuthal scan on the reflection at  $2\theta = 2.14^\circ$  of HP2 polymer membrane prepared by baking process in: a) reflection mode b) transmission mode

Figure 4.16. Comparison of hydrophobicity by contact angle method of oriented HP2 polymer membrane a) air-side b) teflon-side and c) unoriented membrane

Figure 4.17. ESEM image of cross-section of orientated HP2 membrane by baking process

Figure 4.18. AFM phase image pattern of oriented membranes of HP2: a) on glass surface b) on teflon (air side) c) on teflon (teflon side) and topographic image pattern of oriented membranes of HP2: d) on glass surface e) on teflon (air side) f) on teflon (teflon side)

Figure 4.19. AFM phase image pattern of surface morphology of HP2 membranes: a) unoriented b) shear oriented and topographic image pattern of surface morphology of HP2 membranes: c) unoriented d) shear oriented

Figure 4.20. AFM phase image pattern of air side surface morphology of CP2 membrane prepared by baking process a) phase image b) topographic image

Figure 4.21. XRD diffraction pattern of intensity vs  $2\theta$ : a) oriented HP2 membrane b) oriented CP2 membrane

Figure 4.22 a) Measurement of thickness of one lamellar band in AFM phase image b) size of thickness of one lamellar band is approximately 4 nm.

Figure 4.23. The orientation of block copolymer domains with respect to the substrate surface: (A) Lamellae lying parallel to the substrate, (B) lamellae aligned perpendicular, (C) cylinders lying parallel, (D) cylinders perpendicular, and (E) spheres

Figure 4.24. Schematic representation of the formation of finger print like lamellar structure a) supramolecular self assembly of the lamellar structure showing different regions b) formation of ion conducting band (This image is just a schematic representation and not to the scale)

Figure 4.25. Intrinsic electrical conductivity measurement by sensitive ohm meter

Figure 4.26. Schematic diagram of the AC current and voltage measuring circuit for 4-probe (P1, P2, P3, and P4) configurations

### *Tables*

Table 4.1. Calculated peak width at half of the height and angle of orientation of different membranes prepared by baking process

Table 4.2. RMS values of the samples of HP2 and CP2, investigated by AFM

Table 4.3. Proton conductivity versus temperature and relative humidity for samples HP2, HP3, CP1 and CP2



## **Appendix B: Publications, meeting contributions and abroad research stay**

### *Publications*

- 1) Bhosale, S. V.; Rasool, M. A.; Reina, J. A.; Giamberini, M., New liquid crystalline columnar poly(epichlorohydrin-co-ethylene oxide) derivatives leading to biomimetic ion channels. *Polymer Engineering & Science* 2013, 53 (1), 159-167
- 2) Synthesis of side-chain liquid-crystalline polymers based on linear and hyperbranched polyglycidol. *Under preparation*
- 3) Proton exchange membranes based on side-chain liquid-crystalline polyethers. *Under preparation*

### *Meeting contributions*

Bhosale, S. V.; Rasool, M. A.; Reina, J. A.; Giamberini  
“Side-chain liquid-crystalline copolyethers with tapered mesogenic groups”  
European Polymer Congress (EPF). Granada, June 2011. Poster Presentation.

### *Abroad research stay*

Three month research stay: (July-September, 2012)  
“Conductivity measurements of proton exchange membranes based on Side-Chain liquid-crystalline polyethers”  
Supervisor: Prof. Ivo Vankelecom (Faculty of bioscience engineering)  
Centre for surface chemistry and catalysis, Katholieke Universiteit Leuven  
Leuven, Belgium

**Appendix C: New Liquid Crystalline Columnar Poly(epichlorohydrin-co-ethylene oxide) derivatives leading to biomimetic ion channels**

# New Liquid Crystalline Columnar Poly(epichlorohydrin-co-ethylene oxide) Derivatives Leading to Biomimetic Ion Channels

Suryakant Vilasrao Bhosale,<sup>1</sup> Muhammad Azam Rasool,<sup>2</sup> José Antonio Reina,<sup>1</sup> Marta Giamberini<sup>2</sup>

<sup>1</sup> Departament de Química Analítica i Química Orgànica, Universitat Rovira i Virgili, Carrer Marcel·li Domingo s/n, Campus Sescelades, 43007 Tarragona, Spain

<sup>2</sup> Departament de Enginyeria Química, Universitat Rovira i Virgili, Av. Països Catalans, 26 Campus Sescelades, 43007 Tarragona, Spain

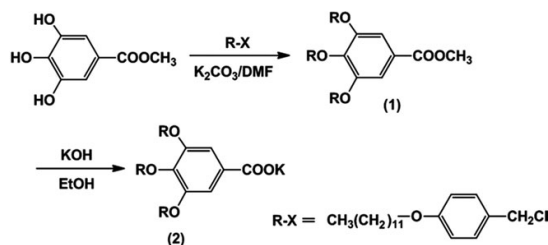
A new family of liquid crystalline columnar polyethers was obtained by modification of Poly(epichlorohydrin-co-ethylene oxide) (P(ECH-co-EO)) with the dendron 3,4,5-tris[4-(*n*-dodecan-1-yloxy)benzyloxy]benzoate, under different conditions. The highest modification degree that we could achieve was 69%. The copolymers were fully characterized by <sup>1</sup>H and <sup>13</sup>C nuclear magnetic resonance (NMR), differential scanning calorimetry (DSC), polarized optical microscopy (POM), and X-ray diffraction (XRD). All copolymers exhibited liquid-crystalline columnar behavior whose range of stability depended on the modification degree. X-ray diffraction experiments on oriented samples showed that the dendrons are approximately perpendicular to the column axis and that their average number per unit cell ranged from 5 to 6. The formation of a stable columnar mesophase in the polyether should determine the presence of a continuous ion channel along the column axis. Therefore, these copolymers are suitable candidates for the preparation of membranes for small cation transport, in agreement with the results that we obtained by using poly(oxy-1-chloro methylethylene) (PECH) modified with the same dendron. POLYM. ENG. SCI., 53:159–167, 2013. © 2012 Society of Plastics Engineers

## INTRODUCTION

Proton transport and transfer phenomena have been the object of extensive research from rather different points of view by materials scientists, chemists, physicists, and biologists [1, 2]. Over the past three decades, most research in the field of proton conductivity has been undertaken by the materials science community, mainly for the development of new proton-conducting materials

to be used in electrochemical cells (e.g., fuel cells, batteries, sensors). Perfluorosulfonic acid (PFSA) membranes, such as Nafion<sup>®</sup> (marketed by DuPont), have aroused great interest in recent years for their proton-conducting properties [3]. To achieve optimum performance for these materials, it is essential to control properties such as proton conductivity, water management, relative affinity of methanol and water in direct methanol fuel cells (DMFCs), mechanical, thermal, and oxidative stability, etc. This is a challenge for Nafion<sup>®</sup> materials, in which the possible chemical variations are quite limited; furthermore, PFSA membranes are expensive. Another serious drawback of membranes of this sort is their environmental inadaptability. For this reason, more than 200 patents and papers have been recently published on the preparation of new proton-conducting membranes [4–8]. One of the possible approaches is to design materials containing ion transport channels, in which the channels localize the permeation path and simultaneously protect the transport process against the environment, like an ion-transporting molecular cable [9–12]. Percec and coworkers [13–17] have comprehensively investigated the self-organization of supramolecular monodendrons and styrene-, methacrylate-, or oxazoline-based polymers for the design of ion-active nanostructured supramolecular systems. The polyethers like poly(oxy-1-chloro methylethylene) (PECH) and its copolymer with ethylene oxide P(ECH-co-EO) have chloromethyl units, which can be easily nucleophilically substituted [18–20]. These polyethers are of low cost and commercially easily available materials. In a very recent paper, we have reported on the preparation of oriented membranes based on a novel liquid crystalline polyether [21]. This polyether was obtained by chemical modification of commercial PECH with the dendron potassium 3,4,5-tris[4-(*n*-dodecan-1-yloxy)benzyloxy]benzoate [22]. As we reported, this polymer self-assembles into a columnar structure, due to an exo-recognition of the side-chain

Correspondence to: M. Giamberini; e-mail: marta.giamberini@urv.cat  
Contract grant sponsor: Ministerio de Ciencia e Innovación; contract grant number: MAT2008-00456/MAT.  
DOI 10.1002/pen.23240  
Published online in Wiley Online Library (wileyonlinelibrary.com).  
© 2012 Society of Plastics Engineers



SCHEME 1. Synthetic path for potassium 3,4,5-tris[4-(*n*-dodecan-1-yloxy)benzyloxy]benzoate).

dendrons. In the resulting structure, the polyether main chain forms a channel in the inner part of the columns, while the hydrophobic side-chain dendrons lie in the outer part. The presence of the polar ether linkages in the inner channel favors the interaction with proton and other cations, in the same way as crown ethers would do [23]. For this reason, the inner polyether chain could work as an ion channel. Satisfactory orientation of the polymer was achieved by sandwiching the polymer solution between a water layer and a wet glass layer to induce unfavorable surface interactions between the outer, hydrophobic portion of the columns and their surroundings. The presence of oriented channels in the polymeric membrane resulted in remarkable proton permeability, around  $2 \times 10^{-6} \text{ cm}^2 \text{ s}^{-1}$ , comparable to that of Nafion N117.

In this article, we modified P(ECH-*co*-EO) with the dendron potassium 3,4,5-tris[4-(*n*-dodecan-1-yloxy)benzyloxy]benzoate, to obtain liquid crystalline columnar polyethers. According to our previous experience, the formation of a stable columnar mesophase should lead to a continuous ion channel along the column axis. A degree of modification from 57 to 69% was achieved and all the modified copolymers exhibited a liquid crystalline columnar mesophase. Therefore, these polyethers are suitable candidates for the preparation of small cation transporting membranes.

## EXPERIMENTAL PART

### Materials

All organic and inorganic reagents were supplied by Fluka or Aldrich and used as received. Tetrahydrofuran (THF) was freshly distilled from sodium benzophenone ketyl under argon. P(ECH-*co*-EO) with PECH/PEO 1:1 ( $M_w = 5.01 \times 10^5$ ,  $M_n = 1.08 \times 10^5$  determined by gel permeation chromatography) was used as received. Tetrabutylammonium bromide (TBAB)  $\geq 99\%$  (Fluka) was dried at  $50^\circ\text{C}$  *in vacuo* for 24 h.

### Synthesis of Dendritic Mesogenic Groups

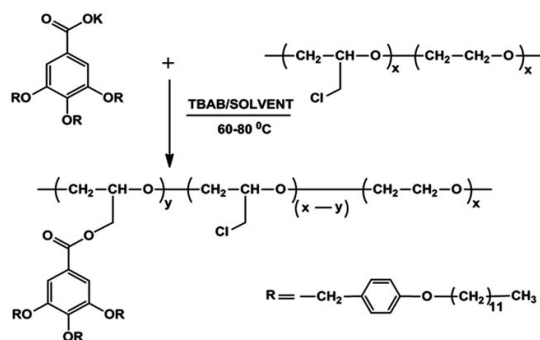
The potassium carboxylate (potassium 3,4,5-tris[4-(*n*-dodecan-1-yloxy)benzyloxy]benzoate) (2) was prepared

from methyl 3,4,5-tris[4-(*n*-dodecan-1-yloxy)benzyloxy]benzoate (1) as described elsewhere (Scheme 1) [22]. The reported procedure was slightly modified, to convert (1) directly to (2), instead of converting it before to 3,4,5-tris[4-(*n*-dodecan-1-yloxy)benzyloxy]benzoic acid, as follows: a solution of 6 N KOH in  $\text{C}_2\text{H}_5\text{OH}$  (34.3 g potassium hydroxide in 102 mL ethyl alcohol) was added to methyl 3,4,5-tris[4-(*n*-dodecan-1-yloxy)benzyloxy]benzoate (10.2 g, 0.01 mol) in a 500-mL round bottom flask. The reaction mixture was heated at  $100^\circ\text{C}$  on oil bath. After 1 h, the reaction mixture was poured into ice cold water (500 mL). A yellow solid material was filtered and vacuum dried at room temperature. It was recrystallized twice from hot absolute ethanol with active charcoal to yield a light yellow solid (yield 85%). Its structure was confirmed by  $^1\text{H}$  and  $^{13}\text{C}$  NMR spectroscopy.

### Copolymer Modification: Synthesis of Copolymers CP1, CP2, CP3, CP4, and CP5

About 0.5 g (0.0036 mol) of P(ECH-*co*-EO) was dissolved in a 125-mL round bottom flask under argon in freshly prepared dried THF (60 mL) by stirring overnight at room temperature (Scheme 2). A viscous solution was obtained. The necessary amounts of potassium carboxylate and tetrabutylammonium bromide (TBAB) were added under argon atmosphere, with inert atmospheric techniques. The reaction mixture was heated under magnetic stirring to the desired temperature. It was heated to  $60^\circ\text{C}$  in THF, and in case of *N*-methyl-2-pyrrolidone (NMP), it was heated to  $80^\circ\text{C}$ . In experiment CP3, THF/DMF were used in equal ratio and heated to  $80^\circ\text{C}$ . After 8 days, the reaction mixture was poured into  $\sim 500$  mL of ice cold water.

The modified copolymer obtained after filtration was redissolved in 125 mL of hot THF and precipitated again in 96% ethanol twice (about  $400 \text{ mL g}^{-1}$  of copolymer). After the second precipitation, the rubbery modified copolymer was collected by filtration and dried at  $60^\circ\text{C}$  under vacuum for 48 h. Table 1 shows the experimental



SCHEME 2. Synthetic path for chemical modification of P(ECH-*co*-EO).

TABLE 1. The modification degree and copolymer yield obtained in the modification of P(ECH-co-EO).

Experiment	RCOOK <sup>a</sup> (mmol)	P(ECH-co-EO)/COOK	Solvent	Time (days)	Modification <sup>b</sup> (%)	Modification <sup>c</sup> (%)	Yield <sup>d</sup> (%)
CP1	5.4	1:1.0	THF	8	67	69	83
CP2	7.3	1:1.2	THF	8	58	59	88
CP3	3.6	1:1.2	THF/DMF	8	64	65	85
CP4	3.6	1:1.2	NMP	8	60	62	87
CP5	5.4	1:1.5	THF	8	56	57	82

<sup>a</sup> Stoichiometric amounts of TBAB referred to chlorine were used in each case.

<sup>b</sup> Average value determined by <sup>1</sup>H NMR.

<sup>c</sup> Determined by chlorine elemental analysis.

<sup>d</sup> Calculated from the average degree of modification.

conditions, the yield and degree of modification for the various experiments.

### Characterization and Measurements

Elemental analyses were carried out on a Carlo Erba EA1106 device. The chlorine content was determined with Schöninger's method, which involves the combustion of the sample in a platinum closed vessel and the potentiometric measurement of the HCl evolved.

Average molecular weights were determined in THF by size exclusion chromatography (SEC); analyses were carried out with an Agilent 1200 series system with PLgel 3 μm MIXED-E, PLgel 5 μm MIXED-D, and PLgel 20 μm MIXED-A columns in series, and equipped with an Agilent 1100 series refractive-index detector. Calibration curves were based on polystyrene standards having low polydispersities. THF was used as an eluent at a flow rate of 1.0 mL min<sup>-1</sup>, the sample concentrations were 5–10 mg mL<sup>-1</sup>, and injection volumes of 100 μL were used.

<sup>1</sup>H NMR and <sup>13</sup>C NMR spectra were recorded at 400 and 100.4 MHz, respectively, on a Varian Gemini 400 spectrometer with proton noise decoupling for <sup>13</sup>C NMR. The <sup>13</sup>C NMR spectra of the polymers were recorded at 30°C, with a flip angle of 45°, and the number of transients ranged from 20,000 to 40,000 with 10–20% (w/v) sample solutions in CDCl<sub>3</sub>. The central peak of CDCl<sub>3</sub> was taken as the reference, and the chemical shifts were given in parts per million from TMS with the appropriate shift conversions.

HR-MAS spectra were recorded on a Bruker Avance III 500 Spectrometer operating at a proton frequency of 500.13 MHz. The instrument was equipped with a 4-mm triple resonance (<sup>1</sup>H, <sup>13</sup>C, <sup>31</sup>P) gradient HR-MAS probe. A Bruker Cooling Unit (BCU-Xtreme) was used to keep the sample temperature at 293 or 323 K. Samples conveniently prepared with CDCl<sub>3</sub> were spun at 6 kHz to keep the rotation sidebands out of the spectral region of interest. One-dimensional (1D) <sup>13</sup>C spectra were acquired using power gate decoupling (zpgp Bruker<sup>®</sup> pulse program) and inverse gate decoupling (zg0ig Bruker<sup>®</sup> pulse program) with 4096 scans. The spectral width of 250 ppm was acquired in 64 K points at different temperatures (293 or 323 K). These sets of parameters for <sup>13</sup>C were

used for longitudinal relaxation (*T*<sub>1</sub>) calculation experiments. For *T*<sub>1</sub> calculation, a relaxation time of 8 s (d1) was left between scans and an inversion recovery experiment (t1irpg Bruker<sup>®</sup> pulse) was performed sampling points at 0.0125, 0.05, 0.1, 0.15, 0.2, 0.3, 0.4, 0.5, 0.6, 0.7, 0.9, 1.2, 2.4, and 4.8 s. The following equation was used for curves fitting the magnetization recovery [24]:

$$\ln(M_0 - M(\tau)) = \ln 2 + \ln M_0 - \tau/T_1 \quad (1)$$

where  $\tau$  is the decay time of the experiment and  $M(\tau) = -M_0$  at  $\tau = 0$

If relaxation was due to a single component, then experimental data resulted in a straight line; if this was not the case, multicomponent analysis by computer-aided nonlinear least squares method had to be performed.

Densities were determined by gas pycnometry using Micrometric AccuPyc 1330 machine at 30°C.

Thermal transitions were detected with a Mettler-Torredo differential scanning calorimeter model 822 in dynamic mode at a heating or cooling rate of 10°C min<sup>-1</sup>. Nitrogen was used as the purge gas. The calorimeter was calibrated with an indium standard (heat flow calibration) and an indium–lead–zinc standard (temperature calibration).

Clearing temperature were roughly estimated using polarized optical microscopy (POM); textures of the samples were observed with an Axiolab Zeiss optical microscope equipped with a Linkam TP92 hot stage.

For X-ray experiments, the polymers were mechanically oriented by shearing below clearing temperature on a glass plate. Measurements were made using a Bruker-AXS D8-Discover diffractometer equipped with parallel incident beam (Göbel mirror), vertical  $\theta$ – $\theta$  goniometer, XYZ motorized stage. The GADDS detector was a HI-STAR (multiwire proportional counter of 30 × 30 cm<sup>2</sup> with a 1024 × 1024 pixel). Samples were placed directly on the sample holder for transmission mode. An X-ray collimator system allowed to analyze areas of 100 and 500 μm. The X-ray diffractometer was operated at 40 kV and 40 mA to generate Cu K $\alpha$  radiation. The GADDS detector was 30 × 30 cm<sup>2</sup> with a 1024 × 1024 pixel CCD sensor placed at 30 and 9 cm from the sample. Two analytical conditions were used to measure the sample.

For low  $2\theta$  range: collimator, 100  $\mu\text{m}$ ; distance sample-detector, 30 cm. The collected *frame* (2D XRD pattern) covers a range from 0.9 up to  $9.2^\circ 2\theta$ . The diffracted X-ray beam travelled through a He-filled chamber (SAXS attachment) to reduce the air scattering at low angles. The direct X-ray beam was stopped by a beam stop placed directly on the detector face. The exposition time was of 1800 s per frame and it was first chi-integrated to generate the conventional  $2\theta$  vs. intensity diffractogram and after it was  $2\theta$ -integrated to generate a Chi vs. intensity diffractogram.

Medium  $2\theta$  range: collimator, 500  $\mu\text{m}$ ; distance sample-detector, 9 cm. The collected frame (2D XRD pattern) covers a range from 3.0 up to  $25.5^\circ 2\theta$ . The direct X-ray beam is stopped by a beam stop placed behind the sample with and aperture of  $4^\circ$ . The exposition time was of 300 s per frame and it was first chi-integrated to generate the conventional  $2\theta$  vs. intensity diffractogram and after it was  $2\theta$ -integrated to generate a Chi vs. intensity diffractogram.

## RESULTS AND DISCUSSION

As mentioned previously, the aim of this work was to obtain polyethers bearing the dendron 3,4,5-tris[4-(*n*-dodecan-1-yloxy)benzyloxy]benzoate so that the formation of hexagonal columnar mesophases could be induced. The bimolecular substitution of the chlorine atom in P(ECH-*co*-EO) with the appropriate dendritic potassium carboxylate should give the desired polymer with no substantial modification in either the backbone size or the polymer microstructure (Scheme 2).

The chemical modification of PECH under phase-transfer catalyst conditions with carboxylates has been used by several researchers [25, 26], but few studies have focused on obtaining anisotropic materials [27, 28]. Because we obtained good modification degrees and detected no dehydrochlorination side reactions in the chemical modification of PECH [29, 30], we were encouraged to use the same strategy and reaction conditions for chemically modifying P(ECH-*co*-EO). The given reactions were performed for 8 days in different solvents like THF, THF/DMF, and NMP. As previously stated, the temperature ranged from 60 to  $80^\circ\text{C}$ , depending on the solvent. These conditions were selected on the basis of our previous experience, various substrates and nucleophiles, as they gave high and almost quantitative modification degrees [25, 31]. In this way, the P(ECH-*co*-EO) solutions in different solvents were heated with different ratios of potassium carboxylate in the presence of a stoichiometric amount of TBAB. Table 1 summarizes the  $\text{OCH}_2\text{Cl}/\text{Nu}$  ratio used, the modification degrees and polymer yields obtained in these experiments.

In this case, the modification degree could not be further improved by increasing the nucleophile/ $\text{CH}_2\text{Cl}$  ratio beyond the stoichiometric (see comparison of experiments CP1, CP2, and CP5). Nor could we get higher modifica-

TABLE 2. Molecular weight and densities of the synthesized copolymers.

Polymer	Modification <sup>a</sup> (%)	$M_n \cdot 10^{-4b}$ ( $\text{g mol}^{-1}$ )	$M_w \cdot 10^{-5b}$ ( $\text{g mol}^{-1}$ )	$M_w/M_n^b$	$\rho^c$ ( $\text{g cm}^{-3}$ )
CP1	69	15.40	7.00	4.55	1.053
CP2	59	9.70	3.85	3.97	1.058
CP3	65	5.59	2.33	4.17	1.074
CP4	62	5.88	2.02	3.44	1.057
CP5	57	5.67	2.03	4.16	1.059
P(ECH- <i>co</i> -EO) <sup>d</sup>	—	10.80	5.01	4.61	1.308

<sup>a</sup> Determined by chlorine elemental analysis.

<sup>b</sup> Determined by SEC.

<sup>c</sup> Determined at  $30^\circ\text{C}$ . Error:  $\pm 3\%$ .

<sup>d</sup> Starting copolymer.

tion degrees by increasing solvent polarity (compare experiments CP2, CP3, and CP4). In this case, the modification degree reached a plateau value around 69%. This plateau seems to be related to a progressive compaction of the conformational coil which is induced by the gradual displacement of chlorine: this would finally lead to a decrease in the percentage of accessible reactive sites [32].

Average molecular weights were determined in THF on a SEC system with polystyrene as a reference sample. All values of molecular weights and polydispersity are reported in Table 2. One could expect an increasing trend of the molecular weight with modification degree, since considerably heavy dendritic groups were introduced: however, one should keep in mind that molecular weight values are obtained under the assumption that the copolymer behaves like polystyrene in THF. The introduction of dendrons into the P(ECH-*co*-EO) is expected to greatly modify the hydrodynamic volume of the system. For this reason, it is not easy to predict a trend of the molecular weight with the modification degree, since the introduction of the dendritic groups can lead to significant changes in the hydrodynamic volume with respect to the starting polymer. Density values of modified polymers (Table 2) greatly decrease with respect to the starting P(ECH-*co*-EO), that suggests a considerable change in polymer conformation after modification.

The microstructure and composition of the copolymer were characterized by NMR spectroscopy. Figure 1 reports the  $^1\text{H}$  NMR spectrum of CP1 copolymer as an example. All  $^1\text{H}$  NMR spectra are characterized by broad signals in three regions. The aromatic region shows three partially overlapped signals at 7.20, 6.75, and 6.62 ppm. Considering the relative integration areas and by comparison with the spectrum of methyl 3,4,5-tris(*n*-dodecan-1-yloxy)benzoate, the signal at 7.20 (8H) can be assigned to the protons of the benzoate group plus the benzylic protons ortho to the  $-\text{CH}_2\text{O}-$ . The signals at 6.75 and 6.62 ppm (4H+2H) correspond to the benzylic protons meta to the  $-\text{CH}_2\text{O}-$  of the lateral and central alkyloxybenzyloxy substituents. The characteristic signals, correspond-

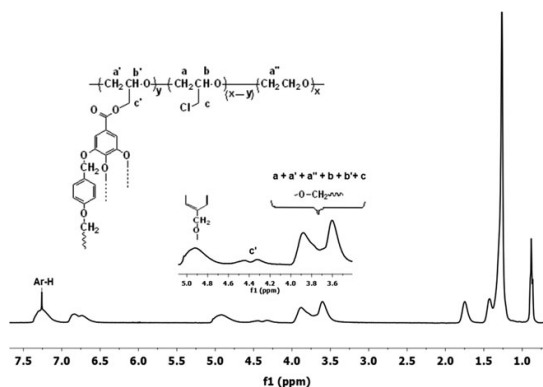


FIG. 1.  $^1\text{H}$  NMR spectrum of copolymer CP1 in  $\text{CDCl}_3$ .

ing to most protons of the dodecyloxy alkyl chains in the dendron, can be observed in the high-field region at 1.7, 1.4, 1.2, and 0.8 ppm. The most interesting region lies between 5 and 3.4 ppm in which five signals can be observed. The two signals centered at 4.42 and 4.24 ppm correspond to the two methylenic carbon  $c'$  protons in the modified monomeric unit; the signal centered at 3.90 ppm corresponds to the methylene attached to the oxygen in the alkyl chains of the mesogenic unit and to the methylenic proton  $b'$ . The partially overlapped broad signal between 3.9 and 3.4 ppm corresponds to the methylenic and methylenic protons  $a$ ,  $a'$ ,  $b$ , and  $c$  in the modified and unmodified monomeric units, as well as to the methylenic protons  $a''$  of the ethylene oxide unit. Finally, the signal centered at 4.82 ppm can be assigned to the benzylic methylenes of the dodecyloxybenzyloxy substituent.

Figure 2 shows the  $^{13}\text{C}$  NMR spectrum of copolymer CP1 with the corresponding assignments. The aromatic carbons and the carbonyl of the benzoate moiety introduced appear between 166 and 108 ppm, whereas carbons 2–12 of the aliphatic alkyl chains appear at the expected displacements in the region between 32 and 14 ppm. The carbons of the main chain units appear in the central

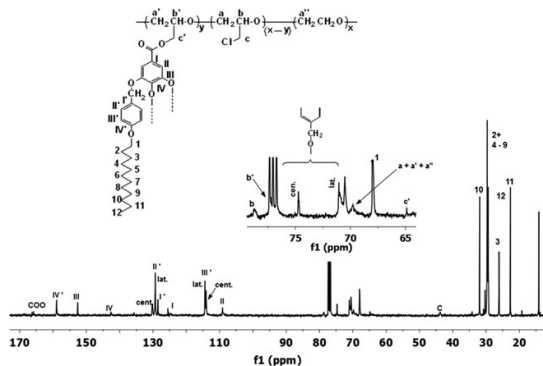


FIG. 2.  $^{13}\text{C}$  NMR spectrum of copolymer CP1 in  $\text{CDCl}_3$ .

TABLE 3. Phase transitions and annealing temperature of the copolymers CP1–CP5.

Sample	Modification (%)	$T_g^a$ ( $^{\circ}\text{C}$ )	$T_m^a$ ( $^{\circ}\text{C}$ )	Annealing temperature ( $^{\circ}\text{C}$ )	$T_c^b$ ( $^{\circ}\text{C}$ )
CP1	69	-12	50	100	115–118
CP2	59	2	34	70	85–90
CP3	65	0	27	90	95–100
CP4	62	3	26	80	100–115
CP5	57	3	29	70	87–90

<sup>a</sup> Determined by DSC from the second heating scan.

<sup>b</sup> Clearing range determined by POM.

region of the spectra. The methine and side methylenic carbons of the modified and unmodified monomeric units appear at different chemical shifts. Therefore,  $b$  and  $b'$  appear at 78.6 and 77.4 ppm, respectively, and  $c$  and  $c'$  appear at 43.5 and 63.8 ppm. The chemical shift of  $b'$  was deduced from reported spectra of modified PECH in  $\text{TCE-d}_2$  [22], since in our case it appears overlapped with the  $\text{CDCl}_3$  signal. The carbons  $a$ ,  $a'$ , and  $a''$  appear as a broad signal at 69.2 ppm. Carbon 1 of the alkyl chains appears as a wide peak at 67.8 ppm. The chemical shifts of the benzylic methylenes depend on their relative position in the aromatic ring. Those in position 3 and 5 appear at 70.7 ppm, whereas the same carbon in position 4 appears downfield at 74.7 ppm. Neither  $^1\text{H}$  NMR nor  $^{13}\text{C}$  NMR spectra showed detectable amounts of any of the signals corresponding to unsaturated vinyl ether units [33]. This indicates that the dehydrohalogenation reaction does not take place under our experimental conditions. The copolymer composition was calculated by NMR spectroscopy because this methodology gave accurate results (as compared with elemental chlorine analysis) in previous studies. Quantification was carried out from the  $^1\text{H}$  NMR spectra by comparing the areas of the aromatic peaks between 7.4 and 6.8 ppm, the benzylic proton signal at 4.8 ppm, and the methylenic protons  $c'$  at 4.4 ppm with the broad signal between 4.0 and 3.5 ppm (see Fig. 1). The results agreed with those of the comparative elemental analysis.

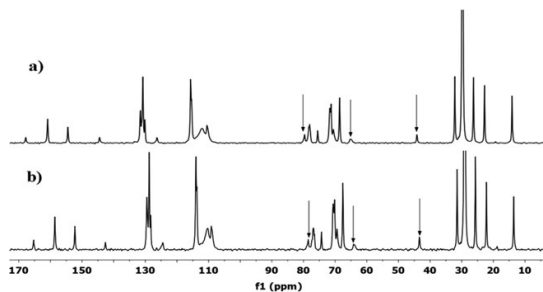


FIG. 3. HR-MAS  $^{13}\text{C}$  spectra of CP2 copolymer at: (a)  $20^{\circ}\text{C}$ ; (b)  $50^{\circ}\text{C}$ . The arrows indicate the peaks considered for  $T_{1\rho}\text{S}$  calculation, located at 43.5, 63.8, and 78.6 ppm.

TABLE 4. Carbon spin-lattice relaxation times of selected peaks of CP2 copolymer at 20 and 50°C.

Peak (ppm)	$T_{1C}$ at 20°C (s)	$T_{1C}$ at 50°C (s)
43.5	1.75 ± 0.09	0.30 ± 0.02
63.8	0.39 ± 0.01, 1.4 ± 0.4	0.22 ± 0.01
78.6	0.70 ± 0.01	0.57 ± 0.03

The characterization of the mesomorphic phases was performed on the basis of DSC, POM, and X-ray diffraction experiments. Table 3 shows the results of POM and DSC characterization. Before DSC and POM experiments, all copolymers were annealed for 2 h in between  $T_g$  and clearing temperature (Table 3). Glass-transition temperatures ( $T_g$ ) were estimated from the second heating on DSC scans in case of all copolymers and ranged between -12 and 3°C.

In all copolymers, DSC analysis put into evidence an endotherm which ranged between 26 and 50°C, which suggested the existence of a crystalline portion in the modified copolymers. XRD experiments performed at room temperature did not put into evidence any peaks attributable to crystallinity in the samples. Nevertheless, we performed HR-MAS NMR experiments on CP2 copolymer at 20 and 50°C, that is, below and above the transition detected by DSC. HR-MAS  $^{13}C$  NMR spectra of CP2 are reported in Fig. 3a and b. We focused our attention on the following peaks: 43.5 ppm, corresponding to the side methylenic carbon (c) of the unmodified unit; 63.8 ppm, corresponding to the side methylenic carbon (c') of the modified unit; 78.6 ppm, corresponding to the methine (b) of the unmodified unit. We did not take into account the peak at 77.4 ppm, corresponding to the methine (b') of the modified unit, because it was partially overlapped with the chloroform signal.

We therefore determined  $T_{1C}$ s by the inversion-recovery pulse sequence as described in the Experimental part. The results are reported in Table 4. In the case of the methylene of the modified unit (63.8 ppm), two components of  $T_{1C}$  were found at 20°C, which reduced to one

TABLE 5. Characteristics of the crystalline phase of copolymers CP1-CP5.

Sample	Modification degree (%)	Melting temperature (°C)	Melting enthalpy <sup>a</sup> (kJ mol <sup>-1</sup> )	Melting entropy <sup>a</sup> (J K <sup>-1</sup> mol <sup>-1</sup> )	$X_c^b$ (%)
PEO	—	62	8.67	25.8	100
CP1	69	50	0.32	0.99	3.7
CP2	59	34	0.16	0.50	1.8
CP3	65	27	0.16	0.42	1.8
CP4	62	26	0.16	0.55	1.8
CP5	57	29	0.15	0.49	1.7

<sup>a</sup> Per mol repetitive unit.

<sup>b</sup> Degree of crystallinity calculated with respect to 100% crystalline PEO.

when temperature was raised to 50°C. In the case of methylene and methine of the unmodified units, only one component was found at 20°C, whose value also decreased on increasing the temperature. In semi-crystalline polymers, double exponential have been observed and they are commonly interpreted by assigning one relaxation process to the crystalline domains and the other relaxation process to the amorphous portion. The longer  $T_{1C}$  value found for c' corresponded to 1.4 s. For the crystalline phase of PEO at room temperature,  $T_{1C}$ s of 14–16 s were reported [34], which are considerably longer than in our case. Taking into consideration that a strict similarity between PEO and CP2 structures should not be sought, there are also several aspects which could further justify such differences in the  $T_{1C}$ s: first, the  $T_{1C}$ s reported for PEO refer to methylene and methine in the main chain, while in our case the relaxation time refers to a side methylene; second, they were determined about 40° below melting temperature, while in our case the relaxation experiment was performed only 14° below the observed transition; third, given the XRD results, in our case it is reasonable to suppose that the amount of crystalline portion in CP2 is quite low when compared to PEO samples reported in the literature. This could also

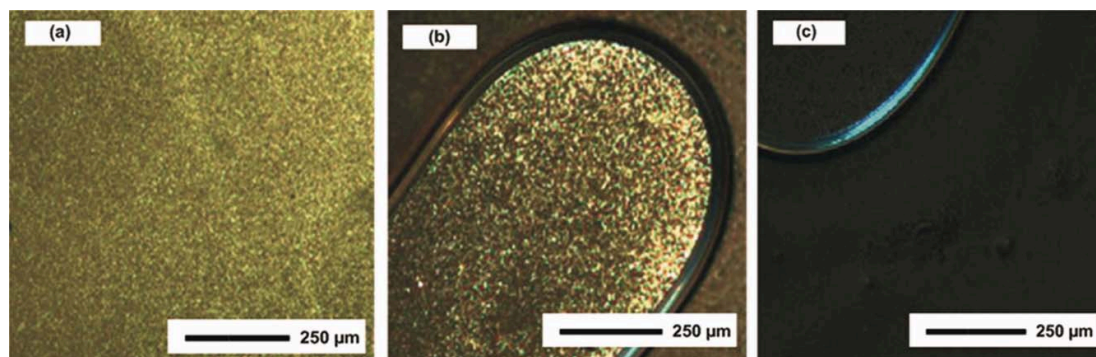


FIG. 4. Optical micrographics between crossed polars of CP1 at: (a) 110°C, (b) 115°C, (c) 120°C. [Color figure can be viewed in the online issue, which is available at wileyonlinelibrary.com.]



TABLE 6. X-ray patterns of oriented samples of copolymers CP1–CP5 at room temperature.

Polymer	Modification (%)	$d_{100}^a$ (Å)	$d_{001}^a$ (Å)	$a^b$ (Å)	$\delta^c$
CP1	69	42	4.7	49	5.1
CP2	59	45	4.7	52	6.0
CP3	65	46	4.7	53	6.0
CP4	62	47	4.7	54	6.4
CP5	57	45	4.7	53	6.0

<sup>a</sup> Planes of the hexagonal prism.

<sup>b</sup> Dimension of the hexagonal unit cell.

<sup>c</sup> Number of disks per unit cell.

affect the value of  $T_{1C}$ , as explained below. Therefore, we attributed the two components of  $T_{1C}$  to the presence of amorphous and crystalline portions in copolymer CP2. Finally, we concluded that the endotherms centered round 40°C could be attributed to main-chain crystallinity for the whole set of polymers. As an approximation, under this assumption, we roughly estimated the degree of crystallinity  $X_c$  in our modified copolymers from the experimental melting enthalpy value and taking as a reference the reported melting enthalpy for 100% crystalline PEO [35]. The obtained values, together with melting temperatures and melting entropies, are reported in Table 5. As expected,  $X_c$  values resulted extremely low, being 1.7–1.8%; in the case of CP1, which has the highest modification degree (i.e., 69%), higher melting temperature, melting entropy, and crystallinity degree were found. This suggests that the presence of the side dendrons, which are responsible for the mesogenic columnar ordering, is also able to induce some crystalline order in the copolymer main chain. In all cases, such low values of  $X_c$  presumably correspond to a great contact surface between the crystalline and amorphous regions, which determines that the crystal carbons can migrate quickly into the noncryst-

talline regions and relax. This could explain the short relaxation time found for the crystalline component of methylene  $c'$ .

All copolymers exhibited liquid-crystalline behavior, as shown by POM and confirmed by XRD. By DSC, we could evaluate neither the clearing temperature nor the clearing enthalpy, since only a very small variation of heat flow signal with respect to the baseline could be observed, even after annealing. The clearing temperature ranges were therefore determined by POM: they were found to depend on the modification degree achieved, as expected, but were all around 90–100°C. For instance, the change in the optical texture of CP1 in the clearing range is shown in Fig. 4a–c.

Table 6 shows the results of X-ray diffraction experiments performed at room temperature on the samples oriented by shearing in the rubbery state. As an example, Fig. 5 shows the X-ray diffraction pattern of CP5 in the low  $2\theta$  range (0.9–9.2°) (a) and in the medium  $2\theta$  range (3–25.5°) (b). In the case of all copolymers, the XRD pattern showed a sharp reflection at  $2\theta = \sim 2.0^\circ$ , and a broad halo at  $2\theta = \sim 20^\circ$ . This diffractogram is compatible with a columnar mesophase, the lower spacing corresponding to the planar distance between disks and the higher one corresponding to the lateral distance between columns. The former  $2\theta$  value corresponded to the  $d_{100}$  plane of a columnar phase and allowed to calculate the dimensions of the unit cell, while the latter corresponded to  $d_{001}$  plane and could be referred to the distance between dendrons [36].

For a hexagonal mesophase, and given the experimental densities  $\rho$ , we can calculate the number of repeat units of copolymer  $\mu$  that are present in a hexagonal prism layer of height  $c$  from the following equation:

$$\rho = \frac{2\mu M}{\sqrt{3}N_A a^2 c} \quad (2)$$

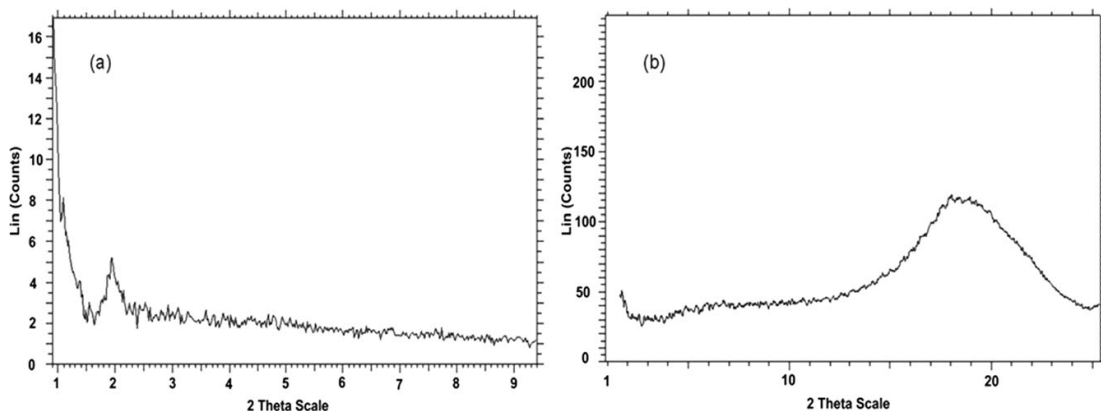


FIG. 5. X-ray diffraction pattern of CP5 in the low  $2\theta$  range (0.9–9.2°) (a) and in the medium  $2\theta$  range (3–25.5°) (b).

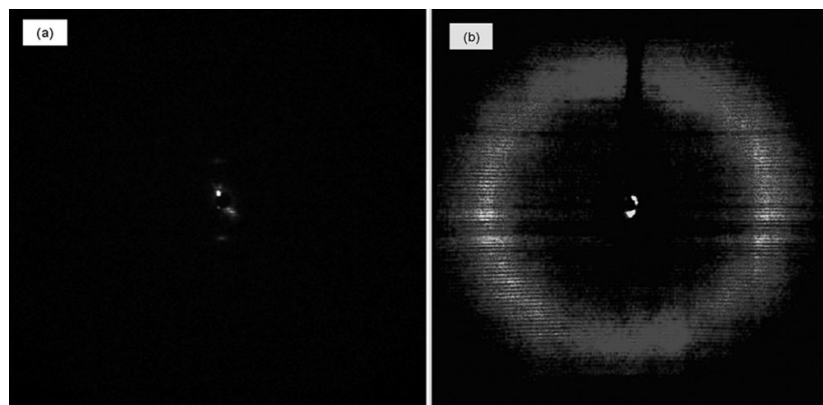


FIG. 6. XRD pattern on flat film of an oriented CP5 sample, in the low  $2\theta$  range ( $0.9\text{--}9.2^\circ$ ) (a) and in the medium  $2\theta$  range ( $3\text{--}25.5^\circ$ ) (b).

where  $M$  is the molecular weight of the repeat unit,  $N_A$  is Avogadro's number,  $a = \langle d_{100} \rangle / \sqrt{3}$  is the dimension of the hexagonal unit cell, and  $c = d_{001} \cos \chi$ , and  $\chi$  are the angles between the prism height and the distance between disks calculated from the XRD pattern of oriented samples. By considering the experimental modification degree of the copolymer  $\alpha$ , we can finally find the number of disks contained in a unit cell,  $\delta = \mu \times \alpha$ . The same calculation can also be applied to columnar samples because geometrical considerations make it possible to assume that in a columnar mesophase the columns self-assemble in a compact hexagonal packing where statistical fluctuations in the column positions do not produce any of the additional reflections that are expected in a  $\Phi_h$  phase: that is, the instantaneous positions of the columns fit a hexagonal organization even if the average positions do not [22].

Figure 6 shows the XRD pattern on flat film of an oriented CP5 sample, in the low  $2\theta$  range ( $0.9\text{--}9.2^\circ$ ) (a) and in the medium  $2\theta$  range ( $3\text{--}25.5^\circ$ ) (b). It can be seen that the reflection at  $2\theta = 1.9^\circ$ , corresponding to the  $d_{100}$  plane, is polarized in the meridian, while the halo at  $\sim 2\theta = 20^\circ$ , corresponding to  $d_{001}$  plane, exhibits polarization at the equator. This experimental evidence showed that dendrons are approximately perpendicular to the column axis and was found in the XRD pattern of oriented samples of the whole copolymer series CP1–CP5. The estimated average number of dendrons per unit cell ranged from 5 to 6. The self-assembling of CP1–CP5 copolymers into columns is schematized in Fig. 7. In the case of the copolymers obtained by chemical modification of PECH with the same dendron, the unit cell had dimensions in the same range, but it was found that the number of dendrons contained in a unit cell ranged between 3 and 6, with a tilt angle comprised between  $23^\circ$  and  $45^\circ$  [36]. This difference can be ascribed to the higher flexibility of the ethylene oxide unit, which allowed the unit

cell to accommodate more dendrons in the case of our copolymers.

## CONCLUSIONS

A new family of liquid crystalline columnar polyethers was obtained by modification of P(ECH-co-EO) with the dendron 3,4,5-tris[4-(*n*-dodecan-1-yloxy)benzyloxy]benzoate. In agreement with our previous experience, the modification degree could not be further improved by increasing either the nucleophile/ $\text{CH}_2\text{Cl}$  ratio beyond the stoichiometric one, or solvent polarity, and was found to

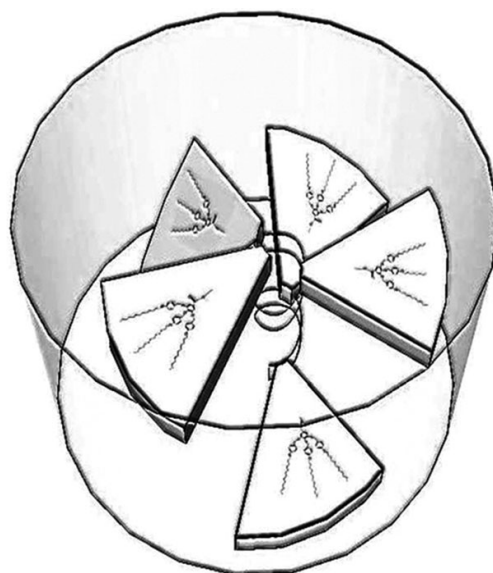


FIG. 7. Schematic representation of columnar structure of CP $n$  copolymers.

reach a plateau value around 69%. NMR characterization indicated that side reactions, such as dehydrohalogenation, did not take place under our experimental conditions. All copolymers exhibited liquid-crystalline columnar behavior, as shown by POM and confirmed by XRD. Moreover, DSC analysis and HR-MAS experiments suggested that the presence of the side dendrons, which are responsible for the mesogenic columnar ordering, is also able to induce small crystalline order in the copolymer main chain. The clearing temperature ranges were determined by POM: they depended on the modification degree, as expected, and were all around 90–100°C. X-ray diffraction experiments on oriented samples showed that the dendrons are approximately perpendicular to the column axis and that their average number per unit cell ranged from 5 to 6. Therefore, these copolymers can be used to prepare oriented membranes for small cation transport, in agreement with the results that we obtained by using PECH modified with dendrons [21]. In the case of the membranes based on modified P(ECH-co-EO), the higher flexibility of the EO moiety and the different modification degrees achieved, could vary the characteristics of the ion channel in the inner part of the columns.

## ACKNOWLEDGMENTS

The authors are grateful to Dr. Miguel Ángel Rodríguez for HR-MAS NMR experiments.

## REFERENCES

1. L.A. Weiss, N. Sakai, B. Ghebremariam, C. Ni, and S. Matile, *J. Am. Chem. Soc.*, **119**, 12142 (1997).
2. G. Brunklaus, S. Schauff, D. Markova, M. Klapper, K. Müllen, and H.-W. Spiess, *J. Phys. Chem. B*, **113**, 6674 (2009).
3. K.A. Mauritz and R.B. Moore, *Chem. Rev.*, **104**, 4535 (2004).
4. F.G. Wilhelm, I.G.M. Pünt, N.F.A.v.d. Vegt, H. Strathmann, and M. Wessling, *J. Membr. Sci.*, **199**, 167 (2002).
5. K. Miyatake, Y. Chikashige, E. Higuchi, and M. Watanabe, *J. Am. Chem. Soc.*, **129**, 3879 (2007).
6. Y. Li, R. Jin, Z. Wang, Z. Cui, W. Xing, and L. Gao, *J. Polym. Sci. Polym. Chem.*, **45**, 222 (2007).
7. G. Alberti, U. Costantino, M. Casciola, S. Ferroni, L. Massinelli, and P. Staiti, *Solid State Ionics*, **145**, 249 (2001).
8. A. Ainla and D. Brandell, *Solid State Ionics*, **178**, 581 (2007).
9. V. Percec, G. Johansson, J. Heck, G. Ungar, and S.V. Batty, *J. Chem. Soc. Perkin Trans.*, **1**, 1411 (1993).
10. U. Beginn, G. Zipp, and M. Möller, *Adv. Mater.*, **12**, 510 (2000).
11. M. Yoshio, T. Kagata, K. Hoshino, T. Mukai, H. Ohno, and T. Kato, *J. Am. Chem. Soc.*, **128**, 5570 (2006).
12. L. Jiménez-García, A. Kaltbeitzel, W. Pisula, J.S. Gutmann, M. Klapper, and K. Müllen, *Angew. Chem. Int. Ed.*, **48**, 9951 (2009).
13. V. Percec, M. Glodde, T.K. Bera, Y. Miura, I. Shiyankovskaya, K.D. Singer, V.S.K. Balagurusamy, P.A. Heiney, I. Schnell, A. Rapp, H.-W. Spiess, S.D. Hudson, and H. Duan, *Nature*, **417**, 384 (2002).
14. V. Percec, D. Schlueter, G. Ungar, S.Z.D. Cheng, and A. Zhang, *Macromolecules*, **31**, 1745 (1998).
15. V. Percec, C.-H. Ahn, G. Ungar, D.J.P. Yeardley, M. Möller, and S. Sheiko, *Nature*, **391**, 161 (1998).
16. H.-T. Jung, S.O. Kim, Y.K. Ko, D.K. Yoon, S.D. Hudson, V. Percec, M.N. Holerca, W.-D. Cho and P.E. Mosier, *Macromolecules*, **35**, 3717 (2002).
17. V. Percec, M.N. Holerca, S. Uchida, D.J.P. Yeardley, and G. Ungar, *Biomacromolecules*, **2**, 729 (2001).
18. T. Iizawa, T. Nishikubo, M. Ichikawa, and Y. Sugawara, *J. Polym. Sci. Polym. Chem.*, **23**, 1893 (1985).
19. T.D. N'Guyen, A. Deffieux, and S. Boileau, *Polymer*, **19**, 423 (1978).
20. J.A. Reina, A. Serra, A. Mantecón, and V. Cádiz, *J. Polym. Sci. Polym. Chem.*, **33**, 941 (1995).
21. B. Tylkowski, N. Castelao, M. Giamberini, R. Garcia-Valls, J.A. Reina, and T. Gumí, *Mater. Sci. Eng. C*, **32**, 105 (2012).
22. J.C. Ronda, J.A. Reina, V. Cádiz, M. Giamberini, and L. Nicolais, *J. Polym. Sci. A Polym. Chem.*, **41**, 2918 (2003).
23. L.M. Dulyea, T.M. Fyles, and G.D. Robertson, *J. Membr. Sci.*, **34**, 87 (1987).
24. F.A. Bovey and P.A. Mirau, *NMR of Polymers*, Academic Press San Diego, USA, 79 (1996).
25. J.A. Reina, V. Cádiz, A. Mantecón, and A. Serra, *Angew. Makromol. Chem.*, **209**, 95 (1993).
26. J.A. Reina, A. Serra, and V. Cádiz, *Makromol. Chem. Phys.*, **197**, 3001 (1996).
27. C. Pugh and V. Percec, *Polym. Bull.*, **16**, 521 (1986).
28. L. Callau, J.A. Reina, and A. Mantecón, *Macromolecules*, **32**, 7790 (1999).
29. M. Pérez, J.A. Reina, A. Serra, and J.C. Ronda, *Polymer*, **41**, 7331 (2000).
30. M. Pérez, J.A. Reina, A. Serra, and J.C. Ronda, *Acta Polym.*, **49**, 312 (1998).
31. M. Pérez, J.C. Ronda, J.A. Reina, and A. Serra, *Polymer*, **42**, 1 (2001).
32. C. Pugh and V. Percec, *Chemical Reactions on Polymers*, J.L. Benham and J.F. Kinstle Eds., ACS Symposium Series 364, ACS, Washington D.C., 97 (1988).
33. J.M. Montornés, J.C. Ronda, and J.A. Reina, *J. Polym. Sci. A Polym. Chem.*, **42**, 3002 (2004).
34. J.J. Dechter, *J. Polym. Sci. Polym. Lett.*, **23**, 261 (1985).
35. C.P. Buckley and A.J. Kovacs, *Prog. Colloid Polym. Sci.*, **58**, 44 (1975).
36. J.C. Ronda, J.A. Reina, and M. Giamberini, *J. Polym. Sci. A Polym. Chem.*, **42**, 326 (2004).